NATIONAL HURRICANE RESEARCH PROJECT

REPORT NO. 66

On the Filling of Tropical Cyclones over Land

U. S. DEPARTMENT OF COMMERCE
Luther H. Hodges, Secretary
WEATHER BUREAU
Robert M. White, Chief

NATIONAL HURRICANE RESEARCH PROJECT

REPORT NO. 66

On the Filling of Tropical Cyclones over Land

With Particular Reference to Hurricane Donna of 1960

by
Banner I. Miller
National Hurricane Research Project, Miami, Fla.

Washington, D. C.
December 1963

NATIONAL HURRICANE RESEARCH PROJECT REPORTS

Reports by Weather Bureau units, contractors, and cooperators working on the hurricane problem are preprinted in this series to facilitate immediate distribution of the information among the workers and other interested units. As this limited reproduction and distribution in this form do not constitute formal scientific publication, reference to a paper in the series should identify it as a preprinted report.

No. 1. Objectives and basic design of the NHRP. March 1956.
No. 2. Numerical weather prediction of hurricane motion. July 1956.
Supplement: Error analysis of prognostic 500-mb. maps made for numerical weather prediction of hurricane motion. March 1957.
No. 3. Rainfall associated with hurricanes. July 1956.
No. 4. Some problems involved in the study of storm surges. December 1956.
No. 5. Survey of meteorological factors pertinent to reduction of loss of life and property in hurricane situations. March 1957.
No. 6. A mean atmosphere for the West Indies area. May 1957.
No. 7. An index of tide gages and tide gage records for the Atlantic and Gulf coasts of the United States. May 1957.
No. 8. Part I. Hurricanes and the sea surface temperature field. Part II. The exchange of energy between the sea and the atmosphere in relation to hurricane behavior. June 1957.
No. 9. Seasonal variations in the frequency of North Atlantic tropical cyclones related to the general circulation. July 1957.
No. 10. Estimating central pressure of tropical cyclones from aircraft data. August 1957.
No. 11. Instrumentation of National Hurricane Research Project aircraft. August 1957.
No. 12. Studies of hurricane spiral bands as observed on radar. September 1957.
No. 13. Mean soundings for the hurricane eye. September 1957.
No. 14. On the maximum intensity of hurricanes. December 1957.
No. 15. The three-dimensional wind structure around a tropical cyclone. January 1958.
No. 16. Modification of hurricanes through cloud seeding. May 1958.
No. 17. Analysis of tropical storm Frieda 1957. A preliminary report. June 1958.
No. 18. The use of mean layer winds as a hurricane steering mechanism. June 1958.
No. 19. Further examination of the balance of angular momentum in the mature hurricane. July 1958.
No. 20. On the energetics of the mature hurricane and other rotating wind systems. July 1958.
No. 21. Formation of tropical storms related to anomalies of the long-period mean circulation. September 1958.
No. 22. On production of kinetic energy from condensation heating. October 1958.
No. 23. Hurricane Audrey storm tide. October 1958.
No. 24. Details of circulation in the high energy core of hurricane Carrie. November 1958.
No. 25. Distribution of surface friction in hurricanes. November 1958.
No. 26. A note on the origin of hurricane radar spiral bands and the echoes which form them. February 1959.
No. 27. Proceedings of the Board of Review and Conference on Research Progress. March 1959.
No. 28. A model hurricane plan for a coastal community. March 1959.
No. 29. Exchange of heat, moisture, and momentum between hurricane Ella (1958) and its environment. April 1959.
No. 30. Mean soundings for the Gulf of Mexico area. April 1959.
No. 31. On the dynamics and energy transformations in steady-state hurricanes. August 1959.
No. 32. An interim hurricane storm surge forecasting guide. August 1959.
No. 33. Meteorological considerations pertinent to standard project hurricane, Atlantic and Gulf coasts of the United States. November 1959.
No. 34. Filling and intensity changes in hurricanes over land. November 1959.
No. 35. Wind and pressure fields in the stratosphere over the West Indies region in August 1958. December 1959.
No. 36. Climatological aspects of intensity of typhoons. February 1960.
No. 37. Unrest in the upper stratosphere over the Caribbean Sea during January 1960. April 1960.
No. 38. On quantitative precipitation forecasting. August 1960.
No. 39. Surface winds near the center of hurricanes (and other cyclones). September 1960.
No. 40. On initiation of tropical depressions and convection in a conditionally unstable atmosphere. October 1960.
No. 41. On the heat balance of the troposphere and water body of the Caribbean Sea. December 1960.
No. 42. Climatology of 24-hour North Atlantic tropical cyclone movements. January 1961.
No. 43. Prediction of movements and surface pressures of typhoon centers in the Far East by statistical methods. May 1961.
No. 44. Marked changes in the characteristics of the eye of intense typhoons between the deepening and filling states. May 1961.
No. 45. The occurrence of anomalous winds and their significance. June 1961.
No. 46. Some aspects of hurricane Daisy, 1958. July 1961.
No. 47. Concerning the mechanics and thermodynamics of the inflow layer of the mature hurricane. September 1961.
No. 48. On the structure of hurricane Daisy (1958). October 1961.
No. 49. Some properties of hurricane wind fields as deduced from trajectories. November 1961.
No. 50. Proceedings of the Second Technical Conference on Hurricanes, June 27-30, 1961, Miami Beach, Fla. March 1962.
No. 51. Concerning the general vertically averaged hydrodynamic equations with respect to basic storm surge equations. April 1962.
No. 52. Inventory, use, and availability of NHRP meteorological data gathered by aircraft. April 1962.
No. 53. On the momentum and energy balance of hurricane Helene (1958). April 1962.
No. 54. On the balance of forces and radial accelerations in hurricanes. June 1962.
No. 55. Vertical wind profiles in hurricanes. June 1962.
No. 56. A theoretical analysis of the field of motion in the hurricane boundary layer. June 1962.
No. 57. On the dynamics of disturbed circulation in the lower mesosphere. August 1962.
No. 58. Mean sounding data over the western tropical Pacific Ocean during the typhoon season. and Distribution of turbulence and icing in the tropical cyclone. October 1962.
No. 59. Reconstruction of the surface pressure and wind fields of hurricane Helene. October 1962.
No. 60. A cloud seeding experiment in hurricane Esther, 1961. November 1962.
No. 61. Studies on statistical prediction of typhoons. April 1963.
No. 62. The distribution of liquid water in hurricanes. June 1963.
No. 63. Some relations between wind and thermal structure of steady state hurricanes. June 1963.
No. 64. Instability aspects of hurricane genesis. June 1963.
No. 65. On the evolution of the wind field during the life cycle of tropical cyclones. November 1963.

TABLE OF CONTENTS

ON THE FILLING OF TROPICAL CYCLONES OVER LAND, WITH PARTICULAR REFERENCE TO HURRICANE DONNA OF 1960

Banner I. Miller
National Hurricane Research Project
U.S. Weather Bureau, Miami, Florida

ABSTRACT

The processes which resulted in the dissipation of a tropical cyclone over land have been investigated. The eddy fluxes of latent and sensible heat and the dissipation of kinetic energy at the earth's surface have been computed for a 3-day period. On the first two days the cyclone was over water, and on the third day the center was over land. Hence it was possible to compare the rates of energy exchange at the surface after the character of the lower boundary had changed. Some significant differences in these rates of exchange were detected.

Over the oceans, air within the boundary layer flowed toward lower pressure, but the addition of sensible heat by the oceanic heat source was large enough to prevent any adiabatic cooling. As a result the temperature of the surface air remained almost constant. Evaporation from the ocean proceeded at increased rates as the center of the cyclone was approached. The eddy fluxes of sensible and latent heat resulted in an increase of the equivalent potential temperature of the air, and a radial gradient of equivalent potential temperature (with values increasing inward) was produced within the boundary layer. With the onset of convection, part of the air within the boundary layer ascended to the upper troposphere. Since air ascended at different radii, a radial gradient of mean virtual temperature from the surface to the upper troposphere was produced, with the warmest air near the core of the cyclone. This warm-core structure was responsible for the intense pressure gradients observed at sea level.

Over land, however, the eddy fluxes of latent and sensible heat were very nearly zero. The air within the boundary layer still flowed toward reduced pressure, but, in the absence of a heat source, moist adiabatic cooling took place. This resulted in the destruction of the radial gradient of equivalent potential temperature within the boundary layer. Following ascent to the middle or upper troposphere, the warm-core structure of the cyclone was destroyed. This cooling resulted in a pressure rise at the center of the cyclone and the circulation decayed.

The land area was rougher than the water. The maximum drag coefficient (C_d) over water was found to be about .0042; over water C_d varied almost linearly with wind speed. Over land the mean drag coefficient was about .0087; there were no indications of a dependence on wind speed. Within a few hours after landfall, the rate of dissipation of kinetic energy due to surface friction was less over land than it had been over water just prior to landfall. This decrease is presumably due to greater vertical shear and reduced pressure gradients over land; the latter resulted in a slowing down of the wind at anemometer level.

The production of kinetic energy by the inflow layer was reduced sharply near the core after the center moved inland. Mass flow changed very little after landfall, and the decrease in the production of kinetic energy was caused primarily by the reduced pressure gradients over land. It was concluded that the primary cause for the dissipation of tropical cyclones over land was the removal of the oceanic heat source. The dissipation of kinetic energy by surface friction was of minor importance during the filling over land.

LIST OF SYMBOLS

C_d a non-dimensional drag coefficient

C_e a non-dimensional coefficient of evaporation

C_h a non-dimensional coefficient of heat flux

C_p specific heat of air at constant pressure

C_v specific heat of air at constant volume

e vapor pressure

e_s saturation vapor pressure

E evaporation per unit area per unit time

F the frictional force per unit mass

g the acceleration of gravity

h the depth of the inflow layer

H sensible heat received by a unit mass

k von Karman's constant

K the kinetic energy per unit mass

k_l the thermal conductivity

K_{ep} Langrangian exchange coefficient for latent heat

K_h the eddy conductivity

K_m the eddy viscosity

K_{sp} Lagrangian exchange coefficient for sensible heat

K_w the eddy diffusivity of water vapor

L the latent heat of condensation

m mass

p	pressure
P	the rate of precipitation
q_s	saturation mixing ratio
Q_e	the flux of latent heat (per unit area per unit time)
Q_s	the flux of sensible heat (per unit area per unit time)
Q_{ep}	flux of latent heat along a trajectory
Q_{sp}	flux of sensible heat along a trajectory
r	radial distance
R	gas constant
R_f	flux form of Richardson number
R_i	gradient form of Richardson number
s	a measure of horizontal distance
t	time
T	temperature
T^*	mean virtual temperature for a layer
u	wind speed
$\mathbf{V}$	two-dimensional wind vector
$\mathbf{V}_3$	three-dimensional wind vector
V_o	surface wind speed
v_r	radial wind speed
v_θ	tangential wind speed
w	vertical wind speed
z	vertical coordinate
Z	height of isobaric surface
Z_t	thickness between two isobaric surfaces
α	specific volume
γ_d	the dry adiabatic lapse rate of temperature (p-system)

Γ_s the moist adiabatic lapse rate of temperature (p-system)

Γ the actual lapse rate of temperature (p-system)

γ_d the dry adiabatic lapse rate of temperature (z-system)

γ_s the moist adiabatic lapse rate of temperature (z-system)

γ the actual lapse rate of temperature (z-system)

ϵ the ratio of molecular weights of water and dry air

ζ_a the vertical component of the absolute vorticity

θ potential temperature, polar angle

θ_e equivalent potential temperature

ρ density

Φ the horizontal shearing stress per unit area

$\mathbb{T}$ the horizontal shearing stress vector

ω dp/dt = the vertical velocity in terms of pressure

Ω the angular rotation of the earth (vector)

∇ the two dimensional differential operator

∇_3 the three dimensional differential operator

1. INTRODUCTION

The tropical cyclone is a thermally driven circulation in the direct sense. The role of the vertical flux of sensible and latent heat in both the formation and maintenance of tropical cyclones has been demonstrated by Palmén and Riehl [37] and by Malkus and Riehl [26]. The dissipation of kinetic energy by friction acts as a brake on hurricane development. It is evident, therefore, that surface exchange processes are of fundamental importance to the hurricane mechanism.

To establish the connection between the growth of the kinetic energy and the heat source, it is necessary to consider both the kinetic energy equation and the thermal energy equation. The kinetic energy equation (neglecting the kinetic energy of vertical motion) is

$$\frac{dK}{dt} = -\alpha \mathbf{V} \cdot \nabla p + \mathbf{V} \cdot \mathbf{F} \qquad (1)$$

in which K is the kinetic energy per unit mass, α is the specific volume, $\mathbf{V}$ is the horizontal wind velocity, ∇ is the two-dimensional differential operator, p is the pressure, and $\mathbf{F}$ is the frictional force. The first term on the right may be interpreted as the rate at which potential energy and enthalpy are converted into kinetic energy. The second term on the right is the rate at which kinetic energy is dissipated by friction.

The first law of thermodynamics for moist air may be written in the form

$$-\alpha \mathbf{V} \cdot \nabla p = -\frac{d}{dt}(gz + C_p T) + \frac{dH}{dt} - L\frac{dq_s}{dt} + \alpha \frac{\partial p}{\partial t} \qquad (2)$$

where gz is the potential energy and $C_p T$ is the enthalpy per unit mass, dH/dt is the sensible heat source, $-Ldq_s/dt$ is the latent heat source, and $\partial p/\partial t$ is the local pressure tendency. The reason for presenting equation (2) here is that it contains the heat sources explicitly. It is not suitable for determining the rate at which kinetic energy is produced. There are several reasons for this.

In a mature tropical cyclone the total of internal and potential energies is about two orders of magnitude larger than the total kinetic energy. The production of kinetic energy is about 3 percent of the latent heat release (Palmén and Riehl [37]), while the sensible heat source is of the same order of magnitude as the production of kinetic energy.

During the growth of a tropical cyclone the increase in the kinetic energy is accompanied by an increase in the internal and potential energies (Palmén and Riehl [37]; Palmén [35]). Spar [54] has shown that developing extratropical cyclones are also accompanied by increased potential and internal energy per unit mass. It is clear, then, that the increase in kinetic energy cannot be calculated by determining the changes in the internal and potential energy.

In mature tropical cyclones, the export of potential energy and enthalpy by the mass circulation at the upper levels exceeds the import of energy (potential, enthalpy, and latent heat) by the mass circulation at the lower levels (Malkus and Riehl [27]; Miller [30]). This points to the importance of the surface heat source in developing and maintaining the cyclone.

As long as the tropical cyclone remains over the oceans where the water is warmer than the air, evaporation and the vertical flux of sensible heat from the ocean to the air contribute to the growth of the energy of the cyclone. Air near the surface spirals inward toward the center of the cyclone, and the trajectory is almost horizontal until the air parcel approaches the core. This flow is in the direction of reduced pressure, but inside a radius corresponding approximately to the radius of the 1000-mb. isobar, the surface temperature is almost constant, indicating that the expected adiabatic cooling does not occur. Such cooling is prevented by the addition of sensible heat from the ocean. This isothermal expansion results in an increase of the equivalent potential temperature (θ) of air, thereby permitting moist adiabatic ascent near the core of the cyclone at higher values of θ_e. As shown by Malkus and Riehl [26] the ascent path (hence the density of the vertical column) is determined solely by the equivalent potential temperature of the rising air. By assuming vertical ascent from the surface to the level of zero buoyancy, that the 100-mb. surface was undisturbed, and that the layer between 100 mb. and the level of zero buoyancy was represented by Jordan's mean tropical sounding (NHRP No. 6), they computed the surface pressures for a series of moist adiabats. They found that within the range θ_e = 350°A. to 365°A., the surface pressure and θ_e are related linearly. Thus

$$-\partial p_s = 2.5\ \partial\theta_e \qquad (3)$$

Since the increase of θ_e is a function of the surface heat and moisture sources, equation (3) gives additional evidence of the importance of the surface heat sources (both sensible and latent) to the development of tropical cyclones.

Over land tropical cyclones usually weaken rapidly. Malkin [25] investigated the changes in central pressure and intensity of 13 selected hurricanes after the centers moved inland. He found that the average change in central pressure was + 2.3 mb./hr. immediately after the center crossed the coastline but that this rate had decreased to about + 1.0 mb./hr. within 24 hr. He developed the empirical formula for the central pressure

$$p_s = p\ (L) + 2.3t - 0.03t^2 \qquad (4)$$

where p_s is the central pressure (in mb.) at the surface, p(L) is the central pressure at time of landfall (t = 0), and t is the time in hours. Equation 4 implies

$$\frac{\partial p_s}{\partial t} = 2.3 - 0.06t \qquad (5)$$

which is an empirical tendency equation for tropical cyclones over land. Malkin made no attempt to evaluate the factors which contribute to the filling process over land.

After a hurricane moves from a water surface to a land surface, the rate of frictional dissipation of kinetic energy at the lower boundary is assumed to change, although this has not been established. For many years, it was believed that increased friction over land was the primary cause for the decay of hurricanes. Hubert [19] attempted to determine the effect of friction on the rate of filling after a hurricane passes from a water to a land surface. He concluded that friction alone is insufficient to account for the decrease in intensity over land. He suggested that a change in the available energy supply was the predominant factor which causes filling over land, but he did not establish this.

The rate of filling over land is a function of the radius, as shown by Myers [32]. The central pressure rises rapidly, whereas the peripheral pressures change more slowly. It is near the center that frictional dissipation of kinetic energy is at a maximum. Over the oceans, the vertical flux of sensible heat from the water to the air is also at a maximum near the center. Over water, presumably, this flux of sensible heat counterbalances the dissipation of kinetic energy due to friction. In a later section it will be shown that near the core of a steady-state hurricane frictional dissipation of kinetic energy and the sensible heat source are essentially equal. Over land the sensible heat source is greatly reduced or may be lacking altogether. Hence, the balance between sensible heat and frictional dissipation is upset after the cyclone moves inland. It has been suggested by Byers([2] p. 392), by Riehl([46], p. 341), and by Bergeron [1] and Palmen [34], that it is the removal of the sensible heat source (hence also the removal of the latent heat source) which makes the most important contribution to the filling process over land. However, no one has ever presented any calculations which establish this view.

The purpose of this paper is to examine in detail the changes in the energy supply which occur after the center of a hurricane moves away from the warm waters of the tropical oceans. We will examine the changes in the flux of energy through the lower boundary. This will include calculation of the vertical flux of both sensible and latent heat over water and over land. Frictional dissipation over land and over water will be compared. Structural and thermodynamical changes which were observed during and after landfall will be related to the surface heat source-frictional dissipation balance (or lack of balance).

The kinetic energy budget for the inflow layer will also be computed, and it will be shown that the production of kinetic energy is less over land than it is over water. This reduction in the production term can be related to the removal of the surface heat source.

The pressure gradient which would be needed to maintain over land the same wind field that was observed while the cyclone was still over water will be computed. This will be done by using the equations of motion with the frictional terms included. It may then be shown that the computed pressure gradient could be maintained over land if a heat source equivalent to the oceanic heat source were present over land.

It is hoped that these calculations will supply partial answers at least to the questions: 1. Is filling and loss of intensity over land due to increased frictional dissipation at the ground? 2. Is filling over land due to a reduced surface heat source? 3. Is filling due to some other causes, e.g. mid-tropospheric ventilation?

2. SOURCES AND ANALYSES OF DATA

Most of the calculations are based on data obtained in the vicinity of hurricane Donna which occurred in September 1960. A portion of the track is shown in figure 1. Donna was selected because the center of the cyclone passed through a region where the density of rawinsonde stations is considerably greater than normal. Also, the surface reporting stations in the Bahamas, Cuba, and Florida provided good data coverage at the surface, necessary for the computation of surface exchanges between the lower boundary and the atmosphere. Research aircraft of the Research Flight Facility of the Weather Bureau flew paths near the core of the cyclone and collected detailed data on winds, temperatures, and relative humidities at three levels on September 9. In addition, the center was under constant radar surveillance for the entire period during which calculations were made. This made it easy to prepare a detailed track of hourly center positions which was necessary in determining the radial component of the wind and in compositing the available data with respect to the center of the cyclone.

Another advantage in using the Donna data resulted from the fact that the thermal structure of the immediate environment of the cyclone remained almost constant before and after the center moved inland over Florida. As a result, one could consider the Donna calculations as very nearly approaching a controlled experiment, in which the only variable allowed to change was the character of the lower boundary. Consequently, it provided an unusual opportunity to examine the effects of changed surface friction and surface heat source after the center of a hurricane has moved inland.

The center of the hurricane passed north of Cuba on the 9th, across the Florida Keys on the 10th, and into central Florida during the early part of the 11th. Calculations will be performed for each of these three days. On the 9th and 10th the center was mostly over water and on the 11th the center was moving over land. The computations should, therefore, provide a basis for comparison of the energy transformations over water with those over land.

The hurricane moved through a region where the density of radiosonde stations is relatively high, as shown in figure 2. Many of these stations made observations at 3-hour intervals during the period when the center of the hurricane was less than 300 n. mi. away, and 6-hourly soundings when the center was 300-800 n. mi. away. For any one synoptic time, however, the data were too few to permit the detailed calculations (such as volume integration of equation (1)) needed to describe the various energy transformations. Consequently, it was necessary to composite the available observations over 12-hr. periods in order to obtain enough data with which to work.

These 12-hr. periods were chosen for compositing the upper-air soundings. These periods included the hours from 0000 GMT to 1200 GMT on the 9th, 10th, and 11th. This choice was dictated by the fact that the center was passing

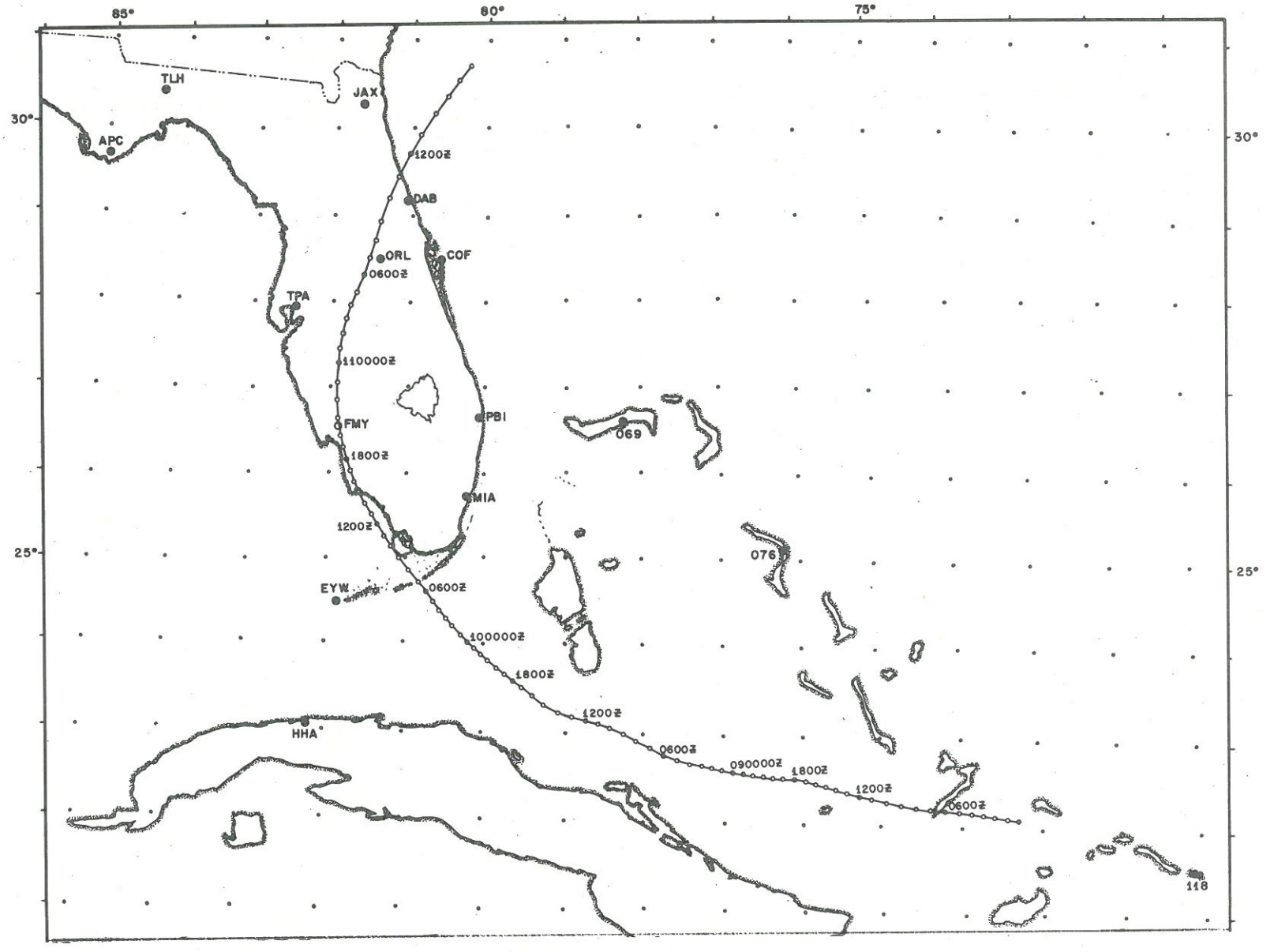

Figure 1. - Track of hurricane Donna, September 8-11, 1960

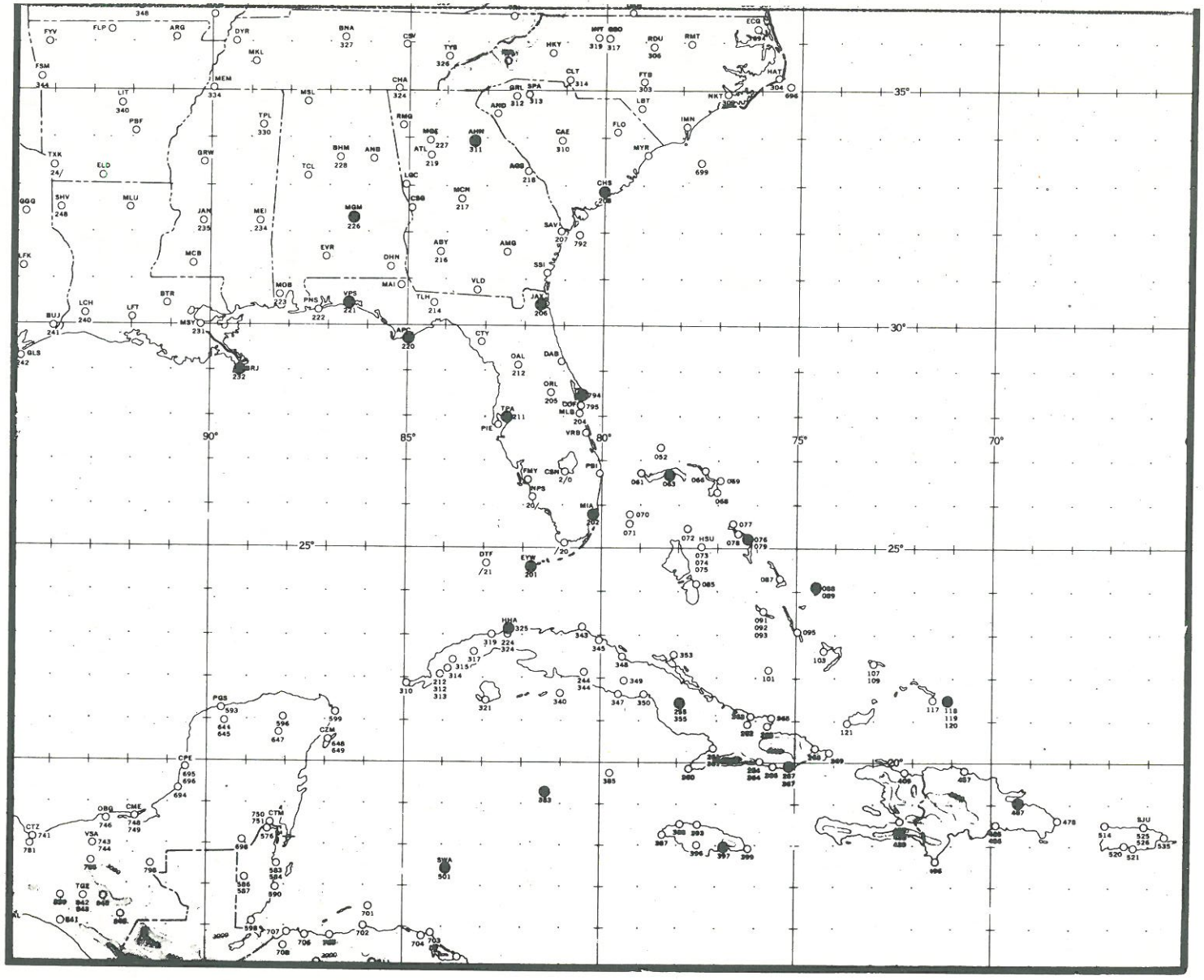

Figure 2. - Network of radiosonde stations in the Caribbean and southeastern United States

over land during these hours on the 11th (fig. 1). The same periods were selected on the 9th and 10th (when the center was over water) to eliminate the necessity for considering possible diurnal effects when over-water and over-land computations were compared.

The data were composited and plotted with respect to the center of the moving cyclone. At all levels data were plotted at the actual position of the balloon at that level (in both space and time) rather than at the position of the observation station and at release time. However, these corrections in position proved to be significant in only a few cases (mostly when the sounding was made within 90 n. mi. or less of the center of the hurricane). The density of the data following the compositing process for the three 12-hour periods is shown in figure 3.

The compositing of data around a tropical cyclone is necessary if one wished to perform any sort of quantitative analyses. It is permissible as long as the cyclone is in a relatively steady state. On the 9th and 10th, Donna was probably as near to being in a steady state as a mature hurricane ever is. Hence, there is not much doubt that the compositing process gives a reasonably accurate picture of the cyclone. On the 11th, however, the cyclone was moving over land and weakening. This casts some doubt on the validity of a composite chart. Figure 4 shows the time variations of the central pressure. It will be noted that most of the rise in the central pressure (more than 30 mb.) occurred between 1200 GMT on the 10th and 0000 GMT on the 11th. This gives some indication that the cyclone was in a quasi-steady state over land during the period for which data were composited. Obviously, it would have been preferable to use only synoptic data, but this was impossible. In fact, no really complete synoptic description of the inner portion of a tropical cyclone has ever been obtained. The nearest thing to such descriptions are those based on aircraft data obtained by the National Hurricane Research Project, but these data are also composited over a period of several hours.

In addition to the radiosonde observations, research aircraft collected some data on the 9th. Extensive flight patterns were flown at 1600, 6400, 14,200 and 18,200 ft. Some useful wind data were obtained by the three lower flights. The tracks are shown in figure 5. None of these flights corresponded in time to the compositing periods (0000-1200 GMT) previously adopted for the radiosonde data. The 1600-ft. level was flown between 1400 GMT and 1530 GMT. These data were therefore used to supplement the composite data for the 9th. The 14,200-ft. flight collected data between 1903 GMT and 2030 GMT, which is nearer in time to the compositing period on the 10th than to that on the 9th. Therefore, the data from this level were used to supplement the rawinsonde data on the 10th. The 6400-ft. flight time was too far away in time from both compositing periods and the data were used mainly as a guide to drawing isotachs near the center of the cyclone and in determining the mass flow on the 9th.

A number of the Coast Guard Lighthouse stations in the Florida Keys are equipped with recording wind instruments, and these also proved to be a good source of wind data. The center of the hurricane passed within 16 n. mi. of Sombrero Light Station, and a maximum speed of about 111 kt. was recorded (fastest mile). The data from Sombrero, Alligator, and Carysfort Light Stations were used as representative of the lowest layer (surface to 900 mb.) on the 10th.

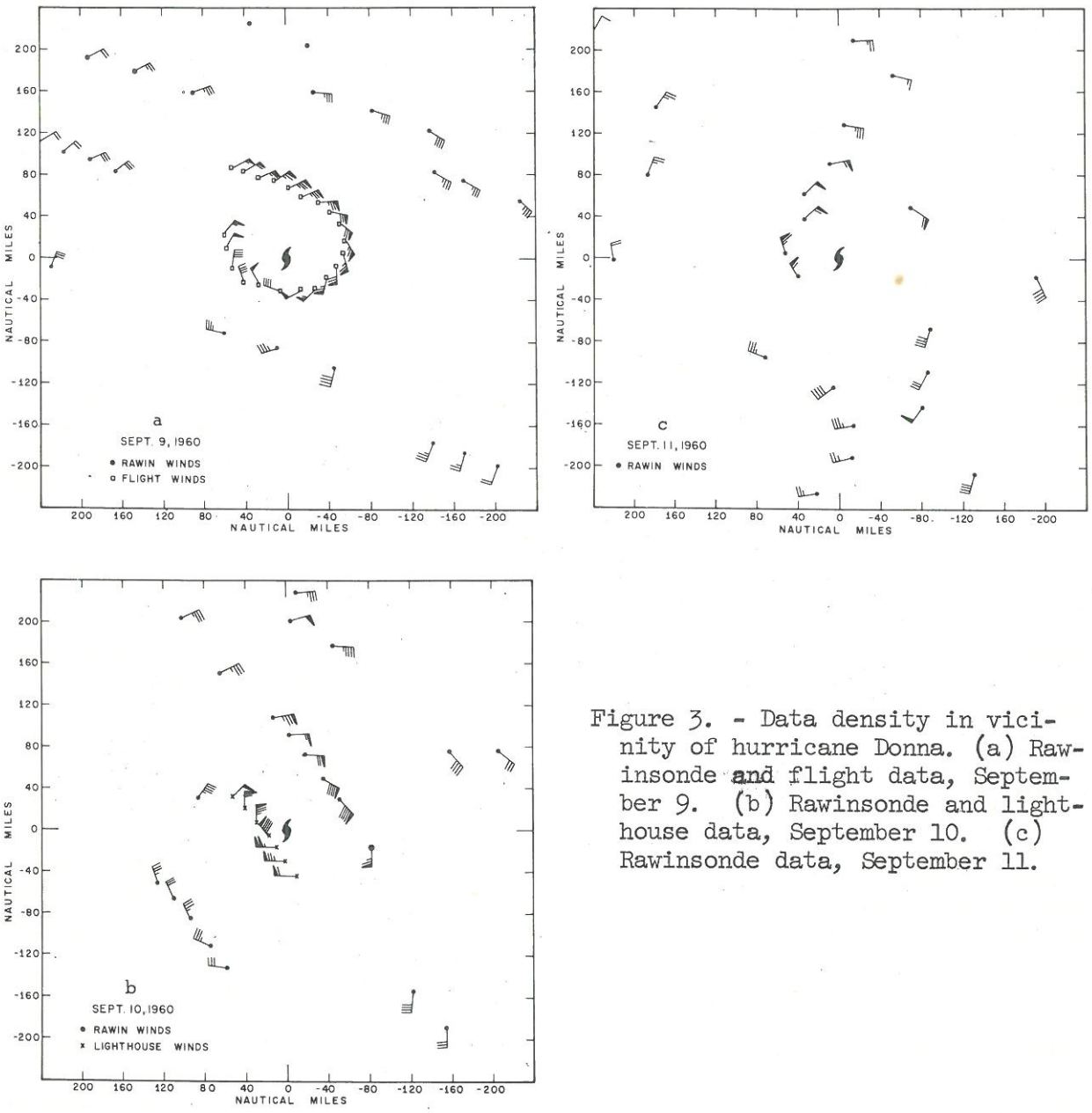

Figure 3. - Data density in vicinity of hurricane Donna. (a) Rawinsonde and flight data, September 9. (b) Rawinsonde and lighthouse data, September 10. (c) Rawinsonde data, September 11.

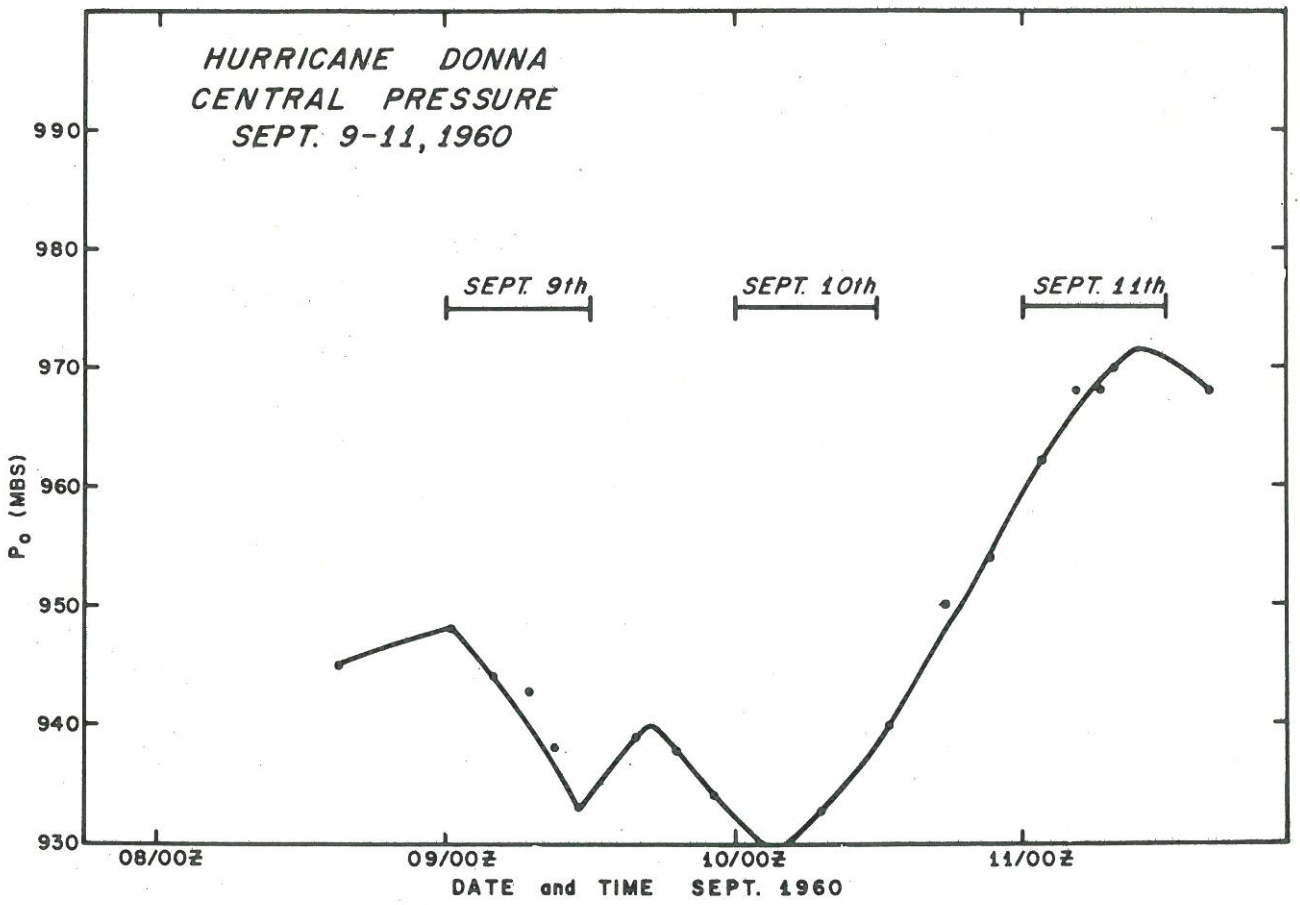

Figure 4. - Variations of central pressure with time, hurricane Donna, September 9-11, 1960.

Other data used included the surface reports from ships (including water temperatures), land stations over Florida and Cuba, and island stations in the Bahama Islands. Several dropsondes made by the Navy from the 700-mb. level were available on the 9th and 10th. These were made mostly in or close to the eye of the cyclone.

Preparatory to analyzing the data, vertical profiles of wind speed and direction were plotted for the individual rawin soundings. Mean winds for layers of 100-mb. thickness from the surface up to 200 mb. were computed. For the 200-100 mb. layer, means were computed for 50-mb. increments. If the vertical variation of the wind direction through a layer was 20° or less, means were computed from the vertical profiles by equal area methods. If the wind direction varied by more than 20° through any layer, means were computed from the balloon trajectory as recorded on the original rawin computation forms. Most of the means for the layers above 300 mb. were computed from the balloon trajectory.

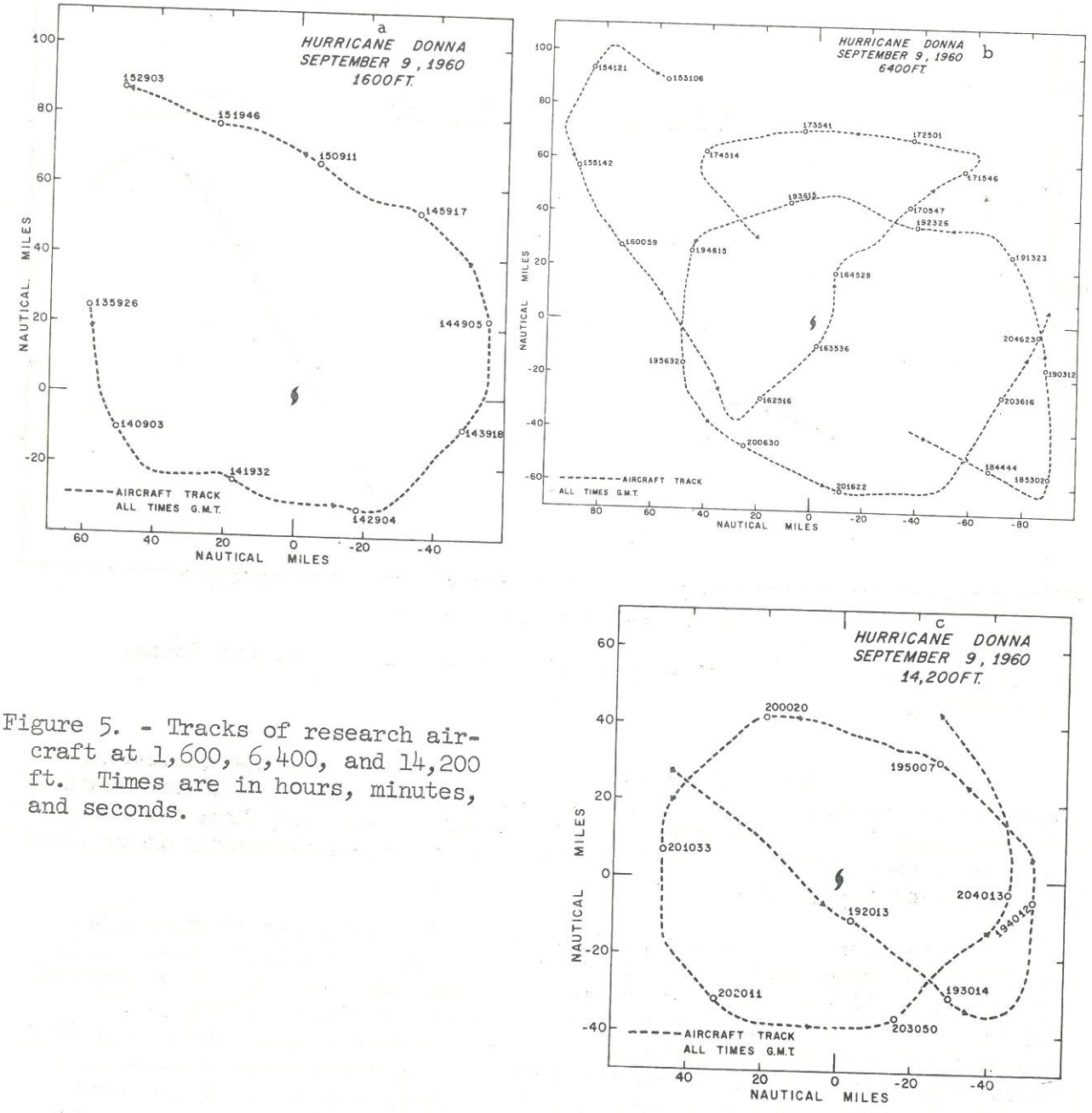

Figure 5. - Tracks of research aircraft at 1,600, 6,400, and 14,200 ft. Times are in hours, minutes, and seconds.

The mean layer winds were then composited with respect to the center of the cyclone. Radial and tangential components of both the actual wind and the relative winds were computed. These wind data and the heights of the constant pressure surfaces, the temperatures, and the mixing ratios (up to 250 mb.) were plotted at the middle of each layer (950 mb., 850 mb., ...125 mb.) for each of the three compositing periods. The height field was carefully analyzed at each level. From the analyses thickness patterns were computed and these were checked for thermal consistency. The thickness patterns were smoothed, where necessary, to make them fit the available temperature data. New height fields were then constructed by differential analysis. These new analyses were then compared with the originals and in most cases the differences were found to be negligible.

The mixing ratios were analyzed for the middle of each layer (950 mb. to 250 mb.). The values obtained from the analyses were compared with the saturation mixing ratios corresponding to the actual temperatures and pressures at each level in order to eliminate any values which would have indicated supersaturation.

No detailed temperature analyses were prepared (aside from the thickness analyses which could have been used to compute the temperature patterns). However, temperatures were used primarily in the computations of the transports of enthalpy. These temperatures were obtained by plotting the temperatures at various radii versus azimuth. Figure 6 shows one example of this type of curve. In regions of no data the temperatures were obtained from the smooth curve drawn to fit the available data. Where the radius for which the data were being prepared fell between reports, linear interpolation was used to obtain the value at that radius.

The tangential component of the actual wind (used in computing the transport of angular momentum) was obtained in the same manner as the temperature. The radial wind analyses were more complicated and will be discussed in the following section.

3. MASS FLOW

A description of the radial mass transport is of fundamental importance in explaining the energy transformations of the tropical cyclone. The rate of conversion of potential energy to kinetic energy depends largely upon the radial wind component. In hurricanes the minimum central pressure is linearly related to the mass flow (Krueger [23]). Much of the latent heat energy is supplied by the radial transport of water vapor from the environment. Some radial transport of kinetic energy inward is apparently necessary to maintain the core of a steady state tropical cyclone (Palmen and Riehl [37]; Rosenthal [49]). Integration of equation (1) over a cylindrical volume requires detailed knowledge of the mass flow inside the cylinder. It is obvious, therefore, that a good radial wind analysis is the most important part of the calculations of the energy transformation in hurricanes.

For each of the three days the radial wind analysis proved to be reasonably easy for the inflow layer, which extended from the surface to about 700 mb. In obtaining the mass flow (and making the subsequent energy calculations) data for the inflow layer were tabulated at radial intervals of 40 n. mi. and at 30° increments as shown by the grid system in figure 7.

Above 700 mb. there was only one common radius for which the mass flow could be accurately determined for all three days. This was the 120-n. mi. radius. For these layers radial wind components were plotted against azimuth (fig. 8). Where the 120-n. mi. circle fell between plotted data, the radial wind was obtained by linear interpolation of the mass flow which is proportional to the product of v_r and r. Smooth curves were then drawn to fit the available data (fig. 8). The radial wind was then read from the curves. These radial winds were means for layers of 100-mb. thickness up to 200 mb. and for 50-mb. layers for the 200-100-mb. interval.

These data were then adjusted for mass balance by setting

$$\oint\int_{p_o}^{p_t} v_r \, dprd\theta = 0 \qquad (6)$$

where p_o is the surface pressure, p_t is pressure at the top of the cyclone (assumed to be at 100 mb.), v_r is the radial wind component, r is the radius, and θ is the polar angle. The adjustments required to achieve mass balance were small, being less than 1 kt. on each of the three days, which probably indicates that the mass flow was determined as accurately as any available observational data permit.

The vertical profiles of radial winds are shown in figure 9. These profiles are similar to those obtained from mean data (E. Jordan [22]; Miller [28]) as well as those observed in several other individual cyclones (e.g. Malkus and Riehl [27]; Miller [30]).

Figure 9 shows that practically all of the inflow into the cyclone occured below 700 mb. This is typical of most hurricanes. The layer from the surface to 700 mb. will be referred to as the inflow layer. There are enough data at the lower levels to permit a detailed energy budget for the inflow layer. This is fortunate, since the inflow layer is, in essence, the engine which drives the cyclone. Because of its importance, the means of determining the mass flow for the inflow layer will be discussed in some detail.

On the 9th the flight data at 1600 ft. were obtained within a few millibars of the 950-mb. level. These wind data were used to represent the mean layer winds for the lowest (surface to 900 mb.) layer. Along the track shown in figure 5 winds were recorded at intervals of from 2 to 20 seconds. Using these data (plus the rawin data whose locations are shown in fig. 3) it was an easy matter to prepare an analysis of the radial wind components. From this analysis the radial wind components (hence the mass flow) for the surface to 900-mb. layer was determined for the 40-, 80-, and 120-n. mi. radii. For the layer centered at 850 mb. the 6400-ft. flight winds (which were obtained at about 800 mb.) were used in conjunction with the rawin data. These data did not correspond in time to the 0000-1200 GMT compositing period. Consequently, it was necessary to make some minor adjustments in the indicated center position of the cyclone in order to obtain a mass flow pattern consistent with the other data. For the 800-700-mb. layer, the mass flow at the 80- and 40-n. mi. radii were obtained by extrapolation from the 120-n. mi.

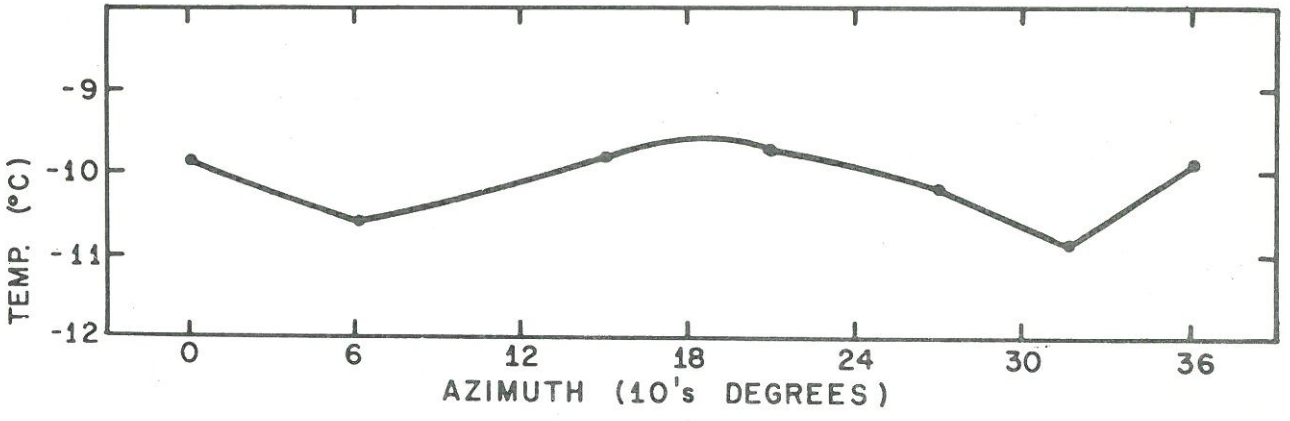

Figure 6. - A plot of temperature versus azimuth. Data are for the 450-mb. level at 120-n.mi. radius on September 9.

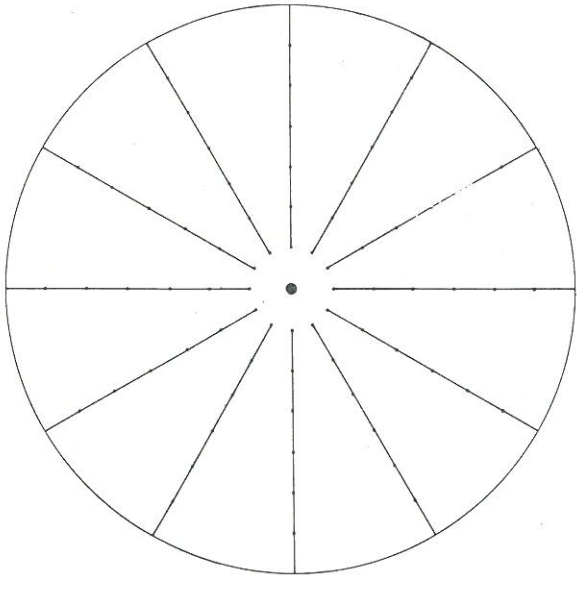

Figure 7. Grid system used in hurricane calculations. Azimuthal interval is 30°; radial interval is 30 or 40 n.mi.

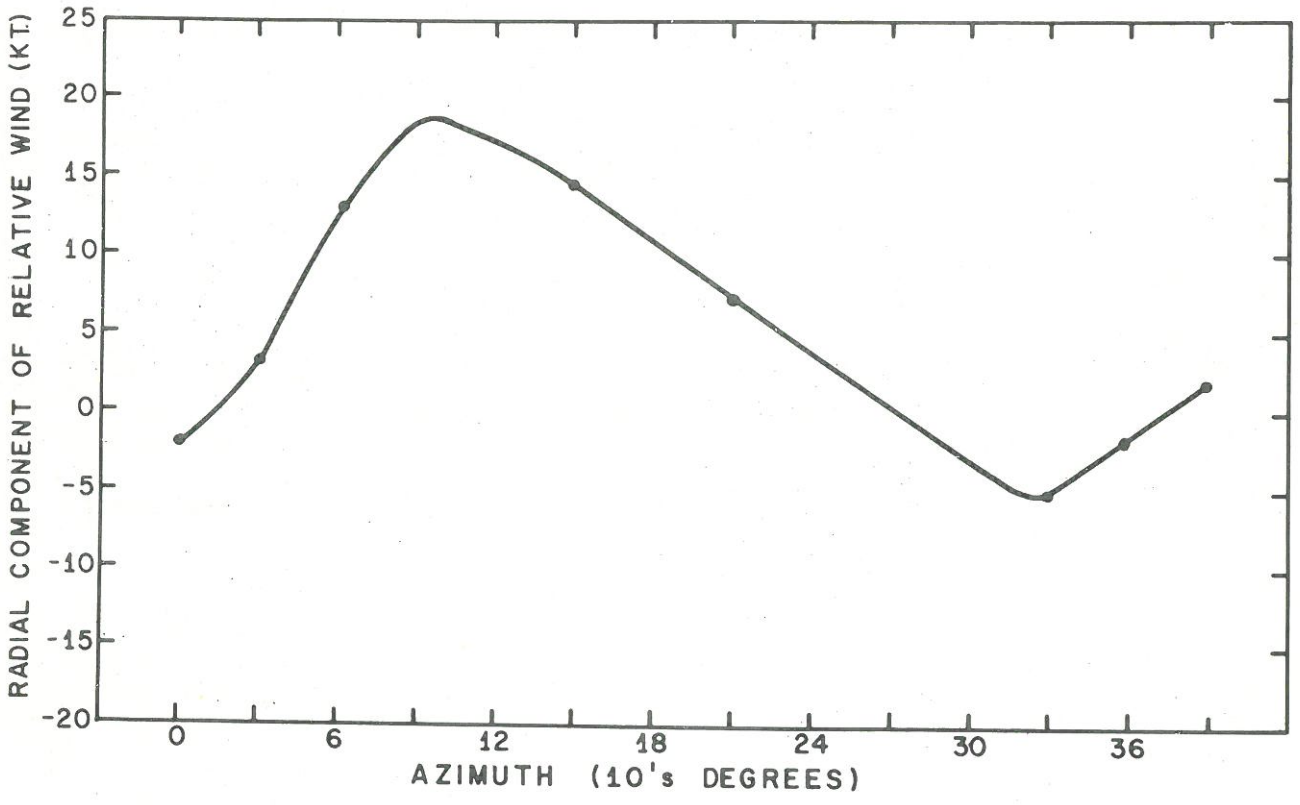

Figure 8. - Radial wind speed versus azimuth. Data are for the 350-mb. level at 120 n.mi. radius on September 9.

radius and from the lower layers. The variations in the mass flow with radius and height are shown in figure 10a.

On the 10th there were enough rawin data to obtain the mass flow at the 80- and 120-n. mi. radii by plotting the radial wind versus azimuth, drawing smooth curves to the available data, and then reading the radial wind components from the curves in regions of no data. This type of curve is illustrated by figure 8. Inside these radii the mass flow was obtained by making use of the lighthouse data and the aircraft winds at 14,200 ft. The data at these two levels were very good and gave an excellent portrayal of the mass flow. The mass flow for the 40-n. mi. radius was obtained by plotting the vertical profiles of radial winds. These profiles were drawn with slopes which followed as closely as possible the already established profiles at the 80- and 120-n. mi. radii. The results are shown in figure 10b. It will be noted that figures 10a and 10b are very similar, as would be expected since the cyclone was approximately steady state.

On the 11th (when the cyclone was over land), mass flow at the 120- and 80-n. mi. radii could be well established by plotting radial wind versus azimuth. At the 40-n.mi. radius, the mass flow was estimated by making use of the available data (mostly to the north and west of the center, as shown by fig. 3) and by extrapolation of the data from the outer radii. Surface

data were used to assist in the construction of the mass flow for the lowest layer. The results are shown in figure 10c. It will be noted that the mass flow changed very little after the cyclone moved inland.

From the mass flow computations, the mean vertical motion for various radial intervals may be computed. The mean horizontal velocity divergence is

$$\overline{\text{Div } \mathbf{V}} = \frac{1}{r} \frac{\partial(v_r r)}{\partial r} \tag{7}$$

The overscore indicating mean values. From (7) the vertical motion was calculated for the 900- 800-, and 700-mb. layers. The results are shown in figure 11, for calculations made for the 10-40, 40-80, and 80-120 n. mi. radial intervals. Inside the 40 n. mi. radius the computed vertical velocities at the 900-mb. level range from 23 to 30 cm. sec.$^{-1}$, which is comparable to the values of 28 to 37 cm. sec.$^{-1}$ obtained inside this radius by Malkus and Riehl [26] at the 1.1 km. level for their semi-theoretical model.

At the top of the inflow layer (700 mb.) the range of vertical motion inside the 40-n. mi. radius is 55 to 65 cm. sec.$^{-1}$ If most of the vertical motion takes the form of updrafts inside undilute cumulonimbus towers which cover up to 10 percent of the inner area (as suggested by Malkus and Riehl [26]), then these updrafts would reach speeds of about 10 to 16 kt. These values are considered reasonable, and are of the order frequently encountered (based on estimates by experienced hurricane reconnaissance pilots) near the eye region of mature hurricanes. Recently, Gray [14] has made some computations of small-scale vertical motions of this magnitude.

On the 11th an independent verification of the mass flow for the 120-n. mi. radius may be obtained by computing the moisture budget. The moisture equation may be written as

$$P = \oint \int_{p_o}^{p_t} v_r \, q \, ds \, \frac{dp}{g} + E - \frac{\partial M}{\partial t} \tag{8}$$

where P is the rate of precipitation, q is the mixing ratio, E is the evaporation, and M is the total moisture content inside the volume, other symbols having been defined previously. Equation (8) can be evaluated for the area inside the 120-n. mi. radius, which yields a mean precipitation value for the area. This can be compared with precipitation measurements on the 11th when the center of the cyclone was over land.

On the 11th, hourly rainfall measurements from a total of 45 recording rain gages were composited with respect to the center of the cyclone for the 12-hr. period 0000-1200 GMT. These values were plotted and then averaged over squares whose sides were 40 n. mi. The mean isohyethal pattern is shown in figure 12. The areal average for the circle with a 120-n.mi. radius was 0.17 in. hr.$^{-1}$ The rate of precipitation for the area was 183.51×10^9 m. sec.$^{-1}$ The rate computed from equation (8) was 249.76×10^9 gm. sec.$^{-1}$ The ratio of observed to computed precipitation is 0.73 (Table 1). This is considered excellent agreement, since rain gages (even when shielded) do not catch the total precipitation in high winds such as those observed in hurricanes

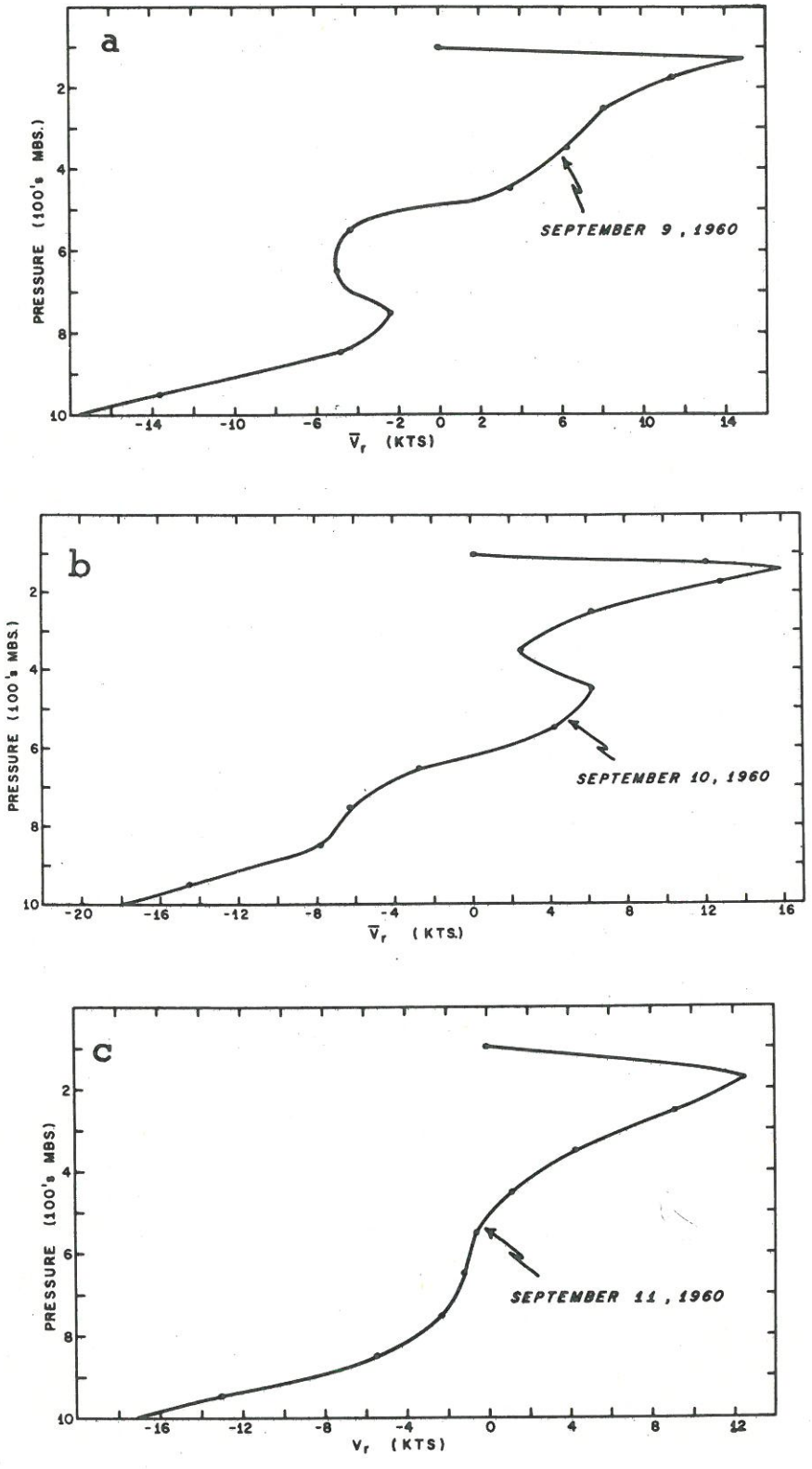

Figure 9. - Vertical profile of radial wind at 120-n.mi. radius, (a) September 9, (b) September 10, (c) September 11.

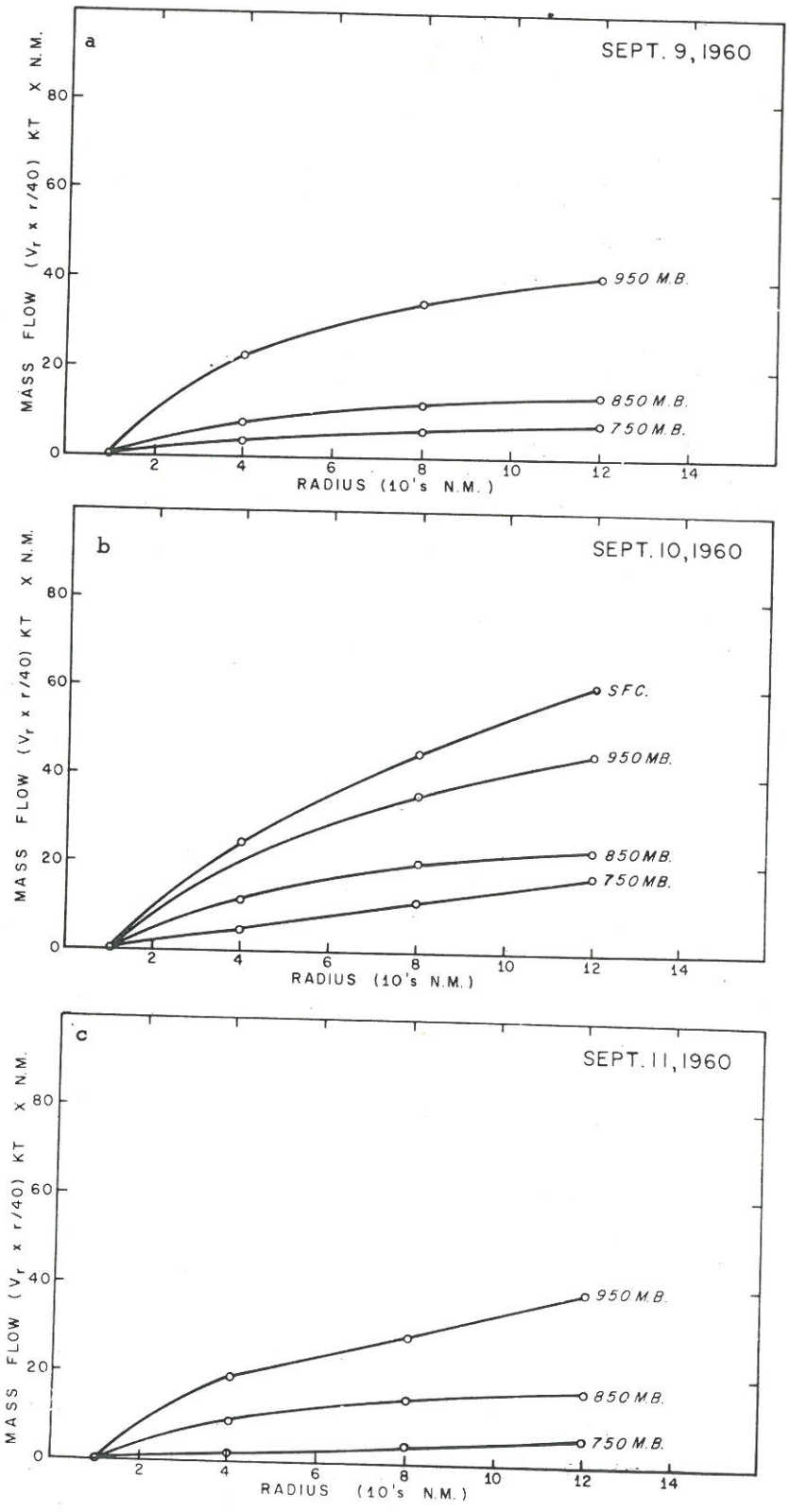

Figure 10. - Radial profile of mass flow (v_r x r/40) for the inflow layer, (a) September 9, (b) September 10, (c) September 11.

1960

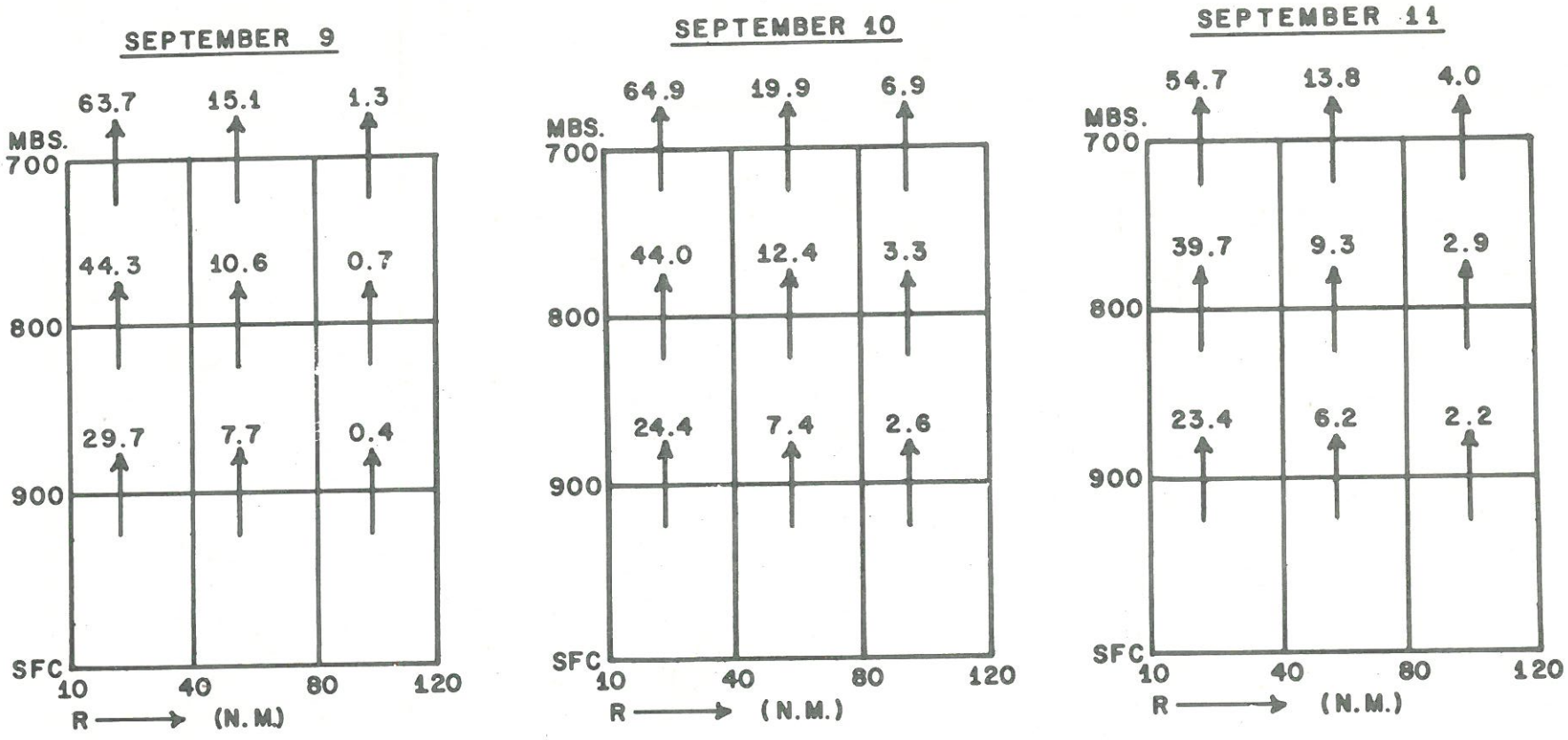

Figure 11. - Vertical motion (cm. sec.$^{-1}$) for the inflow layer. Data represent means for the radial intervals indicated.

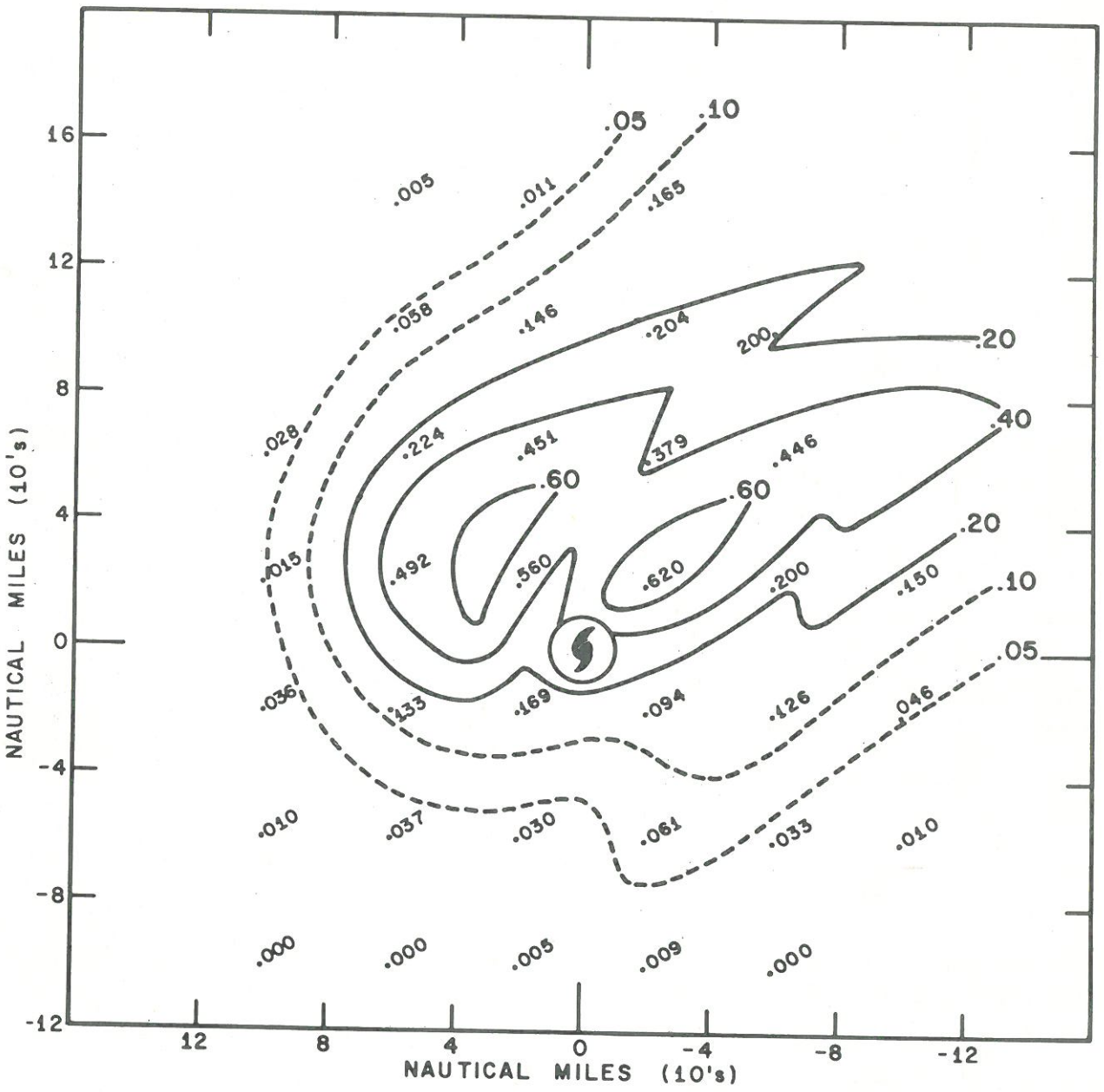

Figure 12. - A composite isohyetal pattern for the period 0000-1200 GMT September 11. Amounts are in inches per hour.

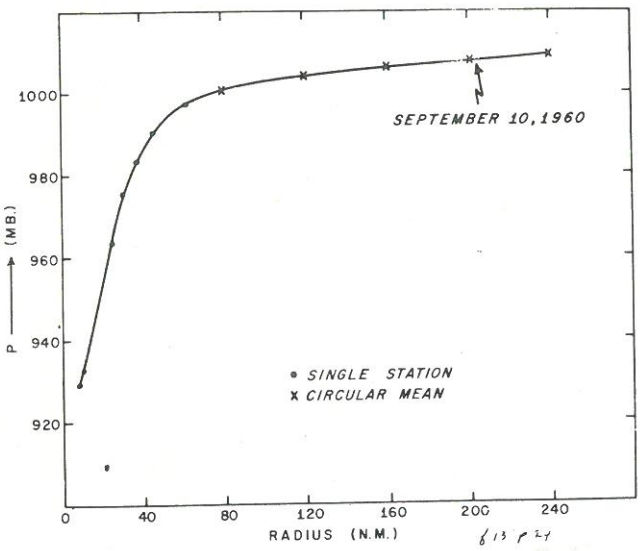

Figure 13. - Radial profile of surface pressure, 0600 GMT September 10.

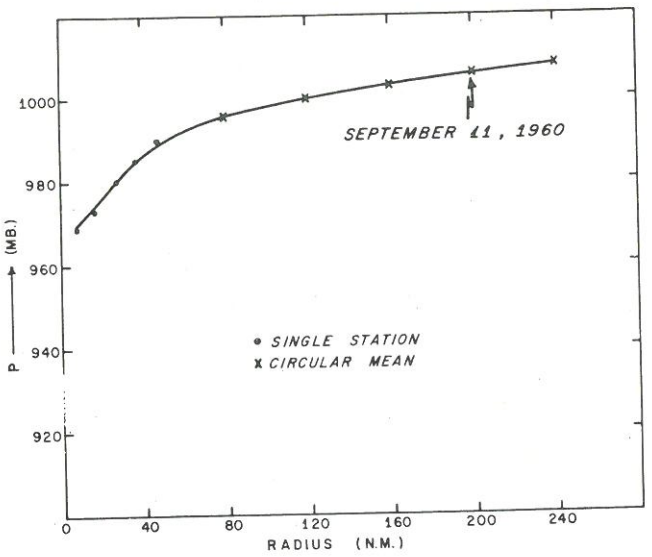

Figure 14. - Radial profile of surface pressure, 0600 GMT September 11.

Table 1. - Measured and computed precipitation (mm. $hr.^{-1}$) for the area of cyclone inside radius of 120 n. mi.

Date	Observed Precipitation	Computed Precipitation	Ratio of Observed to Computed
Sept. 11	4.3	5.9	0.73

(Miller [29]). The computed precipitation is probably more accurate than that obtained from the rain gage network.

The mass flow described by figures 9 and 10 resulted in computed precipitation rates consistent with the measured rainfall (on one day at least). The vertical motions implied by these curves seem reasonable, and the mass flow profiles are not unlike those observed in other tropical cyclones. It is apparent, therefore, that the mass flow has been described with sufficient accuracy for the purpose of computing detailed energy transformations within the cyclone.

4. STRUCTURAL CHANGES IN THE CYCLONE AFTER IT MOVED INLAND

At this point we will examine briefly the changes which occurred in the structure of the cyclone after the center moved inland and then attempt to determine the physical processes which resulted in these changes.

The most pronounced change was in the slope of the surface pressure profile. On the 10th the central pressure was about 929 mb. (fig. 13) and inside the 40- n. mi. radius we have the very steep profile typical of the intense hurricane. Outside the 40-n. mi. radius the data for figure 13 were obtained by averaging around the cyclone. Inside the 40-n. mi. radius the profile is based on the barogram of Sombrero Light Station. The observed time changes have been converted to space changes, and symmetry of the pressure distribution inside the 40-n. mi. radius has been assumed. The averaged data were for the time 0600 GMT on the 10th; the lowest pressure at Sombrero Light Station occurred near 0530 GMT. Hence, these data are synoptic.

By 0600 GMT on the 11th, the central pressure had risen by about 36 mb. (fig. 14). Figure 14 was prepared in the same manner as figure 13, except that the portion inside the 40-n. mi. radius was based on the barogram at Lakeland, Fla., where the minimum pressure occurred at about 0420 GMT. The slope of the pressure profile has decreased by a large amount. While the pressure at the center rose, the pressure outside the 40-n. mi. radius actually decreased after the center moved inland. This represents a redistribution of the mass of the cyclone during the filling process.

The streamline pattern for the low-level wind field did not change very much during the 3-day period. Figure 15a-c shows the streamline and isotach patterns for the surface to 900-mb. layer on the 9th, 10th and 11th. The streamline analysis inside a radius of about 60 n. mi. on the 9th is based on aircraft data at 1600 ft. In addition some winds at 6400 feet were used to assist in construction of the isotach pattern for this layer. On the 10th, the analysis inside a radius of 40-50 n. mi. is based on winds recorded by Lighthouse Stations located off the Florida Keys. These two analyses will be used to represent the surface wind fields in accordance with the well known fact that in tropical cyclones over the water the vertical shear of the wind is small.

On the 11th when the center was over land, it was necessary to use some surface winds to assist in the drawing of streamlines for the surface to 900-mb. layer inside the 40-50-n. mi. radius. Because of the greater vertical shear of the wind over land, however, the surface winds do not represent the true maximum wind. To obtain a reasonable estimate of the actual maximum wind over land, it was necessary to use peak gust data from gust recorders, utilizing an empirical relationship between the peak gust and the wind for the lowest 100 mb.

The mean wind for the surface to 900-mb. layer was plotted against the peak gust for rawin stations which also had gust recorders. These data are shown in figure 16. The peak gust is the highest recorded during the hour when the rawin balloon was released. In general, it will be noted that the mean wind for the surface to 900-mb. layer is about 10 to 15 percent higher than the peak gust. The best estimate of the actual maximum wind over land was taken to be the mean wind for the lowest 100 mb. The peak gust at Lakeland, which was within 8 mi. of the center of the eye, was about 78 kt. Hence, we have estimated the actual maximum wind over land (at 0600 GMT on the 11th) as 85 kt. This value is consistent with the wind profile obtained for the outer portions of the cyclone.

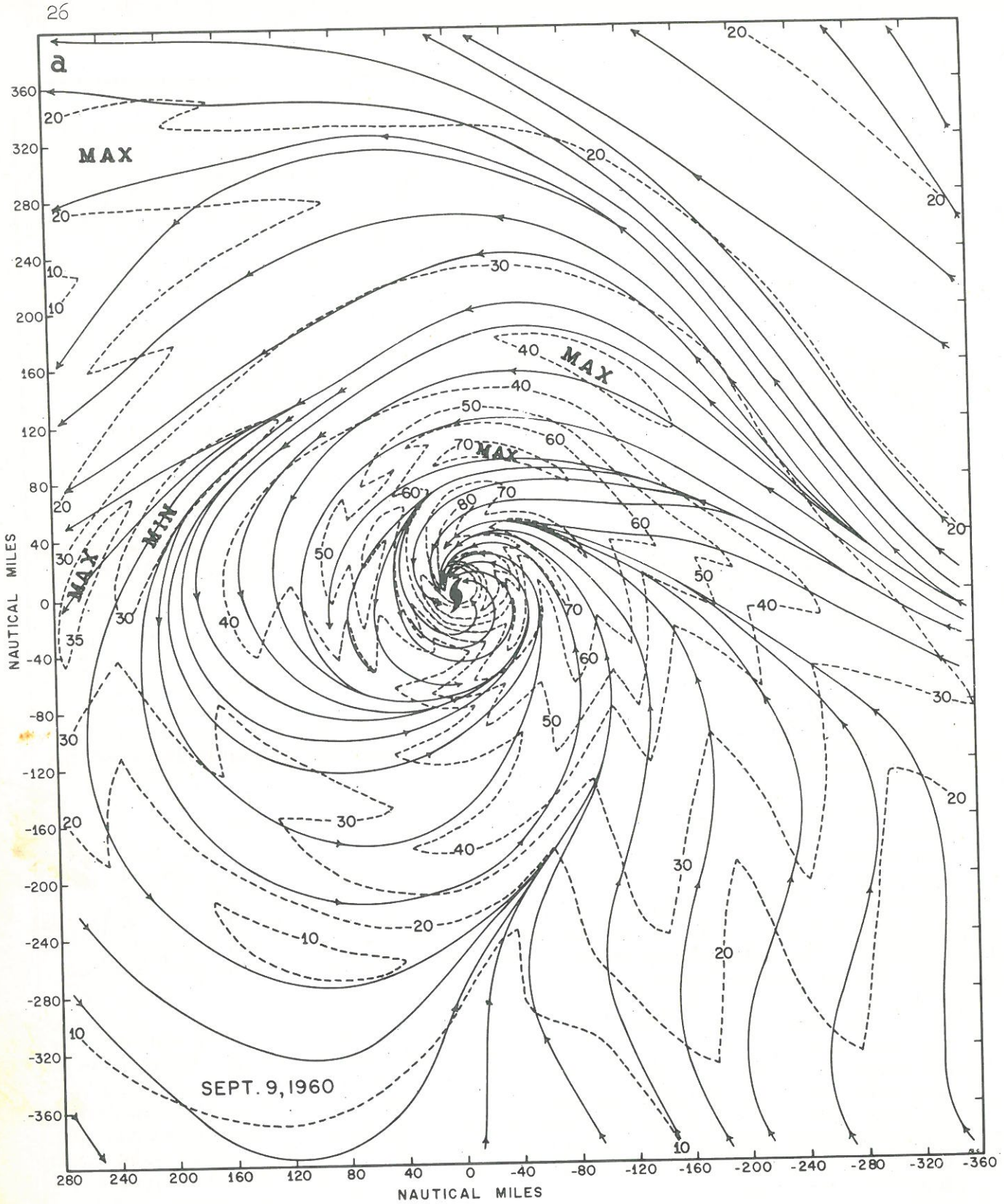

Figure 15. - Streamline-isotach analysis for the mean layer winds (surface to 900 mb.) (a) September 9, (b) September 10, (c) September 11, (d) for the layer 200-150 mb., September 10.

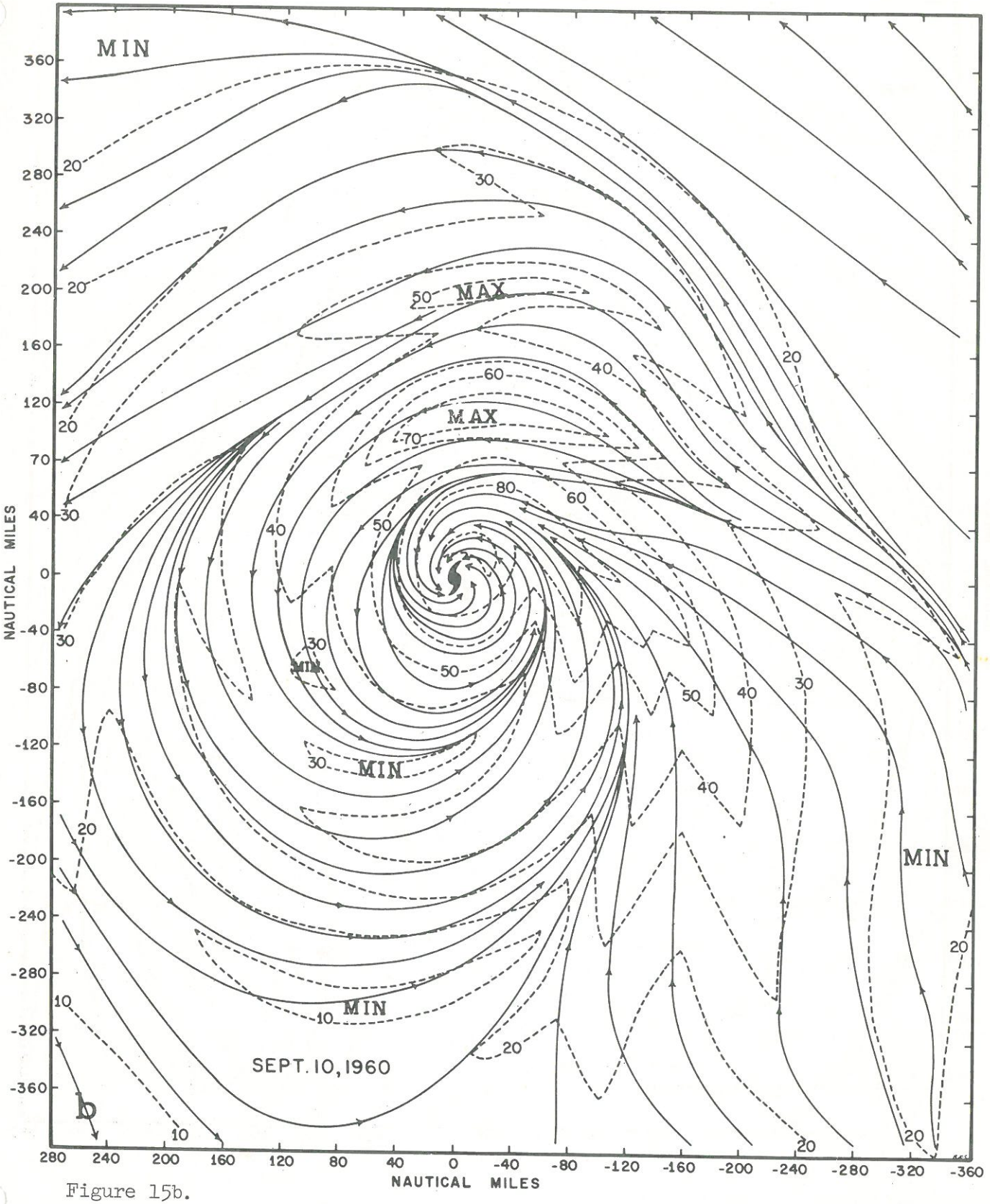
MIN
MAX
MAX
MIN
MIN
MIN
MIN
SEPT. 10, 1960
b
NAUTICAL MILES
NAUTICAL MILES
360
320
280
240
200
160
120
70
40
0
-40
-80
-120
-160
-200
-240
-280
-320
-360
280
240
200
160
120
80
40
0
-40
-80
-120
-160
-200
-240
-280
-320
-360

Figure 15b.

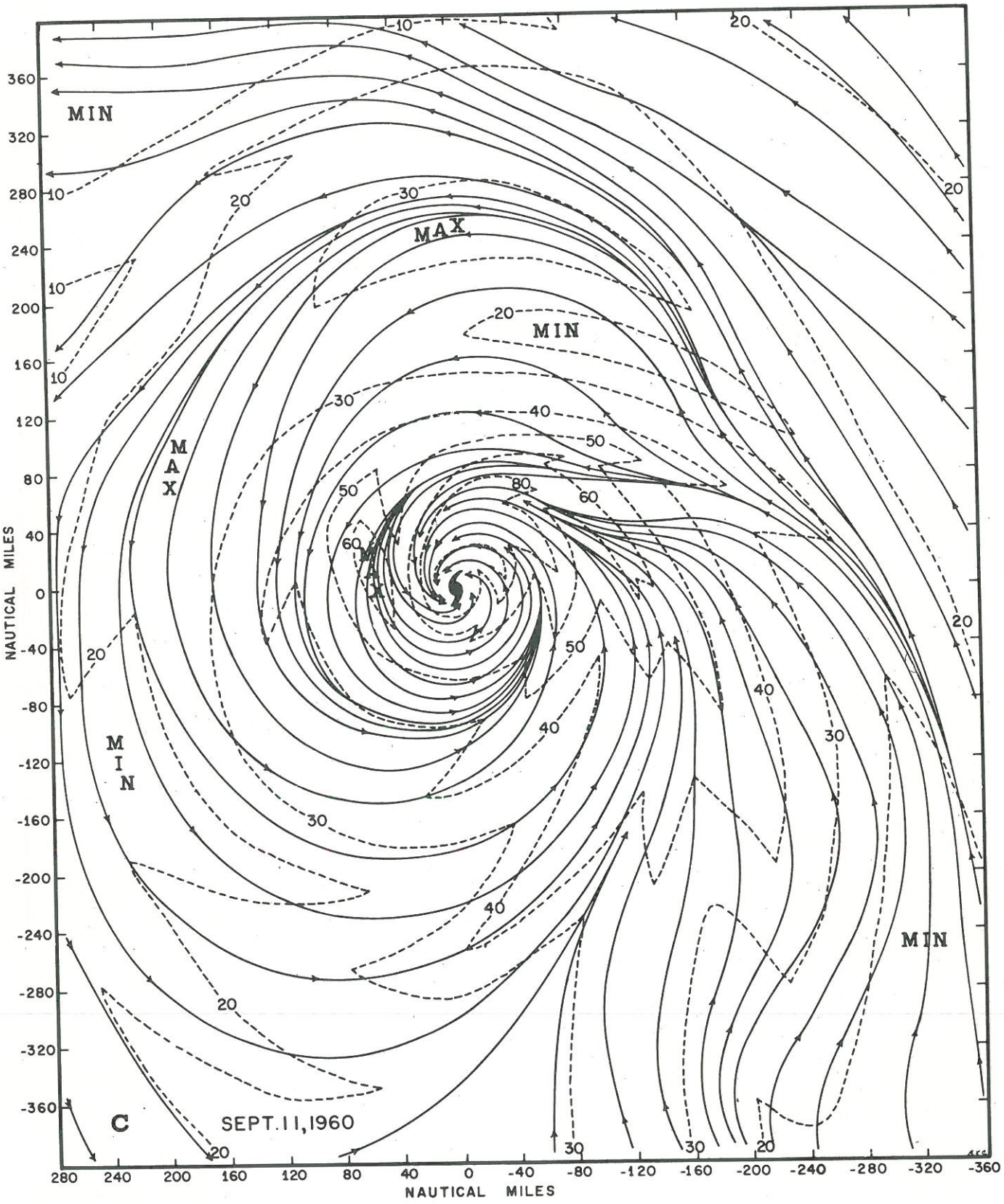
MIN
MAX
MIN
MAX
MIN
MIN
C
SEPT. 11, 1960
NAUTICAL MILES
NAUTICAL MILES

Figure 15c.

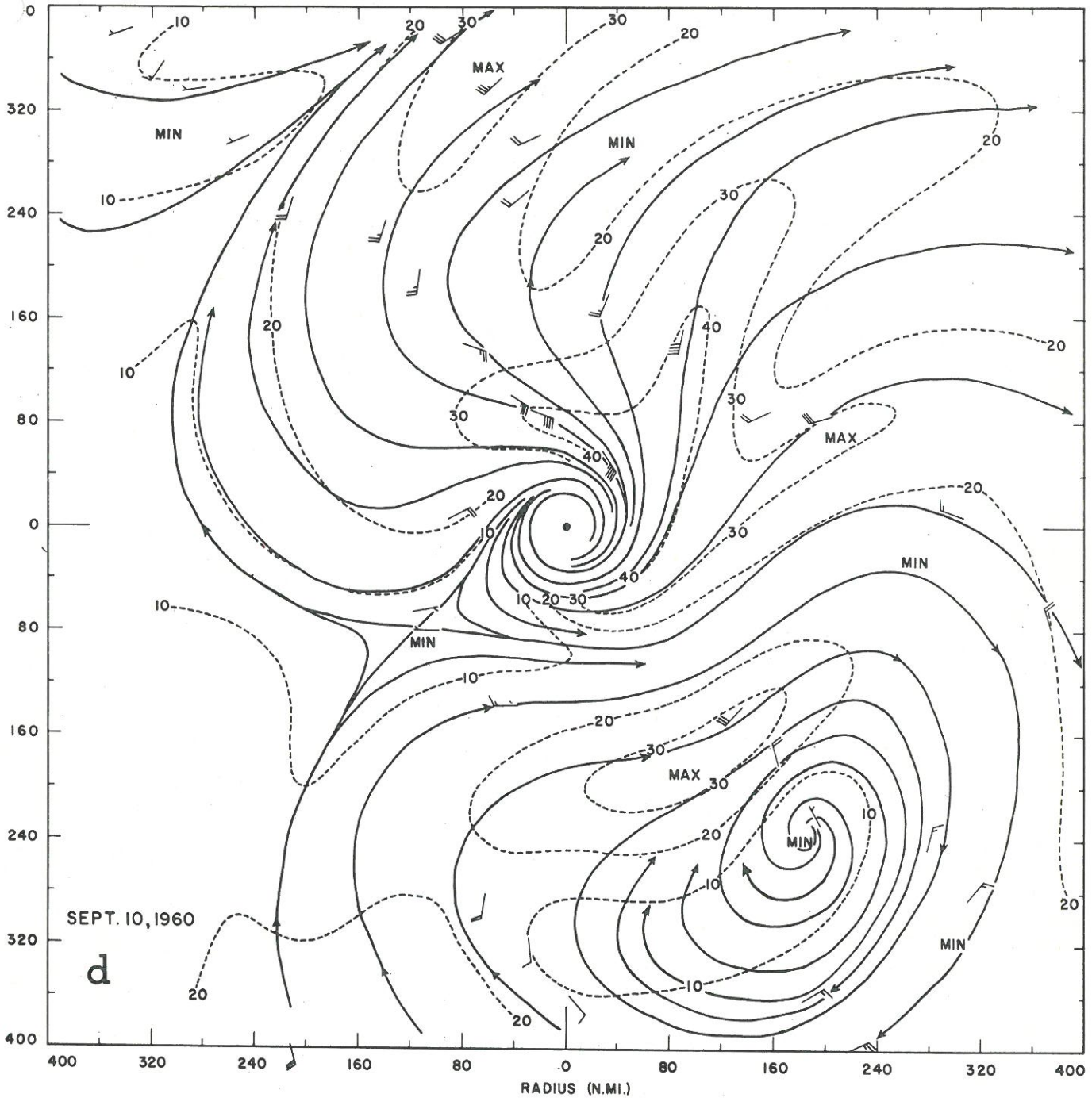

Figure 15d.

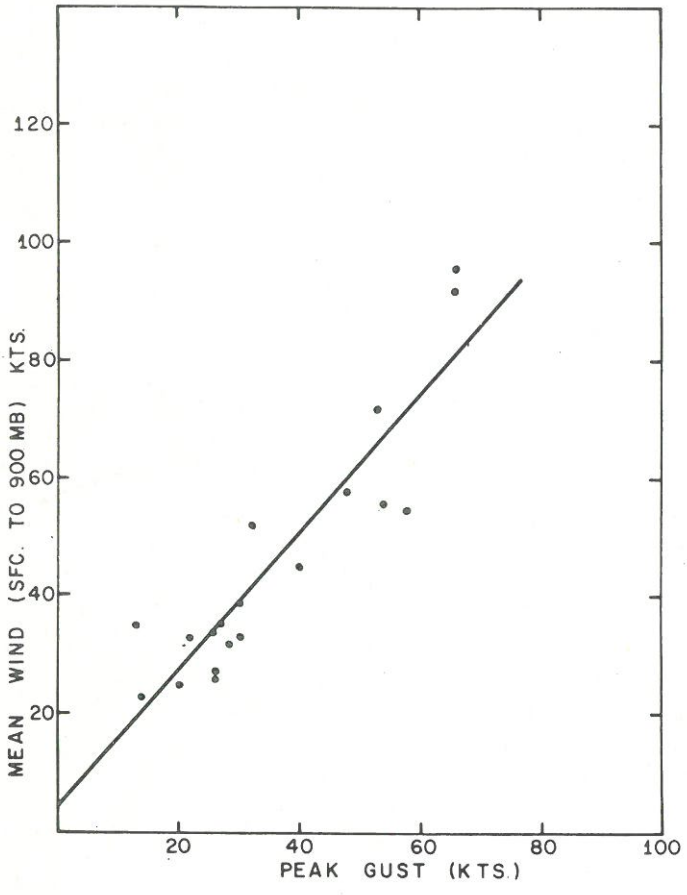

Figure 16. - Mean wind for the surface to 900-mb. layer as a function of the peak gust at the surface.

The wind speeds were averaged around the cyclone and mean wind profiles for the surface to 900-mb. layer were obtained. These are shown in figure 17a-c, plotted on a logarithmic scale. On the 9th and 10th the wind profiles are similar. On these two days the wind field is described reasonably well by a $V r^x$ = constant vortex, with x having values of 0.47 on the 9th and 0.48 on the 10th. On the 11th there is not much change in the wind profile outside the 80-n. mi. radius, but inside this radius a $V r^{0.32}$ = constant yields the line of best fit. The reasons for these changes in slope will be examined later.

The analyses for the inflow layer (fig. 15a-c) probably contain more details than can be supported by the data points shown in figure 3a-c. In regions of no data the streamline and isotach patterns were drawn to conform to typical inflow patterns found to exist in other hurricanes. Isogons were constructed for 10° intervals prior to drawing the streamlines. Some use was made of radar photographs, but this consisted only of comparing the photographs with the completed analyses to see if the confluent regions of the analyses corresponded with the rain bands. The correspondence was reasonably good.

Some of the micro-scale features implied by the analyses of figure 15a-c may be incorrect. However, it is not the purpose of this paper to

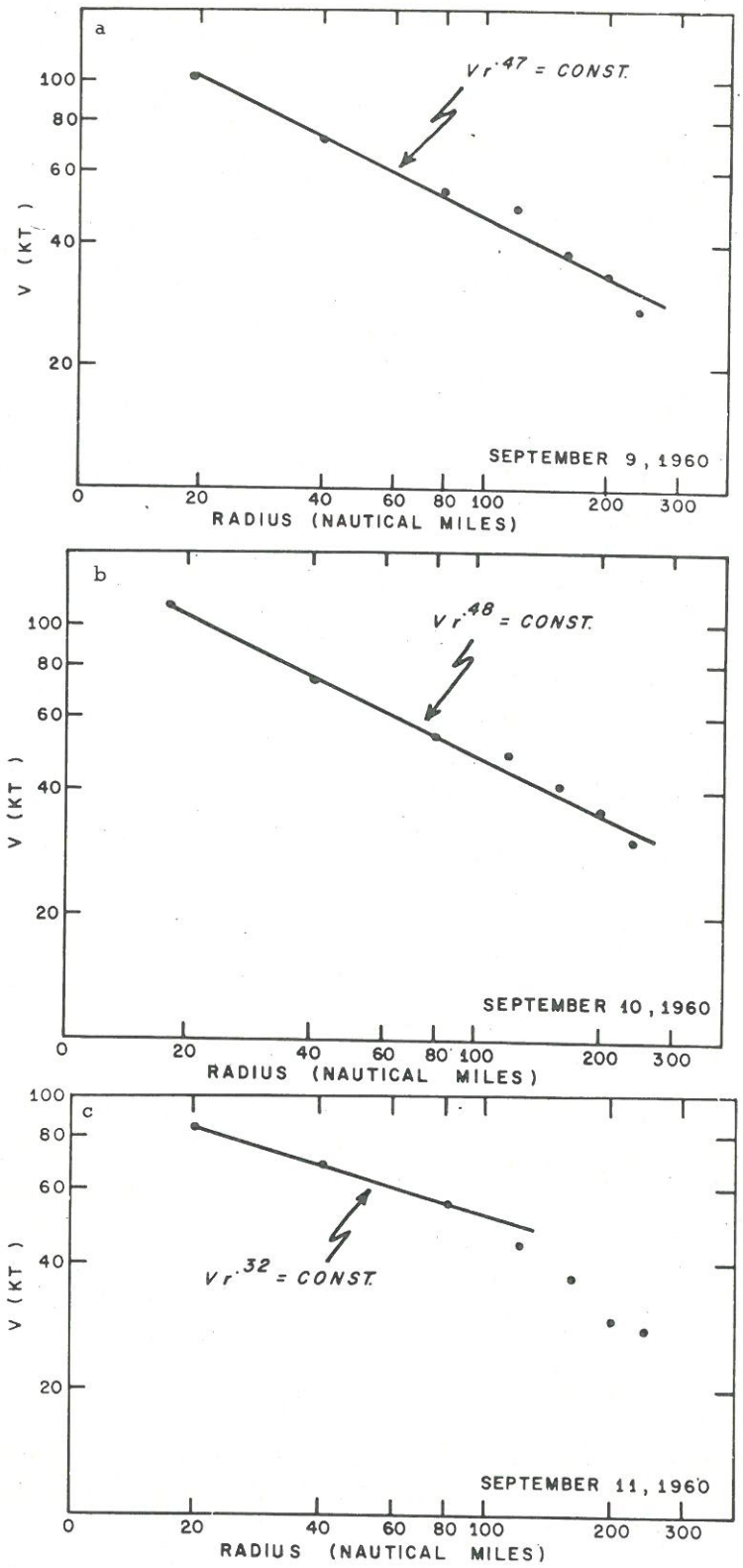

Figure 17. - Radial wind profile for the surface to 900 mb. layer (a) September 9, (b) September 10, (c) September 11.

investigate in detail the small-scale aspects of the hurricane circulation, and the description of the synoptic-scale circulation is considered to be reasonably accurate.

For the upper levels, the analyses were somewhat more difficult and uncertain, since not all rawin soundings extended to 100 mb. or above. However, some useful information could be obtained from these analyses. Figure 15d shows the analysis for the 200-150 mb. layer on the 10th. Data are inadequate to show all the features of the outflow, particularly in the southwest quadrant; however, the neutral point can be located accurately just to the southwest of the center of the cyclone.

Figure 15 d shows that most of the outflow was concentrated within the northeast quadrant. This is in conformity with visual observations of the cirrus shield made by high-level aircraft reconnaissance on the 10th. The main features of the circulation at this level on the 9th and 11th were similar to figure 15d, although the outflow was more concentrated into a single jet on the 11th.

5. THE FLUX OF ENERGY THROUGH THE LOWER BOUNDARY

a. Surface Exchange Coefficients

In any discussion of the energy flux through the lower boundary of the tropical cyclone, the problem of the proper values of the exchange coefficients to be used arises. Since these energy fluxes may be of a paramount importance to our problem, it is necessary to spend some time to obtain the best possible estimate of the exchange coefficients to be used.

We are interested in the vertical flux of momentum, latent heat, and sensible heat. The general equations for vertical flux of heat or a property (such as water vapor) are, in their classical form, similar to those for the conduction of heat in a solid (Byers, [2], p. 330). In a solid the flux of heat is given by

$$H = - k_1 \, \partial T/\partial z \qquad (9)$$

H being the flux of heat, (cal cm.$^{-2}$ sec.$^{-1}$), k_1 the thermal conductivity (cal. cm.$^{-1}$ sec.$^{-1}$ deg.$^{-1}$). and $\partial T/\partial z$ is the thermal gradient. In the atmosphere, however, the flux is achieved mainly be turbulent eddies; hence, the eddy conductivity. In addition, it is necessary to take into account the adiabatic changes in vertically moving eddies. Hence, the vertical flux of heat becomes (Priestley, [43], p. 6)

$$H = - \rho C_p K_h \, (\partial T/\partial z + \gamma_d) \qquad (10)$$

with ρ being the density of the air, c_p is the specific heat of air at constant pressure, K_h is the eddy conductivity, $\partial T/\partial z$ is the actual lapse rate, and γ_d is the dry adiabatic lapse rate.

Similar expressions may be written for evaporation and momentum. These are given by Priestley, [43], (p.6):

$$E = - \rho K_w \partial q/\partial z \tag{11}$$

$$\tau = \rho K_m \partial u/\partial z \tag{12}$$

Here E is the evaporation (gm. cm.^{2} sec.$^{-1}$) K_w is the eddy diffusivity for water vapor (cm.^{2} sec.$^{-1}$), q is the mixing ratio, τ is the stress (dynes cm.$^{-2}$), K_m is eddy viscosity (cm.^{2} sec.$^{-1}$), and u is the wind speed.

Working forms of equations (10-12) are obtained by integration between two arbitrary levels. For application over the oceans (where winds are normally measured at only one level), the upper level is chosen as the anemometer level above the ship's deck. The lower level is taken as the elevation at which the wind speed aproaches zero. This is at or near the ocean surface. Practical forms of the diffusion equations now become

$$Q_s = C_h C_p (T_s - T_a) V_o \tag{13}$$

$$Q_e = LE = L C_e (q_s - q_a) V_o \tag{14}$$

$$\tau = \rho C_d V_o^2 \tag{15}$$

where ρ is the density of the air, C_h, C_e, and C_d are nondimensional exchange coefficients for heat, evaporation, and momentum, V_o is the wind speed at anemometer level, T_s is the temperature of the water, T_a is the temperature of the air, q_s is the saturation mixing ratio corresponding to T_s, and q_a is the actual mixing ratio of the air at anemometer level.

The form and accuracy of equations (13-15) have been the subject of much discussion in the literature (Thornthwaite and Holzman [60]; Jacobs [21]; Sverdrup [55]; Deacon and Swinbank [7]; Sheppard [53]; Priestley [43]; Petterssen et al. [41]). The list could be continued indefinitely. The form of the equations is dictated largely by the fact that winds over the oceans are available at only one level. Their accuracy undoubtedly leaves much to be desired, but they have given some useful results (Jacobs [21]; Montgomery [31]; Riehl et al. [45]; Malkus and Riehl [26]; Colón [5]; Miller [30]). Equations (13-14) will be used in this paper to obtain a first approximation of the flux of latent and sensible heat from the ocean to the atmosphere.

The expression for surface stress (Taylor [58]) may not be applicable under strong wind conditions such as those found in tropical cyclones, particularly near the core. In fact, it will be shown later that C_d over water is a function of the surface wind speed, which may be interpreted as a modification of equation (15) in that stress is then no longer proportional to the square of the wind speed (assuming constant drag coefficients).

The main weakness of using these expressions to determine the vertical flux is the assumption that the various eddy coefficients are equal. This equality implies that not only are the vertical profiles of wind, temperature,

and moisture similar in shape but also that the physical processes responsible for turbulent diffusion of these elements are similar (Priestley [43], p. 93). There is no valid reason to suppose that the physical processes are similar. There is definite knowledge that the orders of magnitude of the eddy coefficients are the same. It is, therefore, convenient and justifiable to assume that these eddy coefficients are equal.

The ratio of eddy conductivity to eddy viscosity (K_h/K_m) is a function of the atmospheric stability. One can find in the literature evidence that it is either 1, greater than 1, or less than 1. During the past few years, however, there is increasing evidence that the ratio varies inversely as the stability. Priestley ([43], p. 9) quotes a correlation coefficient of -0.81 between K_h/K_m and the flux form of the Richardson number, which is defined as

$$R_f = - \frac{gH}{C_p T \rho (\partial u/\partial z)} \qquad (16)$$

Priestley also presents some observational data which show that for a value of R_f near -0.5, the ratio of K_h/K_m may reach a value of 3.0. Swinbank [57] found a correlation of -0.52 between K_h/K_m and the gradient form of the Richardson number, which is

$$R_i = \frac{g}{\theta} \frac{\partial\theta/\partial z}{(\partial u/\partial z)^2} \qquad (17)$$

Priestley says that the correlation of -0.81 is likely to be too high while that of -0.52 is too low, but that the physical reality of the dependence of the ratio on stability is not in doubt.

There is considerable (though not universal) agreement that for neutral stability the ratio of K_h/K_m is about 1.2 to 1.3 (Taylor [59]; Ellison [12]; Panofsky et al. [38]; Miller [30]). These values are also confirmed by laboratory experiments (Hinze [18], pp. 537 ff.). As instability increases, the ratio increases. Ellison suggests that there is an upper limiting value. Taylor [59] used some observational data by Rider and computed a value of 1.67 under free convection, whereas using Swinbank's data he obtained a value of 1.35. Ellison suggested a value of 1.6 for free convection, consistent with the higher value obtained by Taylor.

Tests have also been made to determine the ratio of K_w/K_m. Deacon and Swinbank [7] measured surface stress and evaporation, then calculated evaporation on the assumption that K_w and K_m are equal. The ratio of E (observed) / E (calculated) was $1.04 \pm .09$; this value gives the ratio of K_w/K_m. Rider [44] obtained a value of 1.12 ± 0.04. These values indicate an approximate equality between eddy viscosity and eddy diffusivity.

In this paper, we will use drag coefficients instead of the eddy coefficients. The drag coefficients are a function of surface roughness and static stability. The ratio between C_h/C_d is equal to K_h/K_m, and C_e/C_d to K_w/K_m. Over water the roughness is itself a function of the wind speed,

which makes the determination of C_d somewhat difficult, as a survey of the literature will reveal. Much uncertainty as to the manner of its dependence on wind speed exists. The difficulties involved in determining C_e and C_h over water are even greater. As a result it has been assumed that the best first approximation to the various vertical fluxes can be obtained by making the simple assumption that $C_d = C_h = C_e$.

About the earliest recorded determination of C_d over water was by Colding [4] who obtained a value of 2.6×10^{-3} for winds ranging from about 10 to 30 m.p.s. He determined C_d from the slope of the surface of the Baltic Sea. In 1905 Ekman [11] used the same technique and obtained a value of 2.5×10^{-3} for "strong" winds. Later Rossby and Montgomery [50] used Wüst's [62] wind profile measurements over the Baltic and found that the roughness length was 0.6 cm., which is also equivalent to a C_d (at 15 m. elevation) of 2.5×10^{-3}. Then Rossby [51] developed a technique for computing the roughness length from the angle between the actual wind and the gradient wind, and concluded that the roughness length was independent of the wind speed, confirming the earlier value of 0.6 cm.

Palmén and Laurila [36] determined the stress over the Gulf of Bothnia from the slope of the water surface, obtaining a value of 2.4×10^{-3} for C_d. They considered this value applicable for winds 10 to 26 m.p.s. Sheppard and Omar [52] computed surface stress from pilot balloon observations in the trade wind region by using the approach to the geostrophic wind. They obtained values ranging from 1.0 to 1.5×10^{-3} for winds of 3 to 12 m.p.s. Hay [17] measured the wind at five elevations over the sea and computed the drag coefficient from the wind profile. His values were 1.5 to 2.6×10^{-3} for winds of 6 to 12 m.p.s. Hay's data showed an almost linear variation of C_d when plotted against wind speed.

Darbyshire and Darbyshire [6] used the wind-produced tilt of Lough Neagh to compute C_d, obtaining for all data a range of 1.37 to 2.47×10^{-3} (winds up to 13 m.p.s.). When days were grouped according to atmospheric stability, the unstable days showed values of C_d about twice those for stable days. Lough Neagh ranges in depth from 6 to 12 m. and bottom friction was neglected by the Darbyshires.

Deacon, Sheppard, and Webb [8] computed C_d from wind profile data and obtained 1.0 to 2.8×10^{-3} (winds 5 to 14 m.p.s.), but the increase did not seem to be linear as indicated by the Hay data. From a mean of 466 double theodolite observations at Anegada in the Virgin Islands, Charnock, Francis, and Sheppard [3] calculated a value of 1.24×10^{-3} for a mean wind speed of 5 m.p.s.

Many of the over water values for C_d in the literature show an increase with increasing wind speed. However, Neumann [33] claims that C_d decreases with increasing wind speed. He has presented observational data from which he has derived the statistical relationship,

$$C_d = 9 \times 10^{-3} \left(\frac{1}{V} \right)^{1/2} \qquad (18)$$

where V is in m. $sec.^{-1}$, which indicates a decrease from 9×10^{-3} at 1 m.p.s. to less than 2×10^{-3} at 25 m.p.s. Deacon [9] has challenged Neumann's results, but the matter is not resolved.

Sverdrup [56] summarized the available computations of C_d over water. There is much scatter, but the data may indicate some sort of parabolic distribution, with C_d reaching a minimum near winds of 6 m.p.s., then gradually increasing to about 3.3×10^{-3} at winds of 25 m.p.s. and above. Wilson [61] collected computations from 46 different sources and attempted to adjust all values of C_d to a standard height of 10 m. He then divided the results into "light" and "strong" winds. For strong winds the drag coefficient ranged from 1.5 to 4.0×10^{-3}, with a mean of 2.37×10^{-3}, and a standard deviation of 0.56×10^{-3}, which is an acceptable variation. For light winds the mean was 1.49×10^{-3} and the standard deviation 0.83×10^{-3}, which is much less satisfactory, and probably indicates that part of the scatter is due to the difficulty of accurately measuring the vertical wind profile when the winds are light.

For winds of hurricane force there are almost no estimates of the drag coefficient. Palmén and Riehl [37] used composite wind data compiled by E. Jordan [22] and Hughes [20] to calculate C_d. They obtained a range of 1.1 to 2.2×10^{-3} for winds of about 6 to 26 m.p.s. Miller [30] computed C_d for hurricane Helene, using aircraft data from which he prepared an angular momentum budget, and obtained values for C_d of 2.4 to 3.2×10^{-3} for the 30 m.p.s. to 40 m.p.s. range. The latter results represent an almost linear extension of the Palmen-Riehl data.

For use in making the Donna calculations, C_d was determined by integrating the tangential equation of motion vertically from the surface to the top of the inflow layer. In a cylindrical coordinate system, with the radius, r, and radial velocity, V_r, positive outward, the polar angle, θ, and the tangential velocity, V_θ, positive in a cyclonic sense, and the height, z, and the vertical motion, w, positive upward, the tangential equation of motion is

$$\frac{dv_\theta}{dt} = -\frac{1}{\rho}\frac{\partial p}{r\partial\theta} - fv_r - \frac{v_r v_\theta}{r} + \frac{1}{\rho}\left(\frac{\partial \tau_{\theta\theta}}{r\partial\theta} + \frac{\partial \tau_{\theta r}}{\partial r} + \frac{\partial \tau_{\theta z}}{\partial z}\right) \qquad (19)$$

where p is the pressure, f is the Coriolis parameter, and the τ's are shearing stresses. Other terms have already been defined.

By assuming (1) steady state, (2) that the tangential pressure gradient is negligible, and (3) that lateral mixing of momentum is small, equation (19) may be written

$$\frac{\partial \tau_{\theta z}}{\partial z} = \rho v_r \zeta_a + \rho w \frac{\partial v_\theta}{\partial z} \qquad (20)$$

where ζ_a is the absolute vorticity of the tangential wind. Assumptions (1) and (2) are probably not bad in most mature tropical cyclones (Malkus and Riehl [27]; Rosenthal [49]) but assumption (3) may be less valid. Some of the calculations to be presented in later sections indicate that the lateral

transfer of momentum is quite large near the eye. Such transfer, however, cannot be evaluated with sufficient accuracy to be included here.

Equation (20) can be integrated from the surface to the top of the inflow layer, at which level it is assumed that the shearing stress vanishes. This integration gives

$$\tau_{\theta_o} = \int_{p_o}^{p_h} v_r \zeta_a \frac{dp}{g} + \int_{p_o}^{p_h} w \frac{\partial v_\theta}{\partial z} \frac{dp}{g} \qquad (21)$$

Palmen and Riehl [37] also used equation (21) to estimate the surface stress by using the mean data compiled by Hughes [20] and E. Jordan [22]. They neglected the second term, but applied the integration to the area outside the 120 n. mi. radius only. In this area the cyclone is very nearly non-divergent, so that the omission of the second integral is more exact. Since we are dealing almost exclusively with the region inside the 120 n. mi. radius, we cannot restrict computations to the non-divergent portion of the cyclone. The second integral cannot be evaluated with the data available, however, and must be omitted here also.

Obviously the magnitude of the error introduced by omitting the second integral cannot be determined. Rosenthal [49] has estimated that the second integral is normally less than 10 percent of the first integral, since near the surface where the vertical wind shear is large the vertical motion is negligible, and near the top of the inflow layer where the vertical motion is large the vertical shear is small. This is almost certainly true for mean profiles. If most of the vertical ascent occurs within a few large cumulonimbus towers, the integration of $\int w \, (\partial v_\theta / \partial z)$ becomes more difficult. In any event it probably represents only a small correction to the results obtained by evaluation of the first integral. Consequently, the surface stress was evaluated from the first integral on the right of equation (21).

Calculations of the surface stresses were made for each of the three days at several radii as shown in table 2. The mass flow from figure 10 was used and the vorticity was computed from the winds shown in figure 15. It was assumed that the vorticity was almost constant with height through the inflow layer, so that

$$\widehat{v_r \zeta_a} = \widehat{v_r} \, \widehat{\zeta_a} \qquad (22)$$

where $\widehat{\ }$ indicates the vertical mean. The vorticity of the surface to 900-mb. layer was used to represent the vertically averaged vorticity. Now with sufficient accuracy for these calculations we may write

$$\tau_{\theta_o} = \frac{\widehat{v_r} \, \widehat{\zeta_a} \, (p_h - p_o)}{g} \qquad (23)$$

where p_h is the pressure at the top of the inflow layer and p_o is the surface pressure. After obtaining the surface stress, C_d was calculated by using

equation (15). The surface wind (V_o) was obtained by integrating around the cyclone. The data of figure 15 were used for the 9th and 10th, but for the 11th the vertical shear was too great to permit the use of the mean wind for the surface to 900-mb. layer. Hence the data from figure 27 were used. The results of the calculations are shown in table 2.

Table 2. - Surface stresses and drag coefficients computed by integration of tangential equation of motion through inflow layer, hurricane Donna, Sept. 1960.

Date	Radius (n.mi)	Surface stress (dynes/cm.^{2})	Surface wind V_o (m.p.s.)	Drag coefficient C_d (x 10^3)
9	40	54.00	36.0	3.60
9	80	23.16	27.8	2.61
9	120	11.88	25.2	1.63
9	160	6.39	19.0	1.54
9	200	5.56	17.3	1.62
10	20	130.04	52.0	4.19
10	30	89.04	43.8	4.03
10	40	59.74	38.0	3.60
10	80	30.56	28.3	3.33
10	120	19.25	25.2	2.64
11	40	62.72	24.2	8.73
11	80	34.75	20.0	7.37
11	120	11.76	17.0	3.54

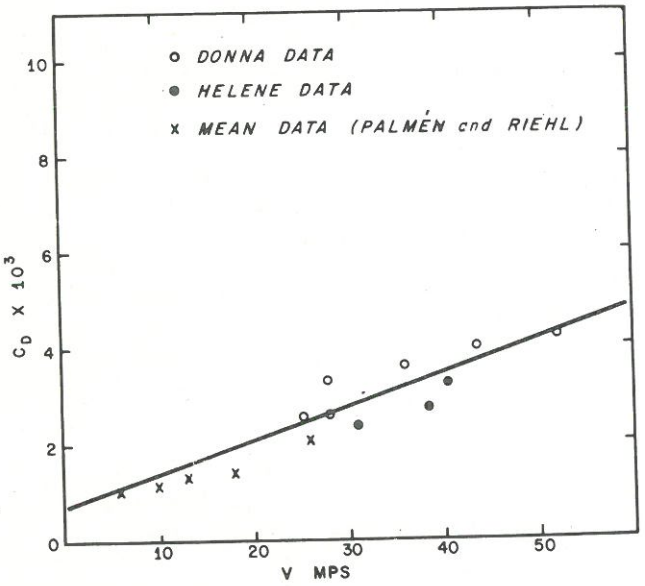

Figure 18. - Drag coefficient (C_d) as a function of wind speed.

The coefficients in table 2 represent means since both v_r and ζ_a were integrated around the cyclone as well as vertically. On the 9th and 10th the cyclone was over water and the results should be comparable to the Palmén-Riehl and Helene calculations, although at radii greater than 80 n. mi. portions of the cyclone were over land on both days. The greater roughness over land undoubtedly has some influence on the results shown in table 2. Figure 18 shows a plot of the drag coefficients against wind speed; the Palmén-Riehl and Helene calculations have been added to the Donna data for the 9th and 10th. It is clear that there is reasonable agreement between the Donna calculations and earlier results.

It should be emphasized that these drag coefficients are means for the radii shown in table 2. Over water, they probably represent reasonably well the local drag coefficients also, since the roughness of the water is a function of the wind speed (though not necessarily of the local wind speed). Over land, however, variations in the surface roughness may be significant. Consequently, the drag coefficients can only be used as means, and cannot be used at the individual stations.

Without wind measurements at more than one level, the roughness lengths at the various surface observations cannot be determined. However, some crude attempts were made to determine the roughness lengths at Key West, Tampa, Miami, and Jacksonville by comparing the wind at anemometer level with the mean wind for the first minute of rawin balloon ascent. This assumes that the logarithmic wind profile is valid from the surface up to the level reached by the sounding balloon at the end of 1 minute; i.e., up to levels of 250-300 m. This assumption is invalid unless the wind is near hurricane force. While the roughness lengths may vary by as much as a factor of two or three, the crudeness of the calculation did not permit one to analyze any fictitious divergences or material accelerations caused by different roughnesses. Hence, no attempts were made to apply any corrections to the trajectories which will be described in a later section.

b. Lagrangian Exchange Coefficients for Heat and Moisture

The calculation of the exchange coefficients for heat and moisture can best be approached in a different way; this involves the computation of the Lagrangian exchange coefficients as described by Malkus and Riehl [26]. The object in making the Lagrangian computations is to compare the heat flux from the underlying surface to the air while the center was over land with the heat flux while the center was over water.

The first law of thermodynamics

$$\delta H = C_p dT - \alpha dp \qquad (24)$$

can be integrated along a trajectory only if the temperature is constant. The integral $\int(\delta H/\delta t)\, dt$, depends upon the path on a thermodynamic diagram, but if the temperature is constant, the path is a simple one, and there is only one way of getting from the initial to the final state. Over land, however, the motion was not isothermal, and as a result an approximate integration must be used. This takes the form (Haltiner and Martin [15], p. 16)

$$H = C_p (T_2 - T_1) + R\bar{T} \ln p_1/p_2 \qquad (25)$$

where $\bar{T}$ is the mean temperature. Equation (25) may be used to approximate the heat transfer along a trajectory, assuming essentially horizontal motion.

We now use the Malkus-Riehl equations for the transfer of sensible and latent heat from the ocean to the air. These are

$$Q_{sp} = K_{sp} (T_s - T_a) V \qquad (26)$$

and

$$Q_{ep} - K_{ep} (e_s - e_a) V \qquad (27)$$

in which Q_{sp} and Q_{ep} are the sensible and latent heat transfer following the motion of a particle, K_{sp} and K_{ep} are the respective Lagrangian exchange coefficients, T_s and e_s are the temperature and the saturation vapor pressure of the underlying surface, T_a and e_a are the actual temperatures and vapor pressure for the air. $\int Q_{sp} dt = H_{s2} - H_{s1}$, and similarly $\int Q_{ep} dt = H_{e2} - H_{e1}$, where H_e designates the latent heat content along the trajectory. These expressions may now be integrated, and combined with (26) and (27) to obtain the exchange coefficients. This gives

$$K_{sp} = \frac{H_{s2} - H_{s1}}{D(T_s - \bar{T}_a)} \qquad (28)$$

$$K_{ep} = \frac{H_{e2} - H_{e1}}{D(e_s - e_a)} \qquad (29)$$

where D is the length of the trajectory. It should be noted that Q_{sp} and Q_{ep} are in cal. gm.$^{-1}$ sec.$^{-1}$, and that K_{sp} has the dimensions of cal. gm.$^{-1}$ cm.$^{-1}$ deg.$^{-1}$, and that K_{ep} has the dimensions cal. gm.$^{-1}$ cm.$^{-1}$ mb.$^{-1}$

Prior to calculating the Lagrangian exchange coefficients, it was neccesary to determine the quantities $(T_s - T_a)$ and $(e_s - e_a)$. Since there were not many ship reports inside the area of interest (within 120 n. mi. or less of the center of the cyclone), this required some extrapolation of available data.

Water temperatures were composited for the 2-day period, September 7 and 8, in order to obtain some idea as to the sea surface temperatures prevailing within the area prior to the passage of the cyclone. These data are shown in figure 19. These were averaged by 5° "squares", and it was found that the average temperature in the area over which Donna was to pass on the 9-11th was about 29.0° to 29.5°C, which is near or slightly above the climatological average for September. Water temperatures were also plotted for the 9th, 10th, and 11th (four map times on one chart). These are shown in figures 20-22. There is some slight indication of cooling of the water

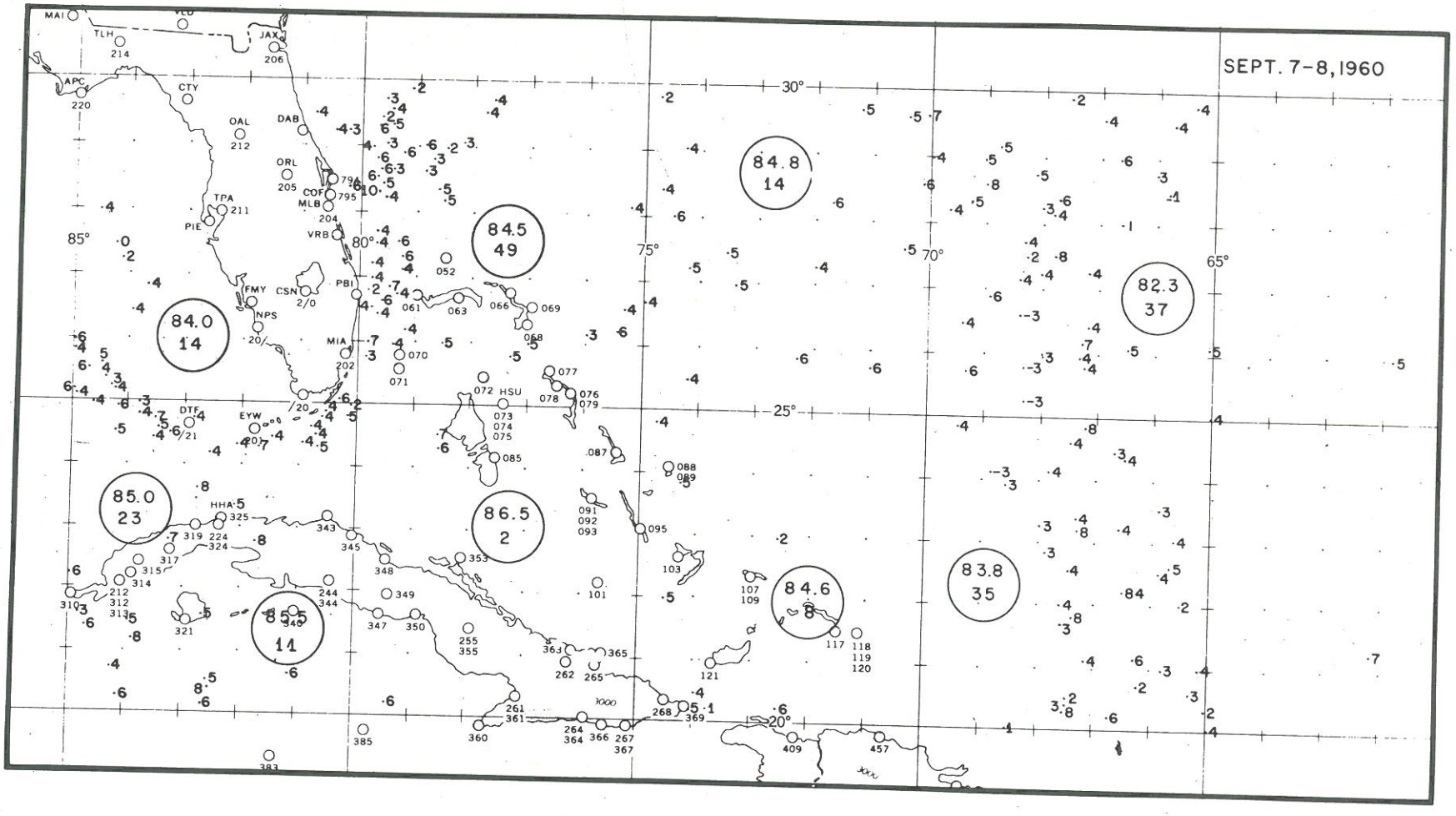

Figure 19. - Sea water temperatures in the vicinity of hurricane Donna, September 7-8. Values are in departures from 80°F. Circled numbers are means and the number of observations per 5° square (except for the square divided by western Cuba where these refer to the indicated area to the north and south of Cuba)

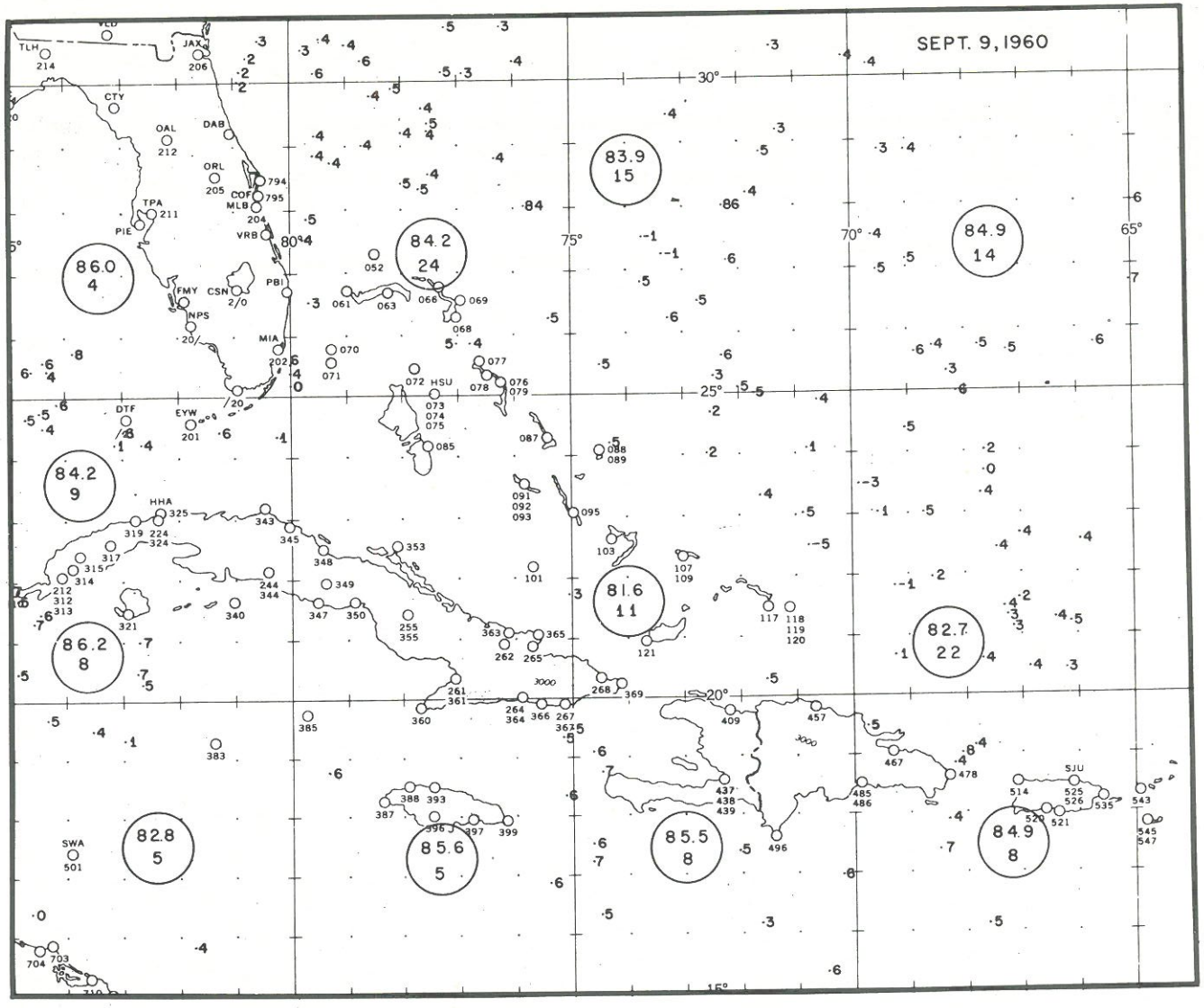

Figure 20. - Sea water temperatures in the vicinity of hurricane Donna, September 9.

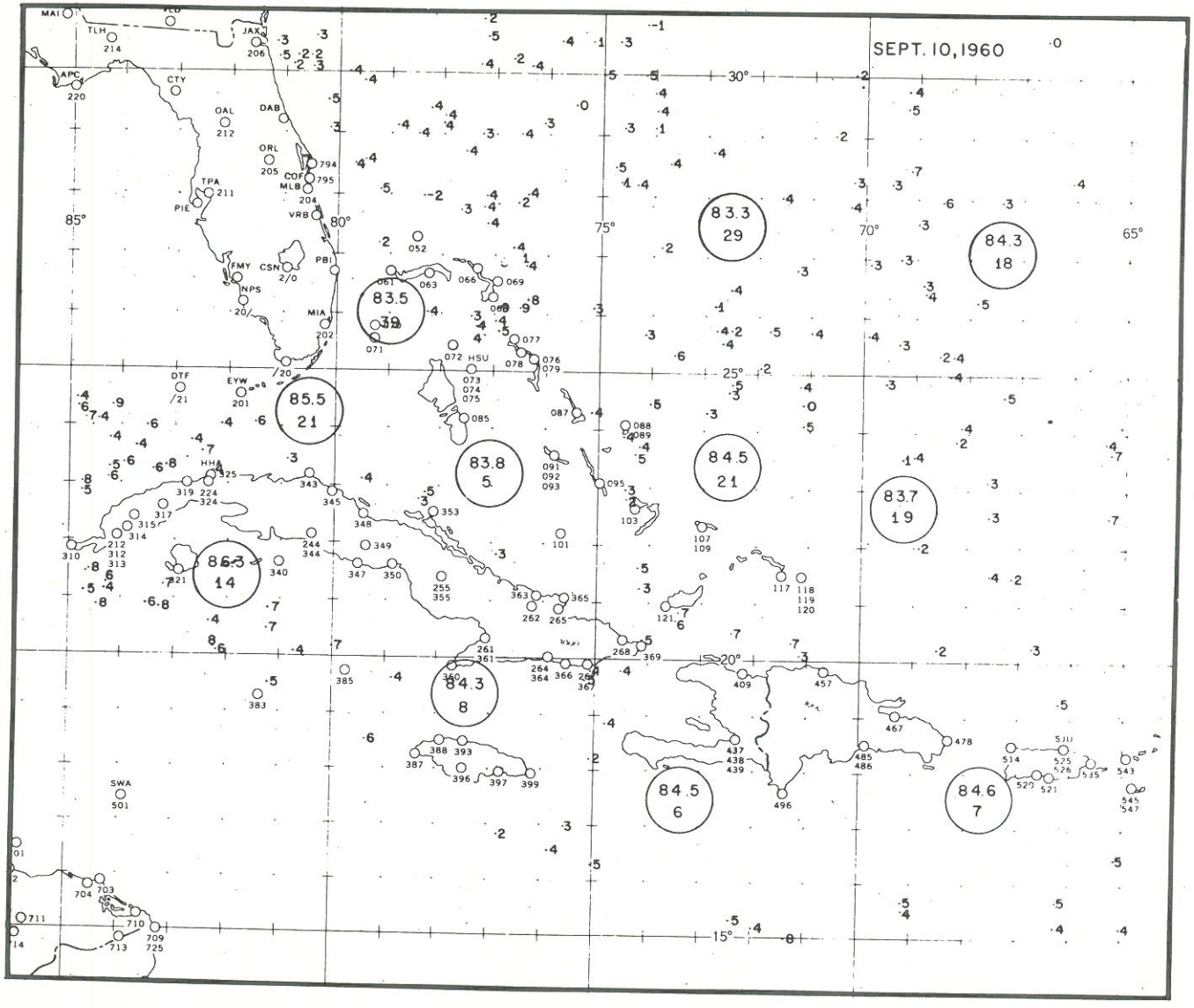

Figure 21. - Sea water temperatures in the vicinity of hurricane Donna, September 10.

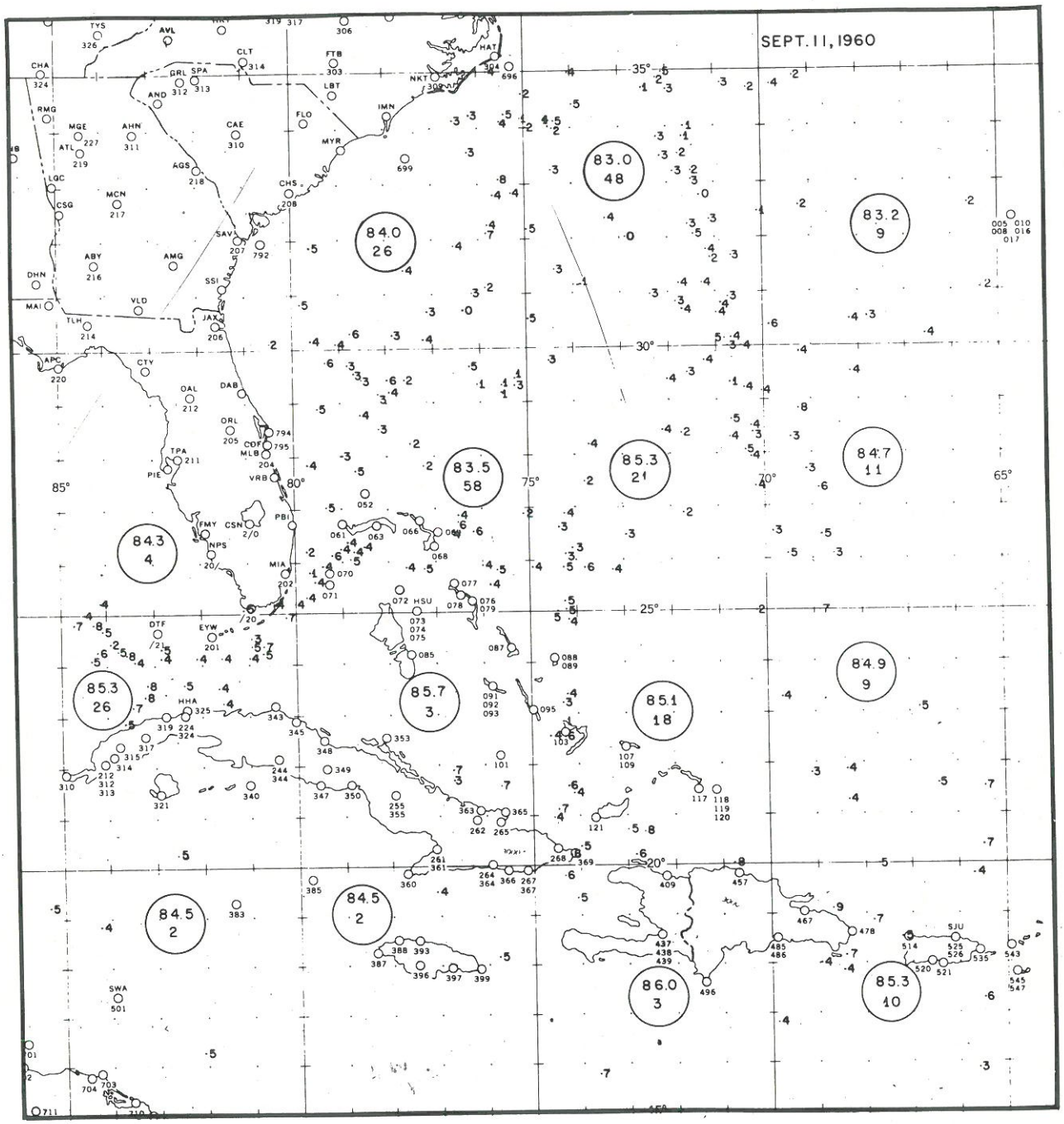

Figure 22. - Sea water temperatures in the vicinity of hurricane Donna, September 11.

after the passage of the cyclone. See figure 20 in the area just to the north of Haiti. Here on the 9th the average water temperature was 81.6°F. (based on 11 observations), compared to an average of 84.6°F. (8 observations) for the same area on the 7th and 8th. This cooling of the water after the passage of the cyclone is not unexpected and has been observed before (Fisher [13] Pike [42]). It is probably due to a combination of (1) removal of sensible heat by the cyclone, (2) upwelling, (3) the mixing with several inches of rain water which is somewhat colder than the sea surface temperature, (4) reduced sunshine due to heavy clouds, and (5) mixing within the ocean.

We will primarily be concerned with the area inside 120 n. mi. radius of the center of the cyclone. The available data are not good enough to permit exact determination of the average sea surface temperatures inside this area. The data do suggest a gradual transition from about 29.0°C. in the forward half of the cyclone to near 27.0°C. to the rear. Accordingly, these values will be used to compute latent and sensible heat transfers on the 9th and 10th. On the 11th, the rear of the cyclone was mostly over land, and since heat transfer occurred mostly in the front half on this day, an average of 29.0°C. will be used.

Temperatures and dew points were also plotted for the two compositing periods (0000-1200 GMT) on the 9th and 10th. These are shown in figures 23 and 24. The average surface air temperature within the 40-120 n. mi. area was about 26.0°C, while the average from 10 dropsonde observations in or near the eye between the hours of 0000 GMT and 1310 GMT on the 9th and 10th was 27.0°C. The corresponding average dew point temperature from these dropsondes was 25.8°C. These data are consistent with an estimate of a surface air temperature of 26.0°C. in the wall cloud region on the 9th and 10th. Hence, this value was used, which gives an average air-sea temperature difference of 3.0°C. in the forward half of the cyclone and 1.0°C. in the rear portion. The areal average was about 2.0°C. which is consistent with estimates for other cyclones in the Atlantic area (Malkus and Riehl [27]; Miller [30]).

Dew point temperatures were even less plentiful than surface air temperatures. The average on the 9th and 10th at 120 n. mi. was about 24.0°C.; this increased to about 25.8°C. in or near the eye. These data were used to compute the quantity $(e_s - e_a)$, which has already been defined.

Over land on the 11th, hourly surface charts were prepared. The density of surface data was great enough so that the determination of temperatures and dew points at the beginning and terminal points of the trajectories did not present any great problems.

The object in making the Lagrangian exchange computations is to compare the heat flux from the underlying surface to the air while the center of the cyclone was over land with the heat flux while the center was over water. Four trajectories were prepared from composite surface data when the cyclone was over the ocean on the 10th. These are shown in figure 25. Seven trajectories were prepared from hourly charts while the center was over land on the 11th. These are shown in figure 26. The results of the calculations from these trajectories are shown in table 3.

Table 3. - Latent and sensible heat flux (Q_{ep} and Q_{sp}) in ca gm.$^{-1}$ following the motion fo a particle at the surface. K_{ep} and K_{sp} are Lagrangian exchange coefficients.

Traj. No	Radial Interval (n. mi.)	Length of Traj. (n. mi.)	Q_{sp} Cal./gm.$^{-1}$	$K_{sp} \times 10^9$ Cal./gm.$^{-1}$ cm.$^{-1}$ deg.$^{-1}$	Q_{ep} Cal./gm.$^{-1}$	$K_{ep} \times 10^9$ Cal./gm.$^{-1}$ cm.$^{-1}$ mb.$^{-1}$
LAGRANGIAN COEFFICIENTS (Over Water Trajectory)						
1	24-66	75	1.22	29.25	1.98	16.88
2	20-65	60	1.09	32.73	1.60	19.04
3	20-65	140	.93	11.96	1.92	20.49
4	12-57	75	1.43	34.29	2.37	20.20
Average				27.06		19.15
LATENT AND SENSIBLE HEAT FLUX (Over Land Trajectory)						
1	32-96	95	.41		-0.29	
2	20-80	60	.51		.43	
3	36-90	75	-.27		-.04	
4	26-78	96	-.20		-1.17	
5	20-80	80	-.13		-.73	
6	7-80	84	-.17		-.91	
7	36-74	70	-.04		.20	
Average			.01		-.36	

Over water, the computations show that the flux of sensible and latent heat from the ocean to the air is very large, as expected. The Lagrangian exchange coefficients are about 3 to 4 times those postulated by Malkus and Riehl [26] in their semi-theoretical model. However, they are not considered excessive, because of the unusual intensity of Donna.

Over land, only two of the seven trajectories show any appreciable sensible heat flux. These two trajectories passed over the Everglades in southern Florida. Since this area is low lying and swampy, some heat flux is not unexpected. The other five trajectories show a decrease in the sensible heat, such that the average is essentially zero. There was some net loss (on the average) in latent heat content, since some condensation took place. Along the trajectory these calculations show that the surface inflow over land is essentially a moist adiabatic process. This effectively demonstrates that following landfall the tropical cyclone is removed from its surface sensible heat source. The importance of this fact will be discussed in more detail in a later section.

The Lagrangian exchange coefficients over land were not computed because of lack of data concerning soil temperatures. It is of interest to compare the Lagrangian exchange coefficients with the drag coefficients computed for the inner region of the cyclone on the 10th. In order to do this, it is necessary to specify the height to which sensible heat is carried by the turbulent diffusion process.

The flux of sensible heat per unit area and per unit time must be independent of the form of the exchange coefficients. Hence

$$\int Q_{sp}\, \rho\, \delta z \delta t = \int Q_s\, \delta t$$

or by use of equations (13) and (26),

$$K_{sp}\,(T_s - T_a)\, s\rho\delta z = \rho C_p C_h (T_s - T_a)\, s$$

Consequently, the relationship between K_{sp} and C_h is

$$C_h = \frac{K_{sp}\,\delta z}{C_p} \tag{30}$$

where z is the depth through which sensible heat is diffused. In order to obtain an estimate of z, we will assume that C_h and C_d are equal, since we are interested only in an order of magnitude calculation. If we use the largest value from table 2 for C_d, we obtain a value of about 150 m. for the depth of the diffusion layer. This value seems reasonable; this elevation lies near or just above the cloud base in tropical cyclones.

It has been suggested by Riehl [48] that the height of the cloud base lies very close to the maximum level to which sensible heat is carried by turbulence. An examination of the temperature data obtained by research flights into tropical cyclones at levels of 1600 and 1800 ft. fails to reveal any significant temperature variations along the radius, as might be expected if sensible heat were advected to these levels. Consequently, it would seem that sensible heat does not rise above the level indicated (i.e., 350 m.). This would also suggest, though not positively, that we are justified in assuming the approximate equality of C_h and C_d.

c. Energy Exchanges at the Surface

It is now possible to determine the flux of energy through the lower boundary of the cyclone for the 3-day period. Sensible and latent heat transfer may be obtained by integrating equations (13) and (14) over the areas. Surface frictional dissipation of kinetic energy may be determined by forming the scalar product of $\mathbf{T}$ and $\mathbf{V}$ and then integrating over the areas involved (Malkus and Riehl [26]). We obtain

$$\text{G. F.} = \int_A \rho C_d\, V_o^3\, dA \tag{31}$$

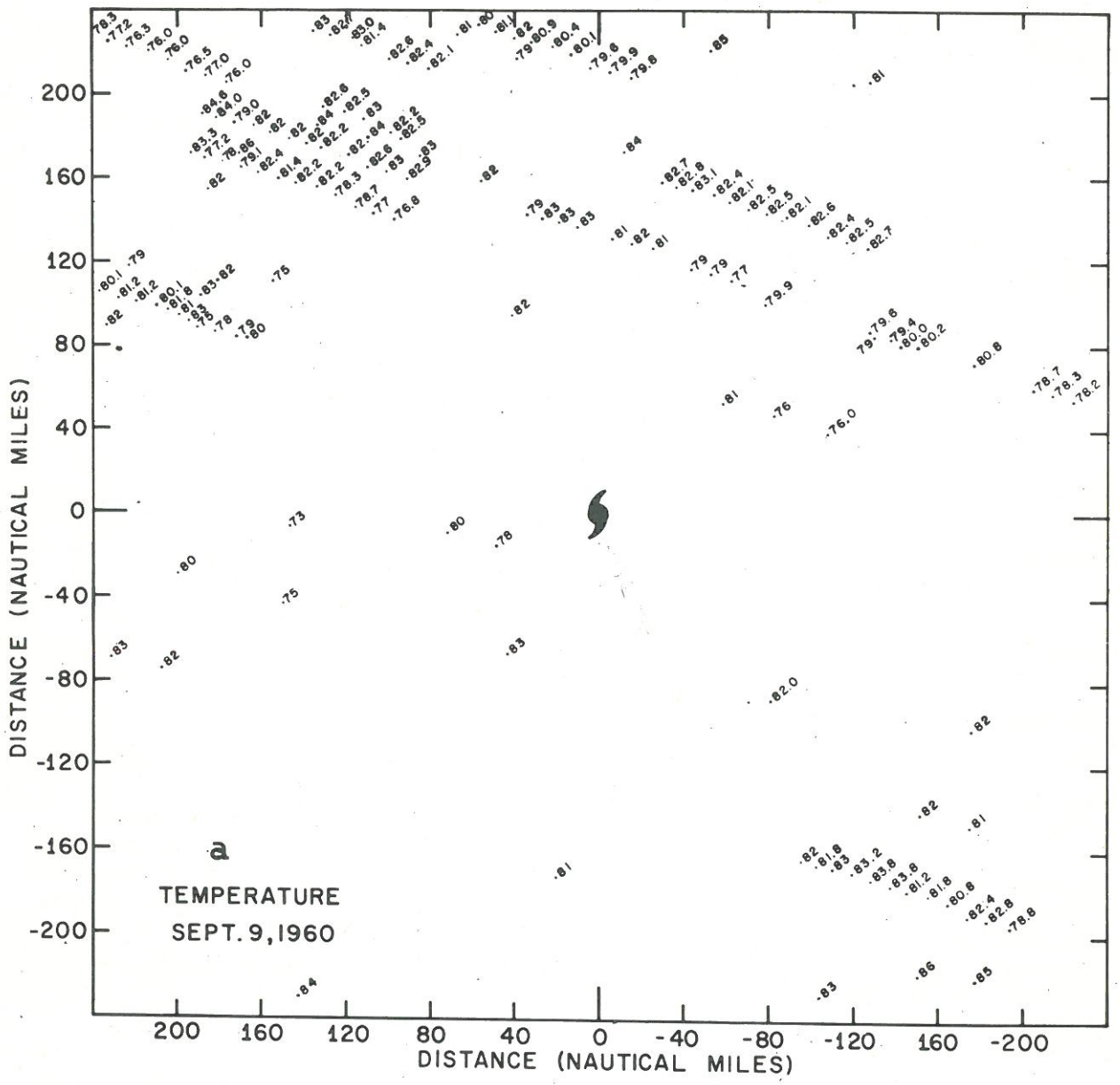

Figure 23. - (a) Temperature of the surface air (°F.), September 9. (b) Dew-point temperature of the surface air (°F.), September 9.

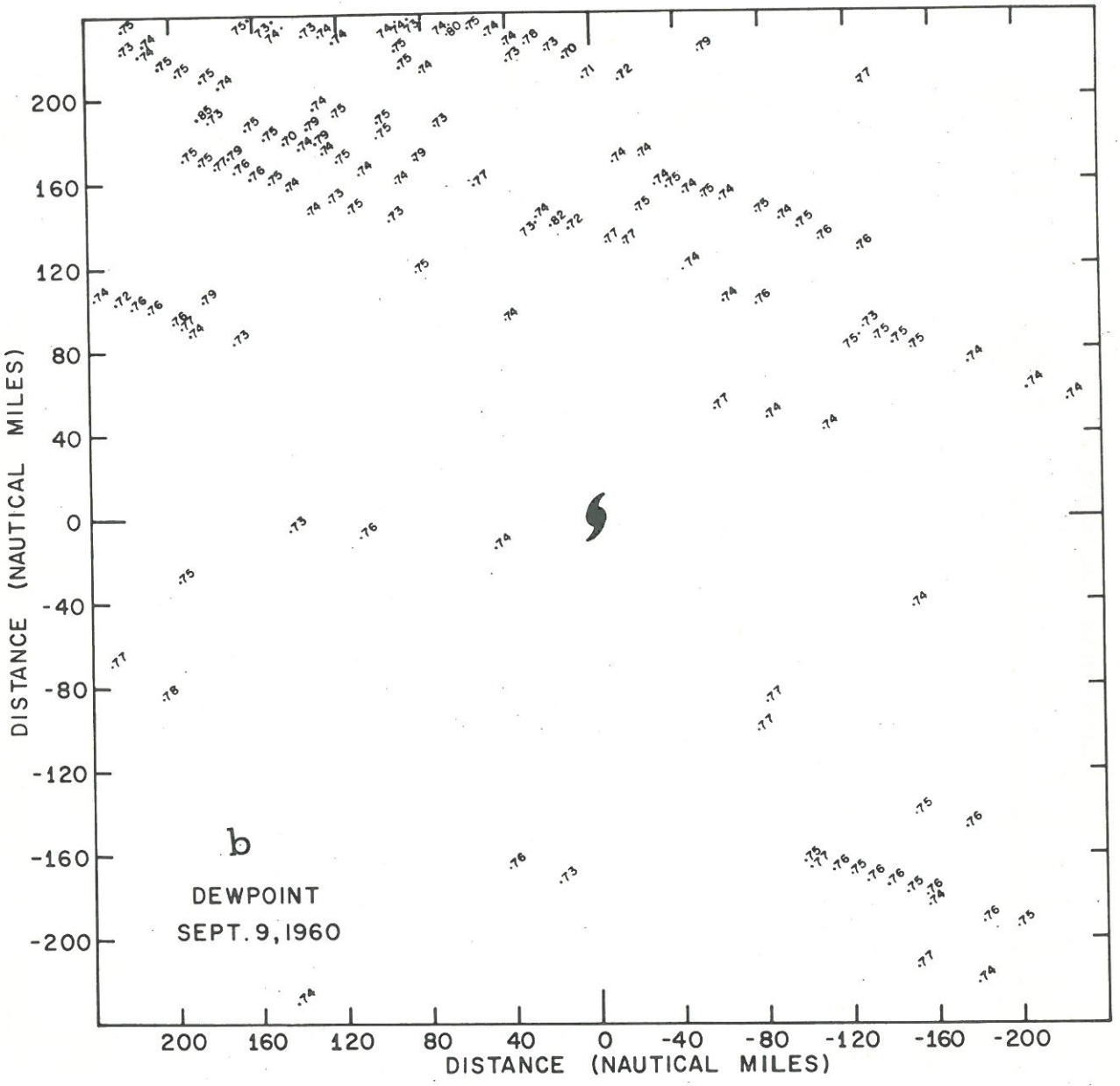
b
DEWPOINT
SEPT. 9, 1960
DISTANCE (NAUTICAL MILES)
200
160
120
80
40
0
-40
-80
-120
-160
-200
DISTANCE (NAUTICAL MILES)

Figure 23b.

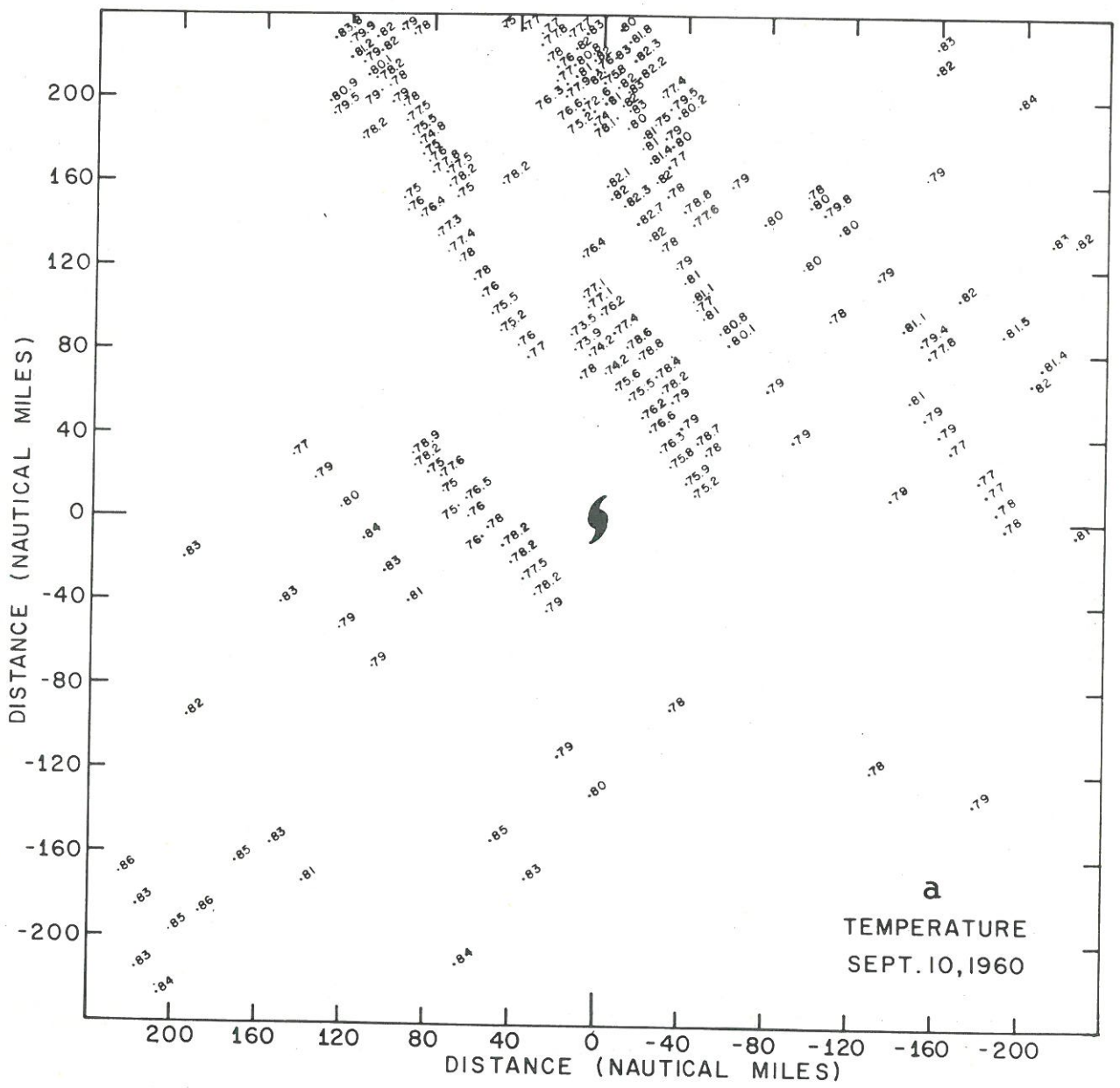

Figure 24. - (a) Temperature of the surface air (°F.), September 10.
(b) Dewpoint temperature of the surface air (°F.), September 10.

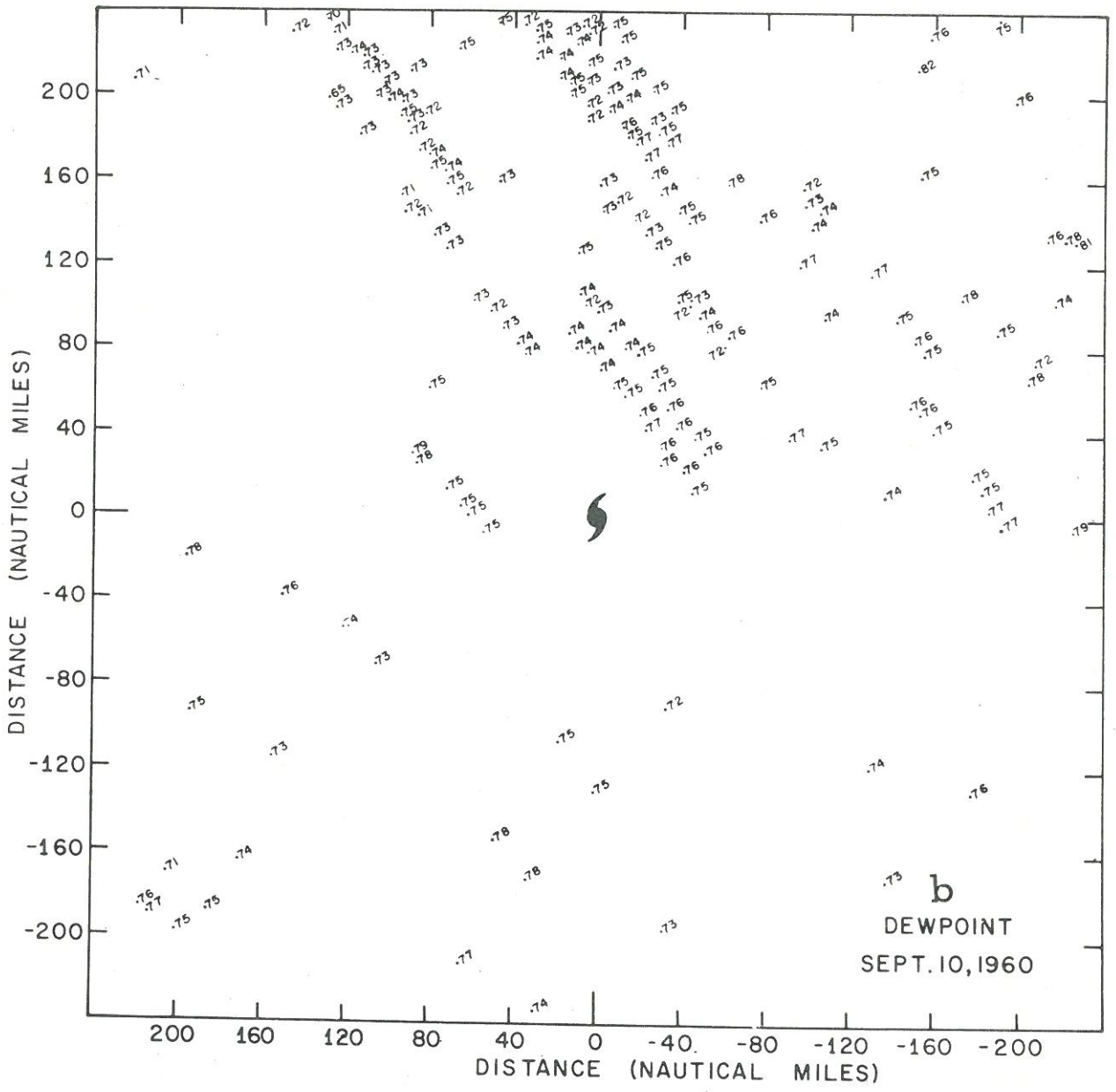
DISTANCE (NAUTICAL MILES)
200
160
120
80
40
0
-40
-80
-120
-160
-200
DISTANCE (NAUTICAL MILES)
200 160 120 80 40 0 -40 -80 -120 -160 -200
b
DEWPOINT
SEPT. 10, 1960

Figure 24b.

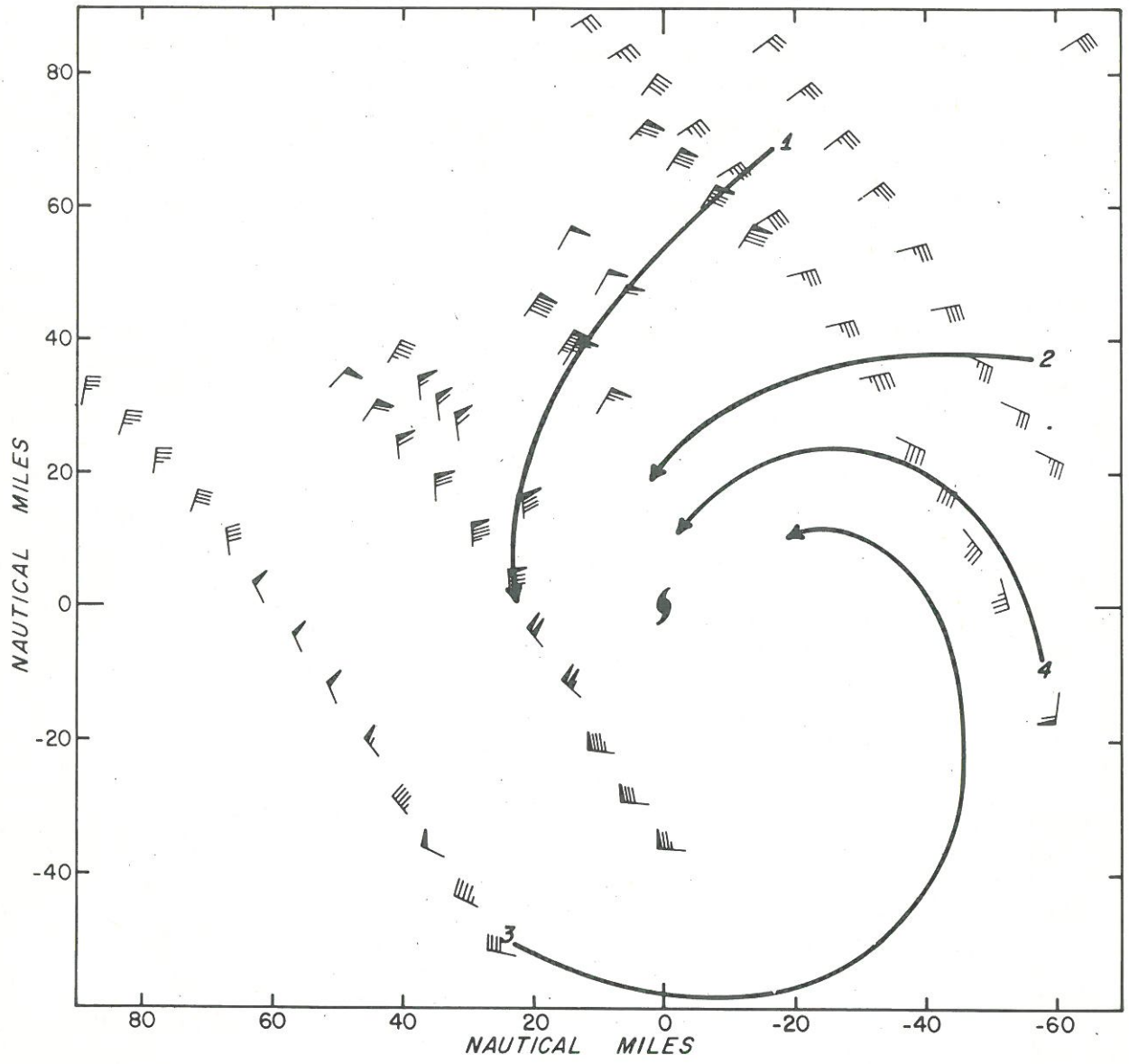

Figure 25. - Trajectories of air parcels relative to the center of the hurricane, September 10. These are over-water trajectories.

in which use has been made of the vector form of equation (15) for the stress and of the assumption that the surface stress is directed opposite to the surface wind.

Drag coefficients from table 2 were used. Surface moisture and temperature were presented in the previous section. On the 9th and 10th the mean winds for the surface to 900-mb. layer were used to represent the surface wind (fig. 15). On the 11th the vertical shear was too large to permit the use of the data of figure 15 to represent the surface winds. An additional isotach chart (fig. 27) was prepared for use over land.

The results of the calculations of the energy exchanges at the surface are shown in table 4. The computations summarized in table 3 have shown that the flux of sensible and latent heat over land are nearly zero. Consequently, zero heat flux from the surface has been assumed for all areas over land.

On the 9th and 10th the vertical flux of both sensible and latent heat was larger than found to exist in either Daisy (Malkus and Riehl [27]) or Helene (Miller [30]). Inside the 80 n. mi. radius on the 10th the average sensible heat flux was 0.62×10^{-2} cal. cm.$^{-2}$ sec.$^{-1}$, or 535 cal. cm.$^{-2}$day^{-1}, and the average latent heat flux was 2.86×10^{-2} cal. cm.$^{-2}$ sec.$^{-1}$or 2471 cal. cm.$^{-2}$ day.$^{-1}$ Average values found in Daisy inside the 80 n. mi. radius on the day of its maximum intensity were 250 cal. cm.$^{-2}$day^{-1} for the sensible heat flux, and 1425 cal. cm.$^{-2}$ day^{-1} for the latent heat flux. The sensible heat flux in Donna was greater by a factor of about 2 than in Daisy, while the latent heat was greater by a factor of 1.7. The Bowen ratio was larger in Donna than in Daisy. The Donna values are comparable to the oceanic heat source predicted by Malkus and Riehl [26] for their semi-theoretical model. For the area lying between radii of 30 and 90 km. in their "moderate hurricane", with maximum winds of112 kt., they obtained a value of 720 cal. cm.$^{-2}$ day^{-1} for the sensible heat flux and 2420 cal. cm.$^{-2}$ day^{-1} for the latent heat flux. The agreement is striking, particularly when one recalls that the maximum sustained winds in Donna were about 111 kt.

On the 11th the surface heat source inside the 40-n. mi. radius was cut off, although there was still some vertical heat flux from the ocean outside this radius, since 35 percent of the area between the 40 and 80-n. mi. radii was still over water. However, it is the heat source near the core of the cyclone which makes the important contribution to the growth of the energy of the cyclone. As soon as this central heat source was cut off, the circulation of the cyclone began to weaken.

Table 4 shows that the frictional dissipation of kinetic energy at the surface is less over land than it is over water. This may be somewhat misleading, since the surface wind data used in computing surface friction were centered around 0600 GMT on the 11th, which was several hours after the center moved inland. It appears likely that during the first few hours after landfall, surface frictional dissipation over land must exceed that over water. If this is the case, the region where frictional dissipation over land is greater may be restricted to the region near the core where there are strong <u>onshore</u> winds.

Table 4. - Surface energy sources and sinks for three day period.
* mean c_d over area used in computing ground friction (G.F)
\# mean c_d for portion of area over water used in computing Q_s and Q_e

Date	9	9	9	9	10	10	10	10	11	11	11	11
Radial Interval (N.M.)	10-40	40-80	80-120	10-120	10-40	40-80	80-120	10-120	10-40	40-80	80-120	10-120
V_o (m.p.s.)	42.0	30.0	24.0	--	45.0	32.0	25.0	--	28.5	22.0	18.5	--
$(T_w - T_a)$	2.0	2.0	2.0	2.0	2.0	2.0	2.0	2.0	3.0	3.0	3.0	3.0
$C_d \times 10^3$	3.90	3.05	2.10		4.00	3.40	2.90		8.70* --	8.25* 2.40#	5.50* 2.00#	
Percentage of area over land	0	15	30	21	0	16	29	21	100	65	33	50
$Q_s \times 10^{-12}$	1.46	2.21	1.68	5.35	1.61	2.60	2.47	6.68	0	.78	1.74	2.52
$(q_w - q_a)$ g/kg	3.08	3.55	4.36	--	3.08	3.55	4.36	--	--	5.30	6.50	--
$Q_e \times 10^{-12}$ cal/sec	5.47	9.57	8.84		6.03	11.25	13.04	30.32	0	3.33	9.34	12.67
Bowen ratio	.27	.23	.19	.22	.27	.23	.19	.22	-	.23	.19	.20
Ground friction $\times 10^{-12}$ cal/sec	1.43	1.42	.80	3.65	1.48	1.64	1.15	4.27	.89	1.34	.84	3.07
Q_s/G.F.	1.02	1.56	2.10	1.47	1.09	1.59	2.15	1.56	0	.58	2.07	.82

The maximum sustained surface wind observed over water was about 111 kt., and the maximum computed value of C_d was 4.19×10^{-3}. Over land the maximum value for C was 8.73×10^{-3}. In order for surface frictional dissipation over land to be equal to that over water, a maximum surface wind over land of about 86 kt. would be required. At no time were there any sustained surface winds with offshore components of this magnitude recorded, although without a dense network of reporting stations with recording anemometers, it cannot be established that no such winds occurred.

The center of the eye passed over Fort Myers about 1930 GMT on the 10th. At this time the central pressure recorded at the Weather Bureau was 951 mb. (a privately-owned barometer recorded a minimum of 940 mb.). The maximum wind at Fort Myers was 92 m.p.h. (fastest mile of record) from the northeast. This is about 80 kt. This value for the surface wind would indicate less frictional dissipation over land than over water just before the eye moved inland. Along the immediate coast, in the region of onshore winds, it is probable that the surface winds exceeded 86 kt. and that the dissipation due to surface friction is here greater over land than it is over water. Turbulence theory would suggest that as a result of the greater surface roughness over land there should be greater vertical shear over land than over water. The wind slows down more at anemometer level than it does at some higher elevation. The peak gust-mean wind data shown in figure 16 would indicate that this is so. This would contribute to a lessening of the surface frictional dissipation over land. Another factor is the decrease in the pressure gradient over land (fig. 13 and 14) which permits the winds to decrease because of reduced pressure forces, thereby resulting in reduced frictional dissipation.

Over water the ratio of sensible heat source to frictional dissipation of kinetic energy is everywhere greater than 1, except near the core where it seems to approach 1 as a limit. It appears that this ratio, not the absolute magnitude of the ground friction, is of fundamental importance to the growth and decay of the tropical cyclone.

Malkus and Riehl [26] have shown that kinetic energy is produced by the oceanic heat source at a maximum rate during horizontal motion and isothermal expansion. That the ratio of sensible heat to surface frictional dissipation has a limiting value of 1 is implied, though not specifically stated in their model. The data from table 4 would seem to support their model, even though these calculations are not restricted by the same assumptions of horizontal motion and isothermal expansion.

It may be of some interest to examine the conditions under which the frictional dissipation could be expected to equal the sensible heat source. Addition of equations (1) and (2) gives a general energy equation

$$\frac{d}{dt}\left(K + gz + C_p T + Lq_s\right) = \frac{dH}{dt} + \frac{\partial p}{\partial x} + V \cdot F \qquad (32)$$

For the present we will restrict our discussion of (32) to the sub-cloud layer where Ldq_s/dt is small and where the frictional dissipation of kinetic

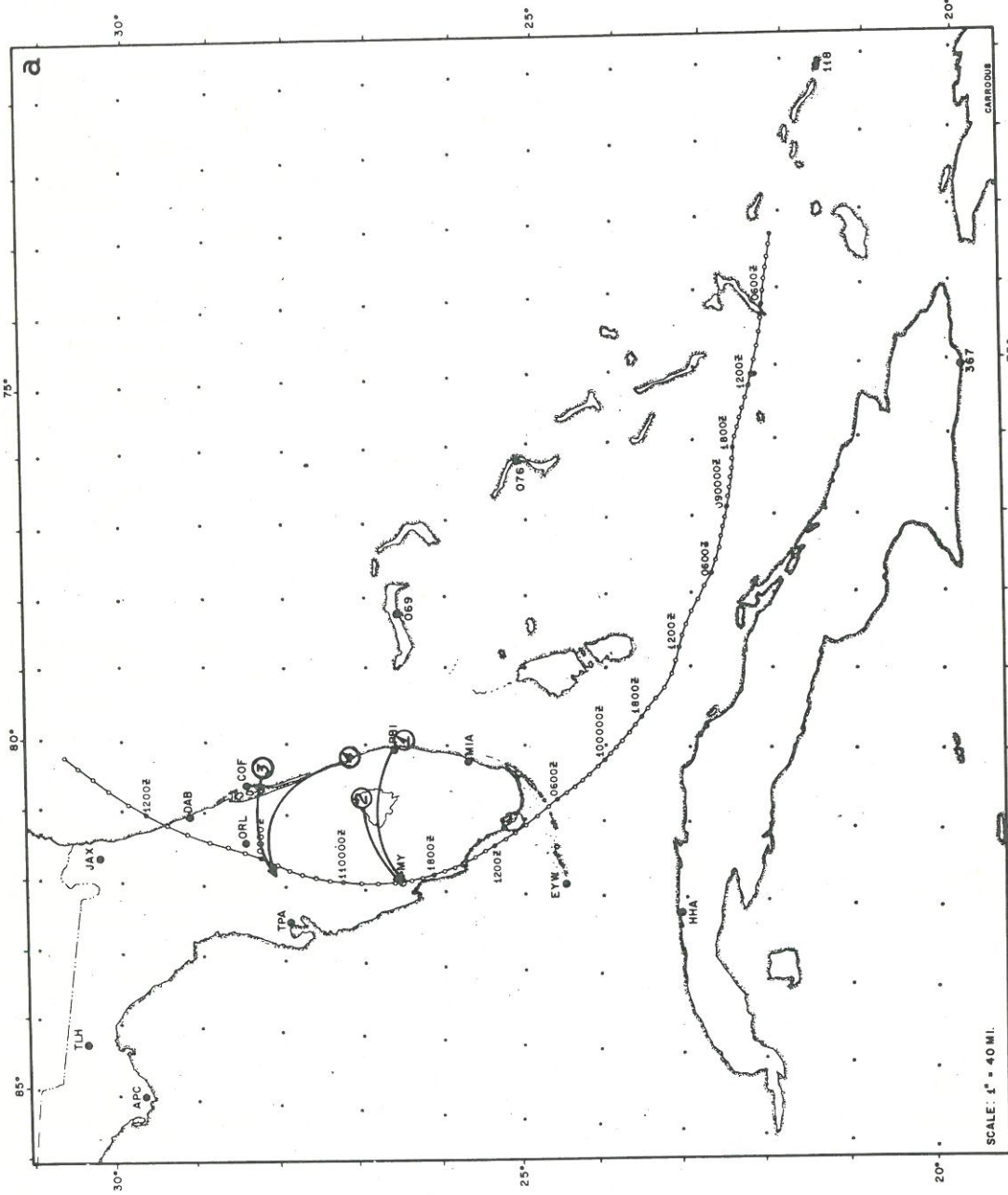

Figure 26. - Trajectories of air parcels at the surface (over land) September 11.

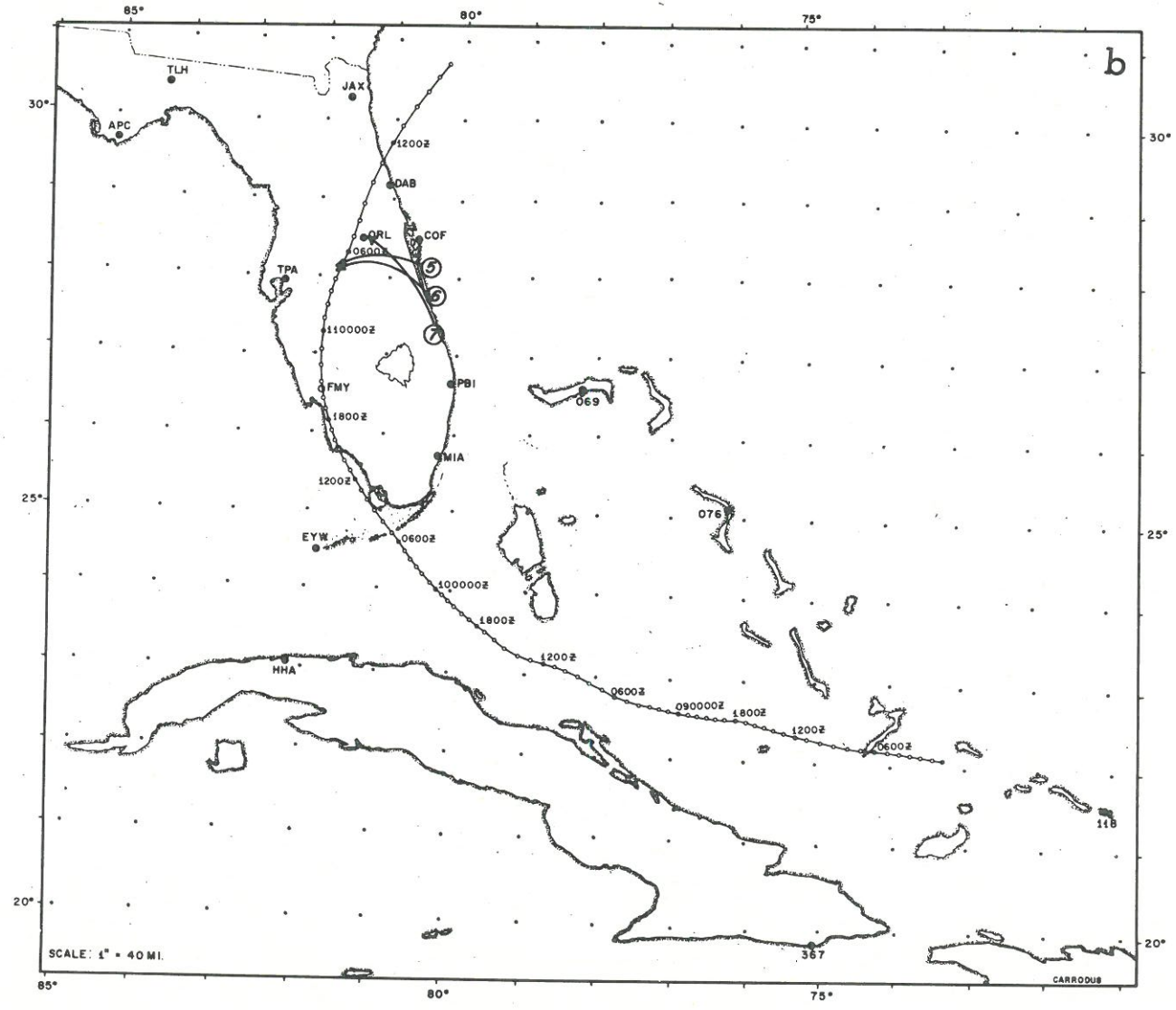

Figure 26. - (continued)

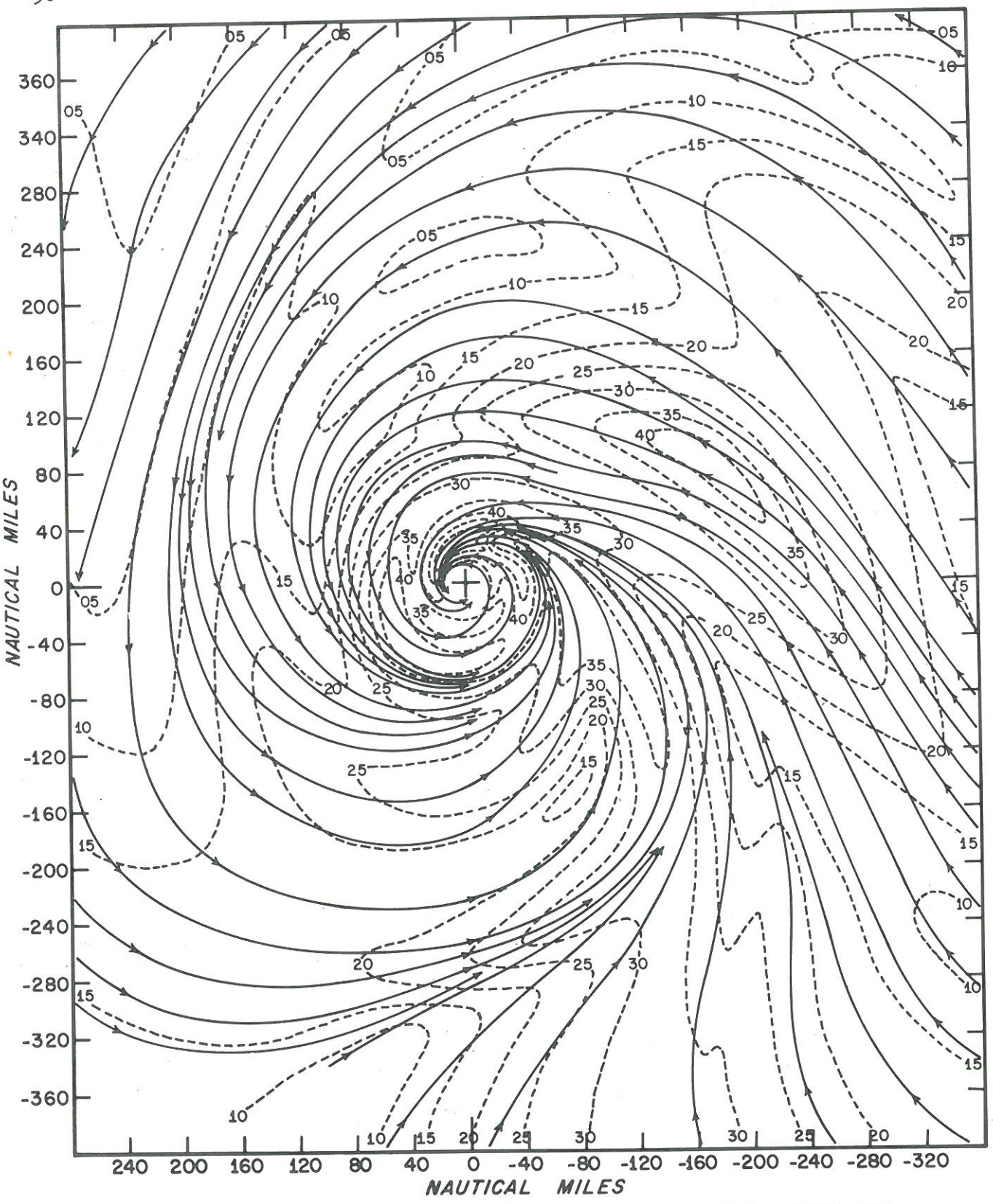

Figure 27. - Streamline-isotach analysis of the surface winds, 0600 GMT, September 11.

energy may be adequately represented by the surface friction. For steady state, the computations of table 4 show that near the core of the cyclone, the right of (32) is zero. Hence (32) may be integrated along a streamline.

$$K + gz + C_p T = \text{constant} \tag{33}$$

which is a generalized Bernoulli equation of compressible flow. Equation (33) indicates that frictional dissipation and sensible heat flux are equal along sub-cloud trajectories where there are two possible cases.

1. K is constant and the sum of $(gz + C_p T)$ is constant, as might occur along horizontal trajectories where the motion is isothermal and the trajectory coincides with an isotach.

2. The increase of the kinetic energy is given explicitly by the decrease in potential energy and enthalpy. If $z_1 = 0$, and $T_2 = T_1 - \gamma z_2$, then

$$(K_2 - K_1) = z C_p J (\gamma - \gamma_d) \tag{34}$$

where K_1 and K_2 are the kinetic energy at successive points along a trajectory and where J is the mechanical equivalent of heat. Hence the energy along the trajectory may be expected to increase if the lapse rate is greater than dry adiabatic.

Over the land the surface heat source is absent, and we have very nearly horizontal motion and moist adiabatic expansion. The cyclone is no longer in a steady state, the core of the cyclone cools, and the pressure at the center rises. The magnitude of this cooling and the associated pressure rise at the surface will be discussed in the following section.

6. THERMODYNAMICAL AND DYNAMICAL CHANGES IN THE CYCLONE AFTER LANDFALL

a. Changes in the Thermal Structure at the Surface and Aloft.

We have already examined the structural changes which occurred after the center of the cyclone was removed from the oceanic heat source. We will now look at the changes in the thermal structure in the light of surface exchange processes and then form some estimates as to how these thermal changes resulted in dynamical changes.

There were not enough data to permit detailed analyses of the temperature field at all levels (although the temperatures could have been computed from the thickness analyses). However, the surface pressure was known with a high degree of accuracy, particularly on the 10th and 11th. It was also possible to prepare good analyses of the 100-mb. chart. From these two levels the mean virtual temperatures for the surface to 100-mb. layer were computed by using the formula

$$z_t = \frac{RT^*}{g} \ln p_o / p_t \tag{35}$$

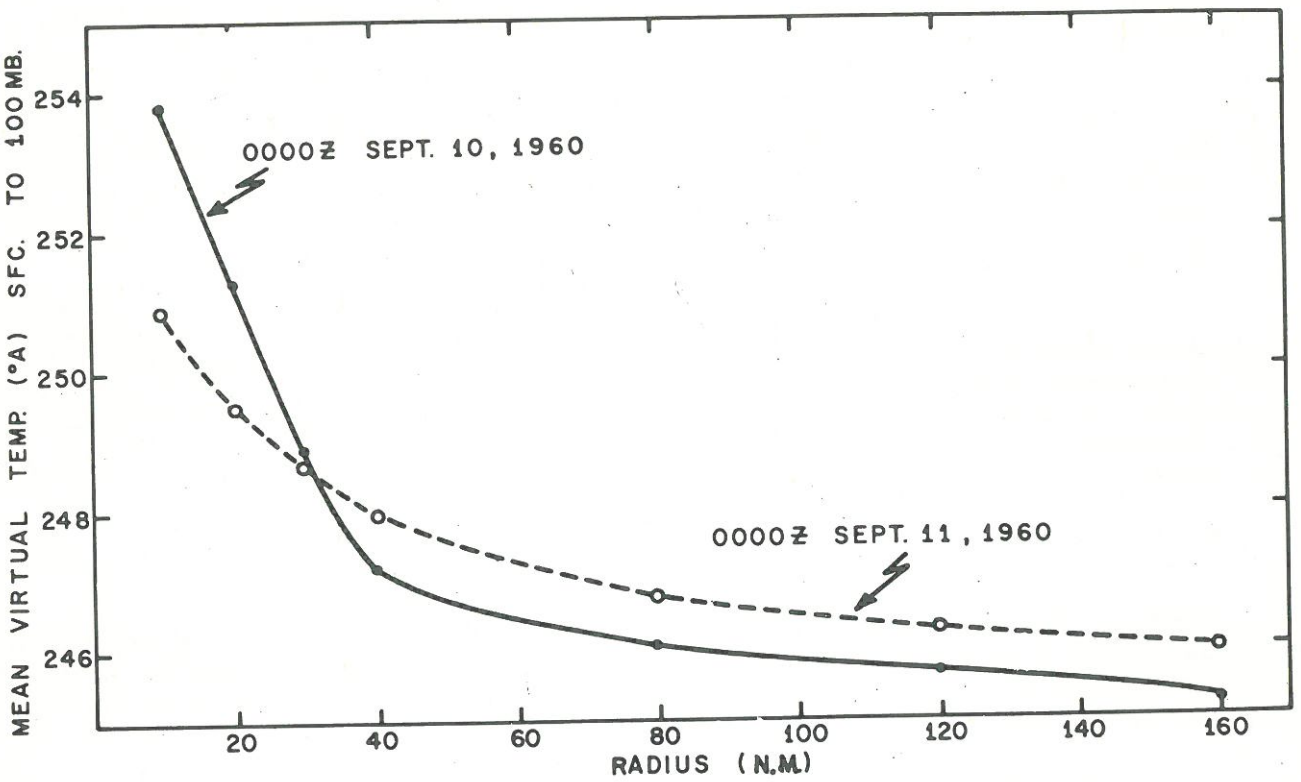

Figure 28. - Radial profile of mean virtual temperature (surface to 100 mb.) on September 10 and 11.

where z_t is the thickness of the column, T^* is the mean virtual temperature, p_o and p_t are pressures at the base and top of the column. The results are shown in figure 28.

During the 24-hr. period between 0000 GMT on the 10th and 11th, the central pressure rose about 36 mb. after the center moved inland, but during this period the pressure outside a radius of about 40 n. mi. fell slightly. This is shown by the indicated cooling of about 3.0°C. in the center of the cyclone and a warming of about 0.6°C. outside the 40-n. mi. radius. This reflects a spreading out of the warm air previously concentrated near the core and a redistribution of the mass of the cyclone during the filling process. In fact, during the period of most rapid filling the total mass of the cyclone remained almost constant.

In equation (35) we may choose p_t as 100 mb. and p_o as the surface pressure. The z becomes the height of the 100-mb. surface. In most tropical cyclones (if not all) the 100-mb. surface is almost flat; i.e., the height is virtually independent of the radial distance from the center of the cyclone. Now differentiate (35) with respect to r and t, and obtain

$$\frac{\partial p_o}{\partial r,t} = - \frac{p_o}{T^*} \frac{\partial T^*}{\partial r,t} \ln \; p_o/100 \qquad (36)$$

which relates the surface pressure gradient to the gradient of mean virtual temperature. Variations in $(p_o/100)$ are small, since p_o will range from about 1000 mb. to near 930 mb.; p_o and T* are inversely correlated, but within the normal range of values, variations of the factor p_o/T^* will alter the pressure gradiently by less than 10 percent. Consequently, it is seen that the surface pressure gradient observed in tropical cyclones is dependent primarily upon the gradient of mean virtual temperature within the column from the surface to about 100 mb. To explain the surface pressure gradient, it is therefore necessary to explain the tropospheric temperature field.

It is evident that the cyclone weakened over land because the core cooled, which resulted in reduced pressure gradients and thereby reduced the conversion of potential energy to kinetic energy (which depends upon the product $v_r\ (\partial z/\partial r)$. It is now possible to deduce the reasons for the cooling of the core of the cyclone.

Time changes in temperatures, mixing ratios, potential temperatures, and equivalent potential temperatures at the surface near the core of the cyclone were plotted. These are shown in figures 29 through 32. These data are based on the surface reports in or near the eye of the cyclone, covering the time period immediately before and after the cyclone center moved inland and weakened. They are intended to represent the best available estimate of surface conditions in the wall cloud region.

The point for the 8th is based on a report from Ragged Island Key. The last temperature and humidity data were recorded when the eye was about 40 n. mi. from the station, but barometric pressures were recorded throughout the passage of the center. Computations were based on the assumption of isothermal expansion and a relative humidity of 95 percent inside this radius. The points for the 9th and 10th each represent the average of five dropsonde observations made in or near the eye between the hours of 0000 GMT and 1300 GMT on each day. Other data are from land station reports; they were recorded at the time of the minimum pressure at each location. All land station data used were within 7 mi. or less of the eye at the time of the lowest pressure.

Note first the changes in the observed surface temperatures. The eye began to move inland between 1200 and 1500 GMT on the 10th. The surface temperature dropped about 3.0°C. between 1200 GMT on the 10th and 0300 GMT on the 11th. The surface air remained near the saturation point throughout; consequently, the reduction in temperature was associated with a sharp drop in the mixing ratio of the surface air (fig. 30). The equivalent potential temperature dropped from a maximum of 374°A. on the 10th to a minimum of 353°A. on the 11th. The potential temperature also dropped, but by a lesser amount.

The potential temperature and the equivalent potential temperature observed near the eye over land are characteristic of their values outside the 60-n. mi. radius while the cyclone was over water. The temperatures and mixing ratios are somewhat less as a result of moist adiabatic cooling. These data confirm the fact of a heat source inside the 60-n. mi. radius, which was demonstrated by the trajectory computations presented in an earlier section.

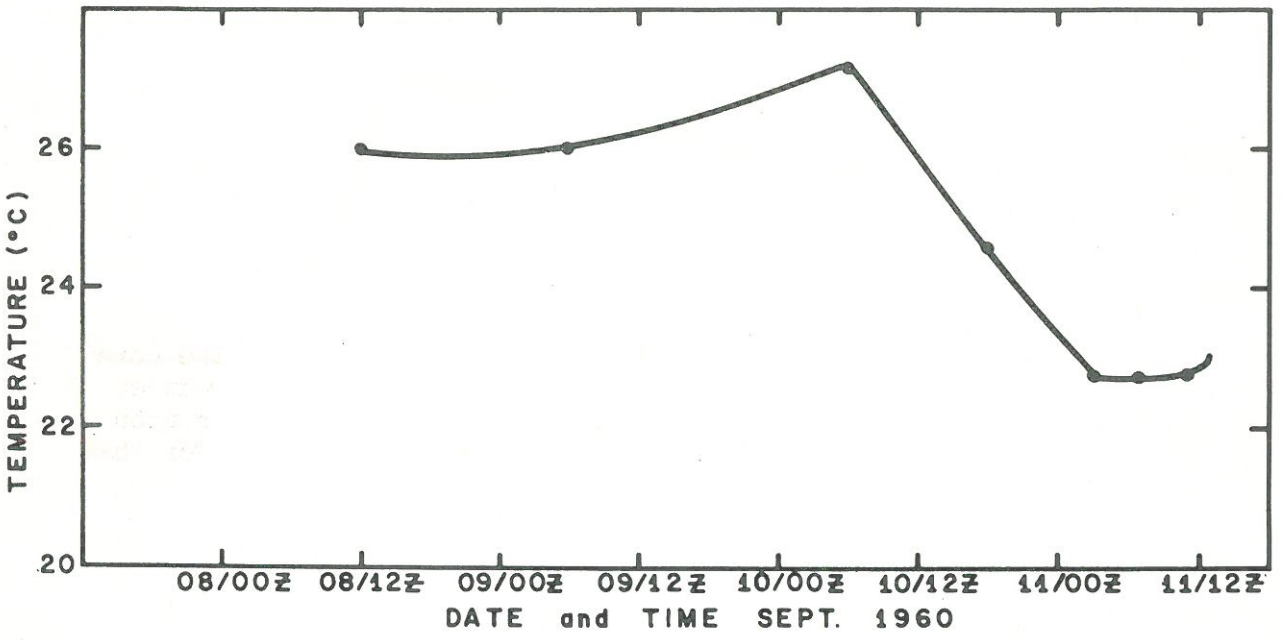

Figure 29. - Changes in surface temperature near the eye of hurricane Donna, September 8-11, 1960.

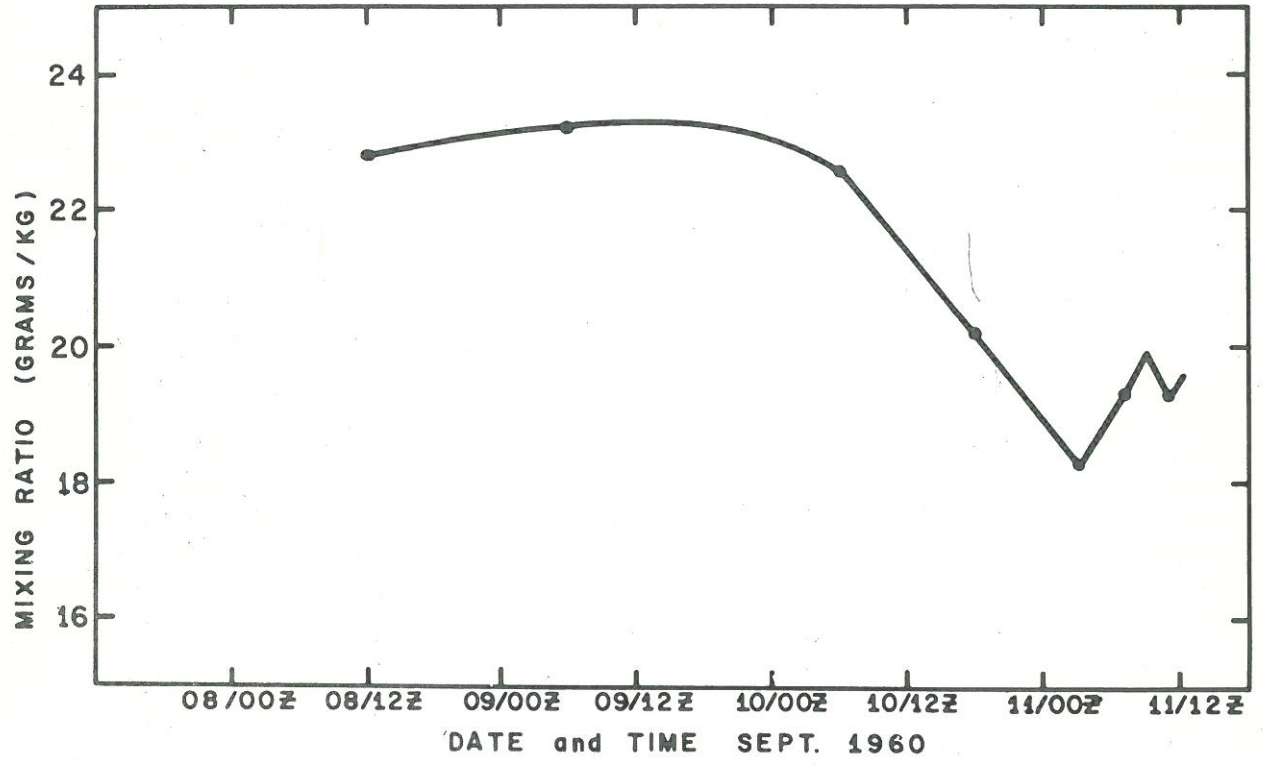

Figure 30. - Changes in mixing ratio of the surface air near the eye of hurricane Donna, September 8-11, 1960

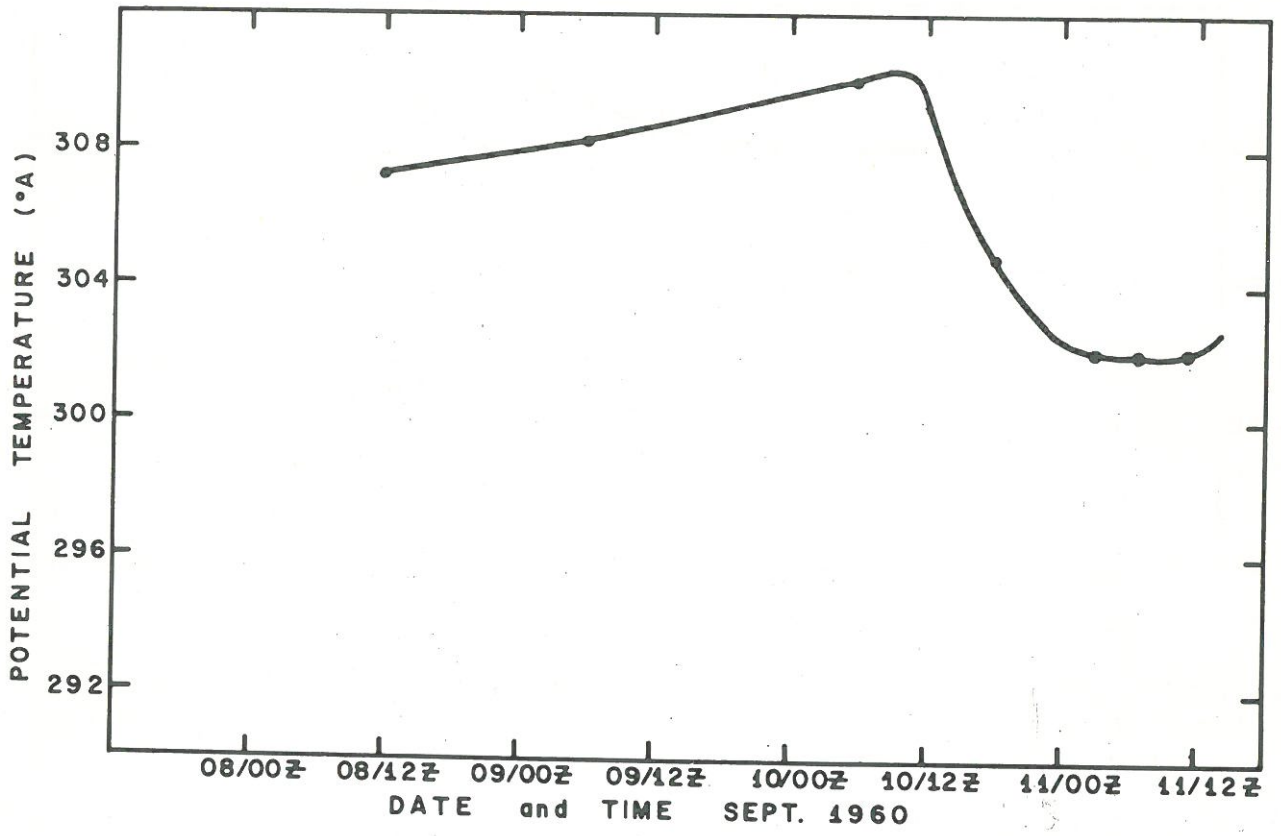

Figure 31. - Changes in the potential temperature of the surface air near the eye of hurricane Donna, September 8-11, 1960

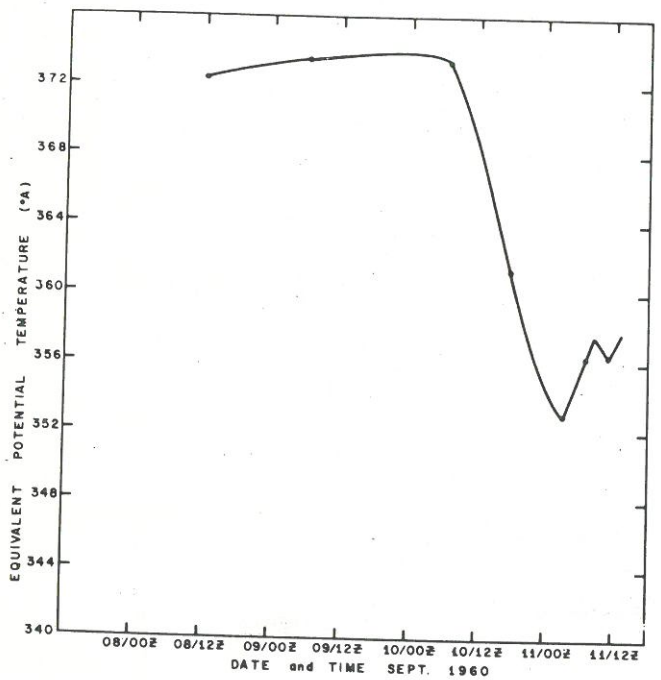

Figure 32. - Changes in equivalent potential temperature of the surface air near the eye of hurricane Donna, September 8-11, 1960

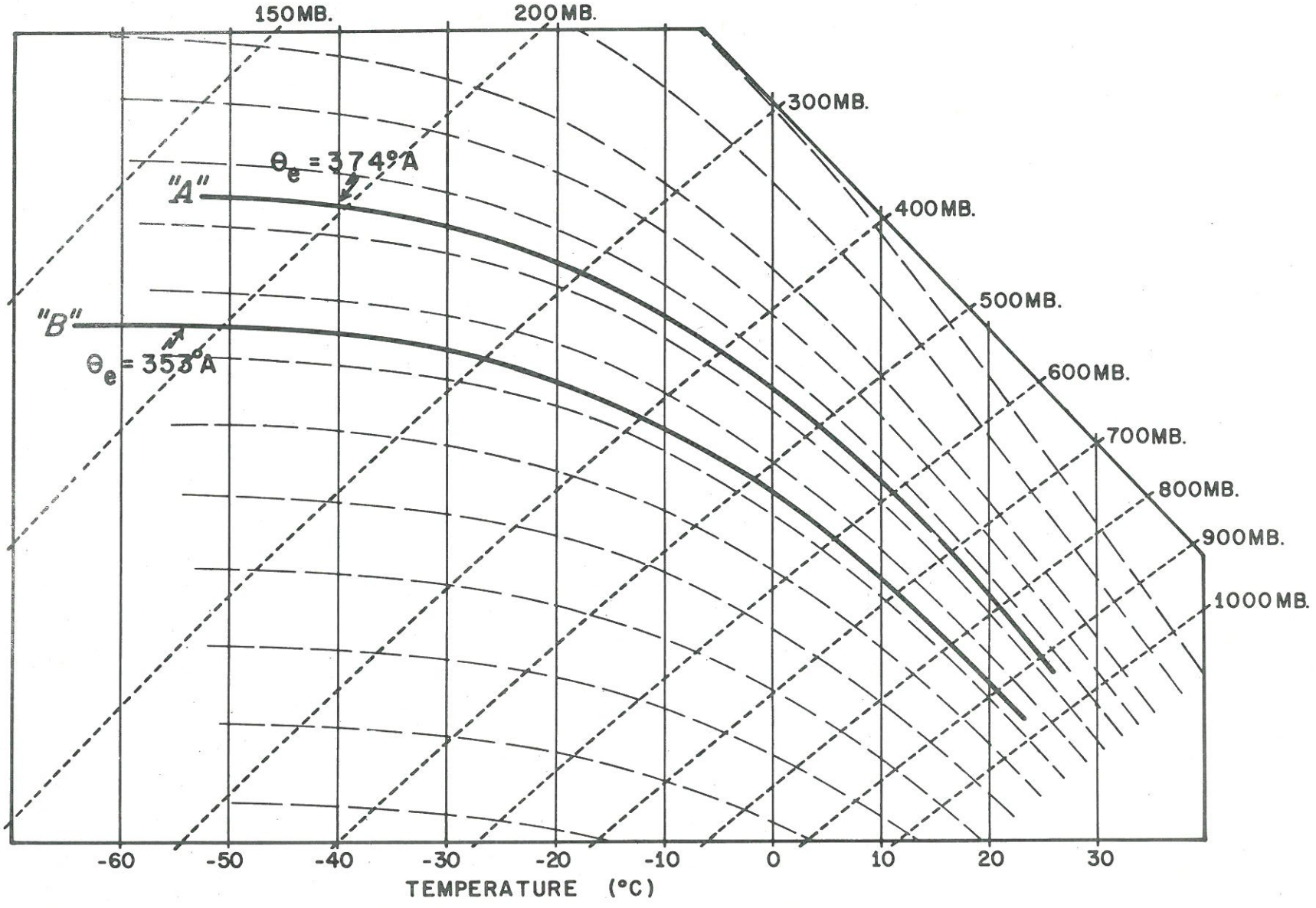

Figure 33. - Vertical temperature profile following vertical ascent of undiluted surface air having equivalent potential temperatures of 353 °A. and 374 °A.

The vertical temperature profiles which would result from moist adiabatic ascent of surface air having equivalent potential temperatures of 37°A. and 353°A. are shown in figure 33. These are characteristic values of θ_e for the intense cyclone over water and for the weakening cyclone over land. For the specified values of θ_e the curves of figure 33 represent maximum values for the temperatures, at the upper levels, which can occur within the cloud area. Values of θ_e in excess of 374°A. have been observed in intense tropical cyclones at the 237-mb. level. Temperatures warmer than the -30°C. indicated by curve "A" for this level have also been observed. In other words observational data obtained by research flights support the concept of undiluted parcel ascent near the core of intense cyclones.

A comparison between curves "A" and "B" shows the very large difference in rate of warming following vertical ascent for surface air having differing θ_e values. At 500 mb. the temperature difference is about 6°C. and at 200 mb. it is near 12°C. It is now clear that the core of the cyclone cooled over land because the air which ascended in the wall cloud region did so at greatly reduced equivalent potential temperatures.

Malkus and Riehl [26] showed that the surface pressure can decrease about 2.5 mb. for each degree increase in θ_e, assuming vertical moist adiabatic ascent from the surface to near 100 mb. If we differentiate equation (3) with respect to time,

$$-\frac{\delta p_s}{\delta t} = 2.5 \frac{\delta \theta_e}{\delta t} \qquad (37)$$

Now apply equation (37) to the data from figure 32 and we get an indicated increase in the central pressure of 52.5 mb. in 24 hr. (θ_e decreased about 21°A.). The actual increase in central pressure was about 36 mb. which is considered good confirmation of the Malkus-Riehl equation.

However, the relation between surface pressure and the equivalent potential temperature at the surface was not intended to apply to cyclones in the dissipating state. It is based on an assumption of very nearly vertical ascent, and the reason for its lack of complete success here can probably be explained by the assumption that the ascent over land deviates from the vertical in the upper levels more than it does over water. A second alternative lies in the possibility that the convective tops are much lower over land. In either case there seems to be a residual pool of warm air at the top of the cyclone. This warm air is apparently advected along with the cyclone, to be gradually destroyed by radiation and lateral diffusion. It is postulated that it is this warm pool which prevents rapid collapse of the cyclone after the surface heat source is cut off.

An examination of the temperature field in the wall cloud region, as obtained from the thickness analyses, would indicate that this is so. These indicate a 24-hr. cooling of the layer from the surface to 500 mb. amounting to about 6° between 0600 GMT on the 10th and 0600 GMT on the 11th, while the cooling of the 500-100-mb. layer was somewhat less than 4°. The cooling of the lower layer can be explained on the basis of moist adiabatic ascent at a reduced equivalent potential temperature. That such ascent did

not continue vertically to the upper troposphere is obvious, since such ascent would have resulted in much more cooling above 500 mb. than actually occurred.

By making use of equation (36) and of the temperature data referred to in the previous paragraph, it can be shown that about 12 mb. of the pressure rise observed to occur at the surface after landfall can be explained by the cooling which took place below 500 mb. The remaining 24 mb. rise in the surface pressure can be explained by the cooling which took place above 500 mb. Both computations are based on the assumption that the height of the 100-mb. surface remained unchanged during the filling process.

The processes by which the core of the cyclone warms or cools may be determined. The first law of thermodynamics for moist air is

$$\frac{dH}{dt} - L\frac{dq_s}{dt} = C_p\frac{dT}{dt} - \alpha\frac{dp}{dt} \qquad (38)$$

By making use of the approximation, $q_s = \epsilon e_s/p$, ϵ being the ratio of the molecular weight of water to that of dry air, we obtain (Rosenthal [49])

$$\frac{dq_s}{dt} = \frac{\epsilon}{p}\frac{de_s}{dT}\frac{dT}{dt} - \frac{\epsilon e_s}{RTp}\alpha\frac{dp}{dt} \qquad (39)$$

The Clausius-Clapeyron equation may be used to eliminate de_s/dT, and (39) becomes

$$\frac{dH}{dt} = \left[C_p + \frac{L^2\epsilon^2 e_s}{RT^2 p}\right]\frac{dT}{dt} - \left[1 + \frac{\epsilon e_s L}{RTp}\right]\alpha\frac{dp}{dt} \qquad (40)$$

The approximate form for the moist adiabatic lapse rate (dT/dp) is (Haurwitz [16], p.55)

$$\Gamma_s = \frac{\alpha}{C_p}\left[\frac{1 + \frac{\epsilon L e_s}{pRT}}{1 + \frac{\epsilon^2 L^2 e_s}{C_p pRT}}\right] \qquad (41)$$

Elimination of $\left[1 + \frac{\epsilon L e_s}{RTp}\right]$ between (40) and (41) gives

$$\frac{dH}{dt} = \left[C_p + \frac{L^2\epsilon^2 e_s}{RT^2 p}\right]\frac{dT}{dt} - \Gamma_s\left[C_p + \frac{L^2\epsilon^2 e_s}{RT^2 p}\right]\frac{dp}{dt} \qquad (42)$$

We now define: $B \equiv \left[C_p + \frac{L^2\epsilon^2 e_s}{RT^2 p}\right]$

expand dT/dt, replace $\partial T/\partial p$ by Γ, and $dp/dt = \omega$ (the vertical motion). The first law of thermodynamics for moist air may then be written as

$$\frac{\partial T}{\partial t} = - \mathbf{V} \cdot \nabla T + \omega (\Gamma_s - \Gamma) + \frac{1}{B} \frac{dH}{dt} \qquad (43)$$

which has the same form as an expression derived by Petterssen [40], (p. 323). In a relative coordinate system (43) becomes

$$\frac{\delta T}{\delta t} = - \mathbf{V}_R \cdot \nabla T + \omega (\Gamma_s - \Gamma) + \frac{1}{B} \frac{\delta H}{\delta t} \qquad (44)$$

Over land the mean temperature of the core of the cyclone decreased. Equation (44) shows three processes by which this cooling may have been brought about. These are by the lateral advection of cooler air into the core region, by the forced ascent of stable air, or by the loss of sensible heat (by radiation or by turbulent transfer to the ground). It has been shown that the flux of sensible heat at the ground is negligible. In heavy cloud areas, radiation is presumably negligible also except for loss of heat from the cloud tops. It is not possible to determine which of the other two processes is the dominant one.

If equation (44) is multiplied by $d\ (\ln p)$ and then integrated between two fixed pressure levels, p_o and p, one obtains (after rearrangement) the thickness tendency

$$\frac{\delta z_t}{\delta t} = \frac{R}{g} \left[\overline{- \mathbf{V}_R \cdot \nabla T} + \overline{\omega (\Gamma_s - \Gamma)} + \overline{\frac{1}{B} \frac{\delta H}{\delta t}} \right] \ln p_o/p \qquad (45)$$

where the bar indicates vertical integration.

Since the tropical cyclone is warm core, its growth or dissipation is determined by the warming or cooling of the core. Equation (45) describes explicitly the thermal processes by which the cyclone intensifies and weakens. The importance of the surface heat source is once again demonstrated in another way; during development it is responsible for the low-level instability which is needed to make the term $(\Gamma_s - \Gamma) < 0$ so that ascending motion near the center results in the production of the warm core. Once this surface heat source is removed, cooling of the core and weakening of the cyclone follow.

b. The Pressure Field

We will now compute from the radial equation of motion the pressure profiles needed to maintain the wind field observed over water against the increased surface roughness over land. We will then ascertain if these pressure profiles are reasonable, and then attempt to determine the magnitude of the surface heat source, which would be required to support the computed pressure profile.

The radial equation of motion is

$$\frac{dv_r}{dt} = \frac{v_\theta}{r} + fv_\theta + \alpha \frac{\partial \tau_{rz}}{\partial z} - \alpha \frac{\partial p}{\partial r} \tag{46}$$

in which τ_{rz} is the radial shearing stress; other terms have already been defined. As a first approximation, we will assume steady state and neglect the horizontal and vertical advection terms. Equation (46) is then integrated over the depth of the inflow layer. This yields

$$\frac{\partial \bar{p}}{\partial r} = \bar{\rho} \left(\frac{\overline{v^2}_\theta}{r} + f\bar{v}_\theta \right) + \frac{\tau_{rh} - \tau_{ro}}{h} \tag{47}$$

In equation (47) the bars indicate mean values for the inflow layer, and h is the depth of the inflow layer. We assume that τ_{rh} is zero and replace the surface stress by

$$\tau_{ro} = \rho_o C_d K_o v_{ro} \tag{48}$$

consequently,

$$\frac{\partial \bar{p}}{\partial r} = \bar{\rho} \left(\frac{\overline{v^2}_\theta}{r} + f\bar{v}_\theta \right) - \frac{\rho_o C_d V_o v_{ro}}{h} \tag{49}$$

Equation (49) was evaluated by computing pressure increments for 5-km. intervals and then integrating graphically. The mean layer wind for the surface to 900-mb. layer was used as the mean for the inflow layer. The surface pressure profile was obtained by joining the solution obtained from (49) with the observed surface pressure at a radius of 220 km.

Three calculations were performed. The first was an attempt to reproduce the observed pressure profile over land by using actual data in integrating equation (49). The results are shown in figure 34. The computed pressure profile is identical with the observed pressure profile (fig. 14) outside the 40 n. mi. radius. Inside this point, the computed pressure deviates slightly from the observed pressure. The computed central pressure is about 5 mb. lower at a radius of 20 km. (12 n. mi.). This is probably as good an agreement as can be expected. Actually, the frictional force in equation (46) is small in comparison with the other terms. A pressure field computed without friction (and without vertical shear) was about the same as that computed with friction outside the 40 n. mi. radius. At smaller radii, the computed pressures were higher, and at the 12 n. mi. radius (20 km.) the computed pressure was about 10 mb. higher than that computed with friction, which is about 5 mb. higher than was actually observed.

The computation of the pressure profile needed over land to sustain the wind field as actually observed over water presented some minor problems, since vertical wind shear in the friction layer could not be ignored. Two possibilities were investigated.

We computed the pressure profile needed to maintain over land the same wind field at the surface (e.g., at a height of 15 m.) which had existed over the ocean prior to landfall. The drag coefficients for the land area and a maximum surface wind of 115 kt. at 15 m. were used. The maximum wind over water was about this value. If we assume that the constant shearing stress layer is 100 m. deep, a value for C_d of 8.75×10^{-3}, and a maximum surface wind of 115 kt. at 15 m., we are implying a vertical shear which would require that the ratio of the mean wind for the inflow layer to the wind at 15 m. be about 1.4. This would require a mean wind for the inflow layer of about 158 kt., a very high value. However, the calculations were performed and the computed pressure profile, under these assumption, is shown in figure 35.

Quite obviously the computed pressure profile is considerably steeper than that actually observed over water, since both friction and mean winds for the inflow layer are greater. The computed minimum pressure is about 895 mb., a value which has been observed to occur only rarely (Dunn and Miller [10], p. 75 ff.), but even this value is not impossible.

The next calculation was performed for the observed mean wind over water and computed surface friction over land. In accordance with the assumptions listed above concerning the depth of the constant stress layer, the wind at 15 m. was allowed to decrease to a value consistent with the surface roughness. This resulted in a maximum surface wind of about 85-90 kt., which is very close to the actual maximum observed immediately after landfall at Fort Myers.

The computed pressure profile (fig. 36) is very similar to that observed on the 10th. It is somewhat less steep, and the minimum pressure is about 940 mb., which is higher than the absolute minimum for the cyclone (929 mb.), the latter value having been recorded in the Florida Keys on the 10th. Since one land station barometer recorded a minimum pressure of 940 mb. at Fort Myers, and since the maximum surface winds at Fort Myers were only slightly less than the maximum surface winds used in computing the pressure profile of figure 36, it is obvious that no unrealistic pressure field is needed to maintain over land the same wind speeds at 100 m. that were observed over water, provided the winds at the surface are permitted to adjust to the greater surface roughness over land.

c. Local Heat Sources Needed to Maintain Computed Pressure Profiles

We will next estimate the surface heat source needed to maintain in steady state an already existing hurricane with the central pressures and pressure profiles just presented, which were computed, using land surface friction and over-water wind fields. The procedure will involve computation of the sensible heat source needed to maintain isothermal expansion inside the 1000-mb. isobar. This isothermal expansion is needed to prevent cooling of the core, which results in lowered capacity to retain moisture. This leads to reduced θ_e and eventual cooling of the core of the cyclone, and resultant loss in cyclone intensity.

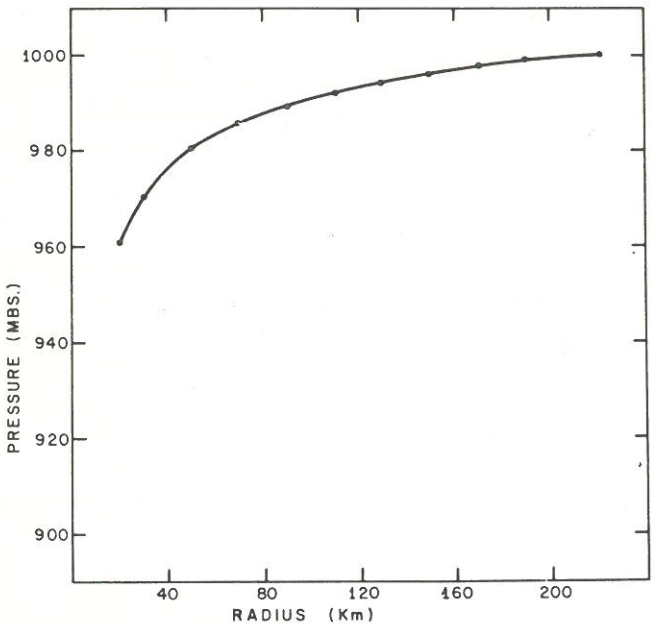

Figure 34. - Radial pressure profile over land, computed by using observed winds and surface friction.

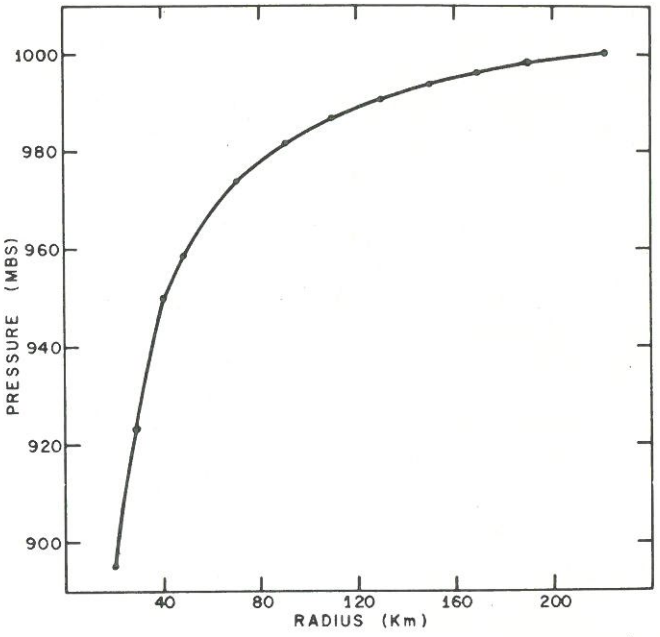

Figure 35. - Computed pressure profile needed to maintain the surface wind over land the same as that observed over water, land friction and vertical shear considered.

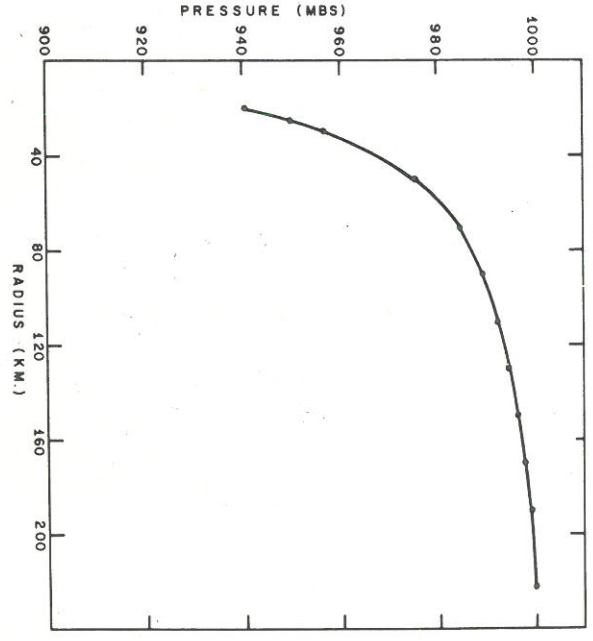

Figure 36. - Computed pressure profile needed to maintain mean wind speed for the inflow layer the same as that observed over water, land friction and vertical shear considered.

We will assume that the radius of the 1000-mb. isobar is 120 km. and that the minimum radius of penetration for a horizontal trajectory is 20 km., that the temperature at 1000 mb. is 26.0°C. and that the relative humidity is 95 percent. Equation (25) will be used in making the calculations. The mean surface inflow angle inside the 120-mb. radius on the 11th, when the cyclone was over land, was 26°. This value will be used in making the calculations.

The results are shown in table 5. The equivalent potential temperature values are comparable in each case to values observed in cyclones of comparable size and intensity. The indicated surface heat sources for "A" and "B" are well within the realm of probability; in fact, they are no greater than those which are known to exist in many tropical cyclones which occur over the oceans. Cyclone "C" would be a super cyclone comparable to the famous Labor Day hurricane which occurred in the Florida Keys in 1935.

As a result of these calculations, it may be concluded that surface friction is not the primary cause for the decay of tropical cyclones over land. In fact, given a surface heat source over land equal to that which exists over the oceans, a tropical cyclone could maintain much of its former vigor after landfall. Surface winds would slow down somewhat, but the pressure profile and the winds above the friction layer could continue with very little change.

7. THE KINETIC ENERGY BALANCE

It was suggested in an earlier section that one of the reasons for reduced frictional dissipation over land is a decrease in the production of kinetic energy. The production of kinetic energy is proportional to the product of $v_r \cdot (\partial z/\partial r)$ (Palmén and Riehl [37]). The mean height gradients decreased after landfall but the mean radial wind did not change very much. Hence, the production of kinetic energy must have decreased. To support this hypothesis, however, we will now compute the kinetic energy budget for the inflow layer. If the computations show that the production did actually decrease, this decrease can then be related to the cooling of the core of the cyclone.

a. The Kinetic Energy Equations

To derive the horizontal kinetic energy equations, we form the scalar product of $\mathbf{V}$ and the two-dimensional vector equation of motion, which is

$$\frac{d\mathbf{V}}{dt} = -g\nabla z - 2\Omega \times \mathbf{V} + \mathbf{F} \qquad (50)$$

Ω being the earth's rotation. Other terms have already been defined. After scalar multiplication by $\mathbf{V}$, we obtain

$$\frac{dK}{dt} = -g\,\mathbf{V} \cdot \nabla z + \mathbf{V} \cdot \mathbf{F} \qquad (51)$$

Table 5. - Surface heat source needed to maintain isothermal expansion inside a 100-mb. isobar with radius of 120 km.

Computed Minimum Pressure (p_c)	Q_{sp} (cal. gm.$^{-1}$)	($T_s - T_a$) (°C.)	$K_{sp} \times 10^9$ (cal.$^{-1}$ cm.$^{-1}$ gm.$^{-1}$ deg.$^{-1}$)	q_s (gm. kg.$^{-1}$)	Q_{ep} (cal. gm.$^{-1}$)	θ_e
960	1.57	2	33.36	21.55	5.44	369.1 A
940	2.40	3	36.04	22.48	8.38	373.0 B
895	4.28	4	48.19	24.18	14.18	382.3 C

Equation (51) is now multiplied by the density, ρ, and then (making use of the equation of continuity, $(\nabla_3 \cdot \mathbf{V}_3 = -(1/\rho)(d\rho/dt)$ transformed into

$$\frac{d\rho K}{dt} + \rho K \nabla_3 \cdot \mathbf{V}_3 = -\rho g \mathbf{V} \cdot \nabla z + \rho \mathbf{V} \cdot \mathbf{F} \qquad (52)$$

Expanding $d\rho k/dt$ and making use of the vector identity,

$$\nabla_3 \cdot (\rho K \mathbf{V}_3) = \rho K \nabla_3 \cdot \mathbf{V}_3 + \mathbf{V}_3 \cdot \nabla \rho K$$

we obtain

$$\frac{\partial \rho K}{\partial t} = -\nabla_3 \cdot \rho K \mathbf{V}_3 - \rho g \mathbf{V} \cdot \nabla z + \rho \mathbf{V} \cdot \mathbf{F} \qquad (53)$$

Equation (53) is now integrated over a volume, α, using pressure as the vertical coordinate, and the divergence theorem is used to transform the first volume integral on the right into a surface integral. This results in

$$\frac{\partial}{\partial t}\int_\alpha \rho K d\alpha = -\int_{p_t}^{p_o}\int_L v_r K \, dL \, \frac{dp}{g} - \int_A \rho a K dA$$

$$-\int_{p_t}^{p_o}\int_A \mathbf{V} \cdot \nabla z dA dp + \int_\alpha \rho \mathbf{V} \cdot \mathbf{F} d\alpha \qquad (54)$$

The first two terms on the right represent the changes in kinetic energy inside the volume due to advection through the boundary. The third integral is the sum of the production of kinetic energy inside the volume by pressure forces and the work done by pressure forces acting on the boundary. The last integral on the right is the frictional dissipation. The "production" term will be evaluated by the approximation

$$\int_p \int_A \mathbf{V} \cdot \nabla z \, dA \, dp \doteq \int_p \int_A v_r \frac{\partial z}{\partial r} \, dA \, dp \qquad (55)$$

since the height field is almost circular. The frictional dissipation can be transformed (Riehl [47]) to

$$\int_\alpha \rho \, \mathbf{V} \cdot \mathbf{F} \, d\alpha = \int_\alpha \mathbf{V} \cdot \frac{\partial \boldsymbol{\tau}}{\partial z} = \int_\alpha \frac{\partial (\mathbf{V} \cdot \boldsymbol{\tau})}{\partial z} d\alpha - \int_\alpha \boldsymbol{\tau} \cdot \frac{\partial \mathbf{V}}{\partial z} d\alpha$$

The first integral on the right gives the dissipation at the upper and lower boundaries, the second, internal frictional dissipation. We assume the frictional stress at the top of the cyclone is negligible. Hence,

$$\int_\alpha \frac{\partial (\mathbf{V} \cdot \boldsymbol{\tau})}{\partial z} \, d\alpha = \int_A (\mathbf{V} \cdot \boldsymbol{\tau}) \, dA = - \int_A \rho C_d v_o^3 dA \qquad (56)$$

Internal friction cannot be determined from the data available.

b. The Kinetic Energy Budget for the Inflow Layer

For the inflow layer the data permitted a detailed calculation of the kinetic energy budget by 40-n. mi. increments. This is fortunate, since the inflow layer is in essence the dynamo which runs the cyclone. The results of the calculations are summarized in table 6. This table shows the production of kinetic energy, horizontal divergence, dissipation by surface friction, and vertical transport through the upper boundary (700 mb.). Internal friction has been omitted. The local change ($\delta K/\delta t$) was derived from a time rate of change curve, which was prepared from the analyses of the isotach patterns.

It will be noted that the production of kinetic energy decreased sharply after the center moved inland. Production for the 10-120-n. mi. ring was 23.36×10^{14} kj./day on the 10th; on the 11th (cyclone over land) this had decreased to 12.24×10^{14} ki./day, which is only 52 percent of the production on the previous day. Within the innermost region (10-40 n. mi. ring) the decrease was even more remarkable. Production dropped from 9.49 units to 3.34 units; production in the core of the inflow layer while the center was over land was 35 percent of its value on the 10th.

This decrease in the production of kinetic energy is due almost entirely to a decrease in the height gradient along the constant pressure surfaces. Some representative curves of the variations of height of the

Table 6. - Kinetic energy budget for the inflow layer (surface to 700 mb.). Units are 10^{14} kj. day^{-1}. Negative values indicate production and inward transport. $\delta K/\delta t$ is the local change of kinetic energy in a moving coordinate system.

Date	9	9	9	9	10	10	10	10	11	11	11	11
Radial interval	10-40	40-80	80-120	10-120	10-40	10-80	80-120	10-120	10-40	40-80	80-120	10-120
Production	-8.09	-4.71	-4.32	-17.12	-9.49	-7.97	-5.90	-23.36	-3.34	-5.10	-3.80	-12.24
Lateral divergence	-4.63	-0.58	-.08	-5.29	-5.37	-1.34	-1.89	-8.60	-4.76	-0.40	0.38	-4.78
$C_d \times 10^3$	3.90	3.05	2.10	--	4.00	3.40	2.90	--	8.70	8.25	5.50	--
Dissipated by surface friction	5.18	5.15	2.88	13.21	5.37	5.92	4.17	15.46	3.21	4.85	3.06	11.12
Vertical transport	5.99	2.30	0.23	8.52	7.18	3.36	1.35	11.89	4.09	2.10	0.68	6.87
$\delta K/\delta t$				0.23				0				-0.42
Residual	-1.55	2.16	-1.29	-0.45	-2.31	-0.03	-2.27	-4.61	-0.80	1.45	0.32	0.55

850-mb. surface along the radius are shown in figure 37. This decrease in height gradient along the radius is brought about by cooling of the core of the cyclone as has been shown previously. The mean values for the radial wind component through the inflow layer are shown in figure 38; it will be seen that the mean v_r on the 11th was about 80 percent of its value on the 10th. Since production was evaluated by use of equation (55), which contains the product of v_r and $\partial z/\partial r$, it is apparent that production did not decrease from a reduction in the radial mass flow.

On the 9th, the cyclone was still intensifying, and the inflow layer produced some excess kinetic energy which may have been either exported by small-scale eddy stresses (either vertically or horizontally) or dissipated by internal friction.

On the 10th there was a large amount left over for either export or dissipation by internal friction. At this time the cyclone was in a steady state. It is postulated that this excess produced by the inflow layer was exported vertically by means of strong updrafts in cumulonimbus clouds, and that it was either exported by the mass outflow in the upper troposphere or dissipated by doing work in the region where the outflow was against the pressure gradient.

On the 11th the inflow layer did not produce enough kinetic energy to overcome surface friction and to provide that exported vertically by the mass circulation. None was left over for internal friction. As a result the circulation of the inflow layer itself must have been weakening. This is indicated by the local change of kinetic energy. Once again, however, it may be emphasized that this weakening of the inflow layer is due to decreased production of kinetic energy and not to increased frictional dissipation.

Reduced production resulted from a decrease in the pressure gradients and not primarily from a reduction in the mass circulation. The greatest decrease in the production of kinetic energy occurred inside the 40-n. mi. radius. It has been shown that the pressure rose in the interior due to cooling of the air column extending from sea level to about 100 mb. Hence, one may conclude that the circulation of the inflow layer weakened primarily as a result of removal of the oceanic heat source and not from increased surface roughness over land.

8. SUMMARY AND CONCLUSIONS

As long as a tropical cyclone remains over the warm waters of the tropical oceans, the surface air temperature is very nearly constant (along a radius). This temperature distribution is due to the oceanic heat source, as large amounts of both latent and sensible heat are added to the parcel along its trajectory. This addition of heat raises the equivalent potential temperature of the surface air. Part of the surface air ascends near the core of the cyclone. Since a radial gradient of equivalent potential temperature exists at the surface, a radial gradient of mean virtual temperature from the surface to the upper troposphere is maintained. This warm core structure is responsible for the intense surface pressure gradients found in tropical cyclones.

Over land, however, a horizontal trajectory takes a path which is very close to moist adiabatic. The oceanic heat source is absent, and the resultant radial gradient of equivalent potential temperature at the surface is destroyed or greatly weakened. Following ascent of this surface air, the gradient of mean virtual temperature from the surface to the upper troposphere is destroyed. The warm air that was previously concentrated near the core of the cyclone is spread out over a larger area. The pressure in the interior rises; at the same time, the pressure at some outer radii (in Donna this was outside the 40-n. mi. radius) falls. This cooling of the core of the cyclone eventually results in weakening and decay of the circulation.

Mass flow through the cyclone remains virtually unchanged after the cyclone moves inland, at least for a period of several hours. However, within a few hours, the radial gradients of heights of the constant pressure surfaces near the core of the cyclone decrease to about one-half their value at the time of landfall. The production of kinetic energy is proportional to the product of the mass flow and the height gradients. Hence, the production of kinetic energy decreases. Since height gradients are known to depend upon thermal gradients, and since the decrease in the height gradients is due to cooling of the core of the cyclone, it follows that the decrease in the production of kinetic energy is due to cooling of the interior of the cyclone.

The surface drag coefficients are larger over land than they are over water by a factor of a little over 2. The dissipation of kinetic energy by surface friction is proportional to the product of the drag coefficient and the third power of the surface wind speed. The increased surface roughness over land results in a decrease in the surface wind speed. Turbulence theory suggests that there must also be greater vertical shear over land than over water; i.e., the decrease in the wind at the anemometer level is greater than it is at some higher level, say 100 m. This, however, cannot be verified with the data available. It can be shown that within a few hours after landfall the dissipation of kinetic energy by surface friction is less over land than it is over water.

The pressure gradients needed to maintain the hurricane over land with the same surface wind speeds that existed over water can be computed by use of the radial equation of motion. If one considers the vertical shear suggested by turbulence theory, the pressure gradient needed is large though not impossible to maintain. This is due to the fact that much larger wind speeds at 100 m. would be required over land than over water (because of larger vertical shear). However, the pressure gradient needed to maintain the same wind speed at 100 m. (with the surface wind allowed to decrease) is about the same as that actually observed over water. A surface heat source over land equivalent to the oceanic heat source could maintain the required pressure gradient.

With all these facts considered, it is concluded that hurricane Donna filled and weakened over land as a result of the removal of the oceanic heat source. Increased surface roughness over land resulted in some reduction in the surface wind speed, but was <u>not responsible</u> for the filling of the cyclone.

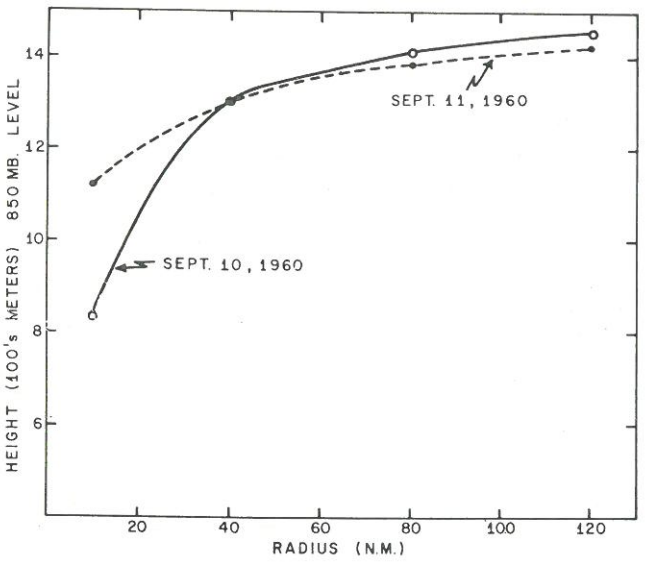

Figure 37. - Radial profile of the height of the 850-mb. surface, September 10-11.

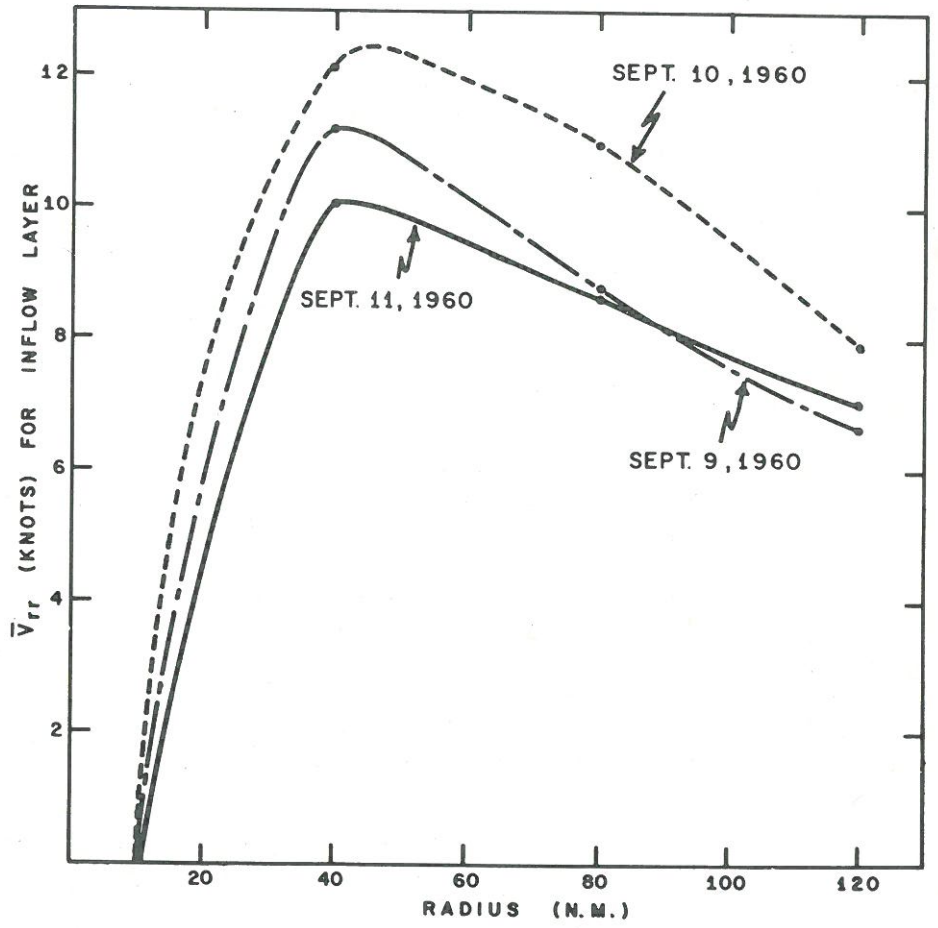

Figure 38. - Radial profile of the vertical mean of the radial wind for the inflow layer, September 9-11.

ACKNOWLEDGMENTS

The author is indebted to Professor Herbert Riehl and Sverre Petterssen for encouragement, advice, and many helpful suggestions throughout the course of this research. Staff members of the National Hurricane Research Project read the manuscript and offered several constructive criticisms. Mr. Daryl T. Rubsam prepared the analyses for figures 15 and 27. Mr. L. F. Conover assisted in the preparation of figure 1. Mrs. Mildred Kirkland assembled much of the data and plotted most of the numerous charts which were used. Mr. Robert Carrodus drafted the illustrations, Mr. Charles True did the photography, and Mrs. Virginia King typed the original manuscript.

REFERENCES

1. T. Bergeron, "The Problem of Tropical Hurricanes," Quarterly Journal of the Royal Meteorological Society, vol. 80, No. 344, Apr. 1954, pp. 131-164.

2. H. R. Byers, General Meteorology, McGraw-Hill Book Co., New York and London, 1959, 540 pp.

3. H. Charnock, J. R. D. Francis, and P. A. Sheppard, "An Investigation of Wind Structure in the Trades: Anegada, 1953," Philosophical Transactions of the Royal Society of London, Series A, vol. 249, No. 963, Oct. 18, 1956, pp. 179-234.

4. A. Colding, "Results of Certain Investigations of the Current in the Sea Caused by the Force of the Wind," Danske Videnskabs, Shrifter, Naturwidenskab Mathematik, Afdel. 11, No. 3, 1876.

5. J. A. Colón, "On the Heat Balance of the Troposphere and Water Body of the Caribbean Sea," National Hurricane Research Project Report No. 41, U. S. Weather Bureau, 1960, 65 pp.

6. J. Darbyshire and M. Darbyshire, "Determination of Wind Stress on the Surface of Lough Neagh by Measurement of Tilt," Quarterly Journal of the Royal Meteorological Society, vol. 81, No. 349, July 1955, 333-339.

7. E. L. Deacon and W. C. Swinbank, "Comparison Between Momentum and Water Vapor Transfer," Paper No. 2, Australian-UNESCO Symposium, Arid Zone Climatology, 1956.

8. E. L. Deacon, P. A. Sheppard, and E. K. Webb, "Wind Profiles Over the Sea and the Drag at the Sea Surface," Australian Journal of Physics, vol. 9, No. 4, Dec. 1956, pp. 511-541.

9. E. L. Deacon, "The Stress of Light Winds on the Sea," Bulletin of the American Meteorological Society, vol. 38, No. 9, Nov. 1957, pp. 540-542

10. G. E. Dunn and B. I. Miller, Atlantic Hurricanes, Louisiana State University Press, Baton Rouge, La., 1960, 326 pp.

11. V. W. Ekman, "On the Influence of the Earth's Rotation on Ocean Currents," Arkiv für Mathematik, Astronomie und Physik, vol. 2, No. 11, 1905, 52 pp.

12. T. H. Ellison, "Turbulent Transport of Heat and Momentum from an Infinite Rough Plane," Journal of Fluid Mechanics, vol. 2, No. 5, July 1957, pp. 456-466.

13. E. L. Fisher, "Hurricanes and the Sea-Surface Temperature Field," Journal of Meteorology, vol. 15, No. 3, June 1958, pp. 328-333.

14. W. M. Gray, Personal communication, 1962.

15. G. J. Haltiner and F. L. Martin, Dynamical and Physical Meteorology, McGraw-Hill Book Co., Inc., New York and London, 470 pp.

16. B. Haurwitz, Dynamic Meteorology, McGraw-Hill Book Co., New York and London, 1941, 365 pp.

17. J. S. Hay, "Some Observations of Air Flow Over the Sea," Quarterly Journal of the Royal Meteorological Society, vol. 81, No. 349, July 1955, pp. 307-319.

18. J. O. Hinze, Turbulence (An introduction to its mechanism and theory), McGraw-Hill Book Co., Inc., New York and London, 1959, 586 pp.

19. L. F. Hubert, "Frictional Filling of Hurricanes," Bulletin of the American Meteorological Society, vol. 36, No. 9, Nov. 1955, pp. 440-445.

20. L. A. Hughes, "On the Low-Level Wind Structure of Tropical Storms," Journal of Meteorology, vol. 9, No. 6, Dec. 1952, pp. 422-428.

21. W. C. Jacobs, "On the Energy Exchange Between Sea and Atmosphere," Journal of Marine Research, vol. 5, 1942, pp. 37-66.

22. E. S. Jordan, "An Observational Study of the Upper Wind-Circulation Around Tropical Storms," Journal of Meteorology, vol. 9, No. 5, Oct. 1952, pp. 340-346.

23. D. W. Krueger, "A Relation Between the Mass Circulation through Hurricanes and Their Intensity," Bulletin of the American Meteorological Society, vol. 40, No. 4, Apr. 1959, pp. 182-189.

24. R. W. Longley, "On the Energy of a Hurricane," Bulletin of the American Meteorological Society, vol. 30, No. 5, May 1949, pp. 194-195.

25. W. Malkin, "Filling and Intensity Changes in Hurricanes Over Land," National Hurricane Research Project Report No. 34, U. S. Weather Bureau, 1959, 18 pp.

26. J. Malkus and H. Riehl, On the Dynamics and Energy Transformations in Steady-State Hurricanes," National Hurricane Research Project Report No. 31, U. S. Weather Bureau, 1959, 31 pp.

27. J. Malkus and H. Riehl, "Some Aspects of Hurricane Daisy, 1958," National Hurricane Research Project Report No. 46, U. S. Weather Bureau, 1961, 64 pp.

28. B. I. Miller, "The Three-Dimensional Wind Structure Around a Tropical Cyclone," National Hurricane Research Project Report No. 15, U. S. Weather Bureau, 1958, 41 pp.

29. B. I. Miller, "Rainfall Rates in Florida Hurricanes," Monthly Weather Review, vol. 86, No. 7, July 1958, pp. 258-264.

30. B. I. Miller, "On the Energy and Momentum Balance of Hurricane Helene (1958)," National Hurricane Research Project Report No. 53, U. S. Weather Bureau, 1962, 19 pp.

31. R.B. Montgomery, "Observations of Vertical Humidity Distribution above the Ocean Surface and Their Relation to Evaporation," Papers in Oceanography and Meteorology, Massachusetts Institute of Technology and Woods Hole Oceanographic Institution, vol. 7, No. 4, 1940, 30 pp.

32. V. A. Myers, "Characteristics of United States Hurricanes Pertinent to Levee Design for Lake Okeechobee, Florida," Hydrometeorological Report No. 32, U. S. Weather Bureau, 1954, 120 pp.

33. G. Neumann, "Wind Stress on Water Surfaces," Bulletin of the American Meteorological Society, vol. 37, No. 5, May 1956, pp. 211-217.

34. E. Palmén, "Formation and Development of Tropical Cyclones," Proceedings of the Tropical Cyclone Symposium , Brisbane, Dec. 1956, pp. 212-231.

35. E. Palmén, "On the Maintenance of Kinetic Energy in the Atmosphere," pp. 212-224 in The Atmosphere and the Sea in Motion, (Rossby Memorial Volume), The Rockefeller Institute and Oxford University Press, 1959.

36. E. Palmén and L. Laurila, "Uber die Einwirkung eines Sturmes auf den hydrographischen Zustand in nördlichen Ostseegebiet," Societas Scientiarum Fennica, Commentationes Physica-Mathematicae, vol. 10, No.1, 1938, 53 pp.

37. E. Palmén and H. Riehl, "Budget of Angular Momentum and Energy in Tropical Cyclones," Journal of Meteorology, vol. 14, No. 2, Apr. 1957, pp. 150-159.

38. H. A. Panofsky, A. K. Blackadar, and G. E. McVehil, "The Diabatic Wind Profile," Quarterly Journal of the Royal Meteorological Society, vol. 86, No. 369, July 1960, pp. 390-398.

39. F. Pasquill, Atmospheric Diffusion, D. van Nostrand Company, Ltd., New York and London, 1962, 297 pp.

40. S. Petterssen, Weather Analysis and Forecasting, McGraw-Hill Book Co., Inc., New York and London, 1956, 428 pp.

41. S. Petterssen, D. L. Bradbury, and K. Pedersen, "Heat Exchange and Cyclone Development on the North Atlantic Ocean," The University of Chicago, Dept. of Meteorology, 1961, 76 pp.

42. A. C. Pike, "The Oceanic Heat Budget as Affected by Hurricane Audrey (1957)," Civil Engineering Dept., Colorado State University, Fort Collins, Colo., 1962, 7 pp.

43. C. H. B. Priestley, Turbulent Transfer in the Lower Atmosphere, University of Chicago Press, Chicago, Ill., 1959, 130 pp.

44. N. E. Rider, "Eddy Diffusion of Momentum, Water Vapour, and Heat Near the Ground," Philosophical Transactions of the Royal Society of London, Series A, vol. 246, 1954, pp. 198-212.

45. H. Riehl, T. C. Yeh, J. S. Malkus, and N. E. LaSeur, "The Northeast Trade of the Pacific Ocean," Quarterly Journal of the Royal Meteorological Society, vol. 77, 1951, pp. 598-626.

46. H. Riehl, Tropical Meteorology, McGraw-Hill Book Co., Inc., New York and London, 1954, 392 pp.

47. H. Riehl, "On the Production of Kinetic Energy from Condensation Heating," National Hurricane Research Project Report No. 22, U. S. Weather Bureau, 1958, 25 pp.

48. H. Riehl, "Surface Processes in Hurricane Donna," Proceedings of the Second Technical Conference on Hurricanes, Miami Beach, Fla., June 27-30, 1961," National Hurricane Research Project Report No. 50, Part II, U. S. Weather Bureau, 1962, pp. 314-316.

49. S. L. Rosenthal, "Concerning the Mechanics and Thermodynamics of the Inflow Layer of the Mature Hurricane, National Hurricane Research Project Report No. 47, U. S. Weather Bureau, 1961, 31 pp.

50. C.-G. Rossby and R. B. Montgomery, "The Layer of Frictional Influence in Wind and Ocean Currents," Massachusetts Institute of Technology, Meteorological Papers, vol. 3, No. 3, 1935, 101 pp.

51. C.-G. Rossby, "On the Momentum Transfer at the Sea Surface," Massachusetts Institute of Technology, Meteorological Papers, vol. 4, No. 3, 1936, 30 pp.

52. P. A. Sheppard and H. M. Omar, "The Wind Stress Over the Ocean from Observations in the Trades," Quarterly Journal of the Royal Meteorological Society, vol. 78, Oct. 1952, pp. 583-589.

53. P. A. Sheppard, "Transfer Across the Earth's Surface and Through the Air Above," Quarterly Journal of the Royal Meteorological Society, vol. 84, No. 361, July 1958, pp. 205-224.

54. J. Spar, "Synoptic Studies of the Potential Energy in Cyclones," Journal of Meteorology, vol. 7, No. 1, Feb. 1950, pp. 48-53.

55. H. U. Sverdrup, "On Evaporation from the Oceans," Compendium of Meteorology, American Meteorological Society, Boston, 1951, pp. 1071-1081.

56. H. U. Sverdrup, "Oceanography," pp. 608-670 in Handbuch der Physik, Band XLVIII, Springer-Verlag, Berlin, 1957.

57. W. C. Swinbank, "An Experimental Study of Eddy Transports in the Lower Atmosphere," Technical Paper No. 2, CSIRO, Div. of Meteorological Physics, Melbourne, 1955, 30 pp.

58. G. I. Taylor, "Eddy Motion in the Atmosphere," Philosophical Transactions of the Royal Society of London, Series A, vol. 215, 1915, pp. 1-26.

59. R. J. Taylor, "Similarity Theory in the Relation Between Fluxes and Gradients in the Lower Atmosphere," Quarterly Journal of the Royal Meteorological Society, vol. 86, No. 367, Jan. 1960, pp. 67-78.

60. C. W. Thornthwaite and B. Holzman, "The Determination of Evaporation from Land and Water Surfaces," Monthly Weather Review, vol. 67, No. 1, Jan. 1939, pp. 4-11.

61. B. W. Wilson, "Note on Surface Wind Stress Over Water at Low and High Wind Speeds," Journal of Geophysical Research, vol. 65, No. 10, Oct. 1960, pp. 3377-3382.

62. G. Wüst, "Die Verdunstung auf dem Meere," Veröffentlichungen, Institut für Meereskunde, Universität Berlin, Neue Folge, A, No. 6, 1920, 95 pp.

TR 3170-66
Miller
ON THE FILLING OF TROPICAL
CYCLONES OVER LAND WITH PARTICULAR
REFERENCE TO HURRICANE DONNA OF
1960